

A Thesis
Entitled

Environmental Impacts on the Development and Dune Activity of Oxbow Lake along the
Southwest Coast of Lake Michigan at Saugatuck, Michigan USA

By
Kira Joy Baca

Submitted to the Graduate Faculty as partial fulfillment of the
requirements for the Master of Science Degree in Geology

Dr. Timothy G. Fisher, Committee Chair

Dr. David E. Krantz, Committee Member

Dr. Richard Becker, Committee Member

Dr. Johan F. Gottgens, Committee Member

Dr. Patricia Komuniecki, Dean
College of Graduate Studies

The University of Toledo
May 2013

Copyright 2013, Kira J. Baca

This document is copyrighted material. Under copyright law, no parts of this document may be reproduced without the expressed permission of the author.

An Abstract of
Environmental Impacts of the Development and Continual Dune Activity of Oxbow Lake
along the Southeast Coast of Lake Michigan at Saugatuck, Michigan, USA

by

Kira J. Baca

Submitted to the Graduate Faculty as partial fulfillment of the
requirements for the Master of Science Degree in Geology

The University of Toledo

May 2013

Coastal dunes of Lake Michigan and corresponding down-wind lakes are studied for links between dune activity and climatic forcing; to date, little is certain about climate control on dune activity. By unveiling relationships between climate variables and dune activity, it becomes possible to associate the activity of dunes with certain climatic conditions. In this study wind, temperature, precipitation, drought, evaporation, and lake level are correlated individually with $^{210}\text{Pb}/^{137}\text{Cs}/^7\text{Be}$ dated sand deposits from core samples taken in a small lake in the lee side of a dune ridge near Saugatuck, Michigan. Linear regressions were run to evaluate the strength of their relationship year-by-year, and offsets of one to two years. Visual correlations were also attempted by evaluating the trends in the annular data sets. While year-by-year R^2 values were not strong, or mixed results made them inconclusive, visually examined trends showed more promising correlations. The strongest correlations existed between sand percent by weight, drought, and lake level. Discrepancies between trends were acceptable within the limits of associated error with isotopic dating methods, and showed a relationship between rising

or high lake levels, wet conditions, and strong eolian activity (based on increased presence of sand in lake sediment). The implications of this research are that dune activity is linked to periods of wet conditions and storminess, and results can be used as a modern analogue for coastal dune activity during times of high lake level.

To all my friends and family who patiently withstood the chronic whirlwinds of stress,
and listened to my frustrations over the span of this study.

Acknowledgments

This Thesis would not have been possible without project advisors, Timothy Fisher and David Krantz for their guidance, many insightful words and field work assistance during the course of this project, Johan Gottgens for his support and facilities, and Richard Becker for his ideas. Also, I would like to thank field assistants Joe Blockland, Janet Traub and her husband Jim Traub, as well as Hope College for their aid in the collecting of cores and GPR data for this project. This project could not have been accomplished without the help and support of the residents and local historians of Saugatuck, Michigan. I dearly thank Norm Deam and family, as well as the Nature Conservancy for their understanding and permission to use their properties for this project. I would also like to extend thanks to the Saugatuck-Douglas Historical Society for their many wonderful historical photographs and sharing the rich history of Saugatuck with me. Many thanks to the data made available by both NOAA and the USACE.

Table of Contents

Abstract	iii
Acknowledgments	v
Table of Contents.....	viii
List of Tables	xi
List of Figures	xii
1 Introduction	1
1.1 Introduction.....	1
1.2 Lake Michigan Fluctuations	2
1.3 Michigan Coastal Dunes	5
1.4 Study Site Overview	8
1.5 Hypothesis and Objectives	14
2 Methodology	15
2.1 Introduction	15
2.2 Historical Data	15
2.3 Sediment Cores and Analyses.....	16
2.3.1 Core Retrieval	17
2.3.2 Core Processing	20
2.3.3 Core Sampling	21

2.3.3.1 $^{210}\text{Pb}/^{137}\text{Cs}/^7\text{Be}$ Dating	22
2.3.3.2 Loss on Ignition	26
2.3.3.3 Particle Size Analysis	27
2.3.3.4 Percent Sand by Weight	29
2.4 Aligning Core Sand Percent Trends	30
2.4.1 Comparison of LOI Organic Trends	30
2.4.2 Constant Sedimentation Rate	31
2.4.3 Aligning of Sand Percent Trends	31
2.5 Correlating Sand Percent and Climate.....	31
2.6 Ground Penetrating Radar	34
3 Historical Data	36
3.1 History of Kalamazoo River	36
3.2 Saugatuck Harbor Research	45
4 GPR Results	48
4.1 Introduction	48
4.2 Ground Penetrating Radar Results	48
4.3 Summary	61
5 Sand Percent and Climate Results	62
5.1 Introduction	62
5.2 Livingstone Core Analysis	63
5.3 Glew Core Analyses	66
5.3.1 Loss on Ignition Organics	67
5.3.2 Particle Size Analysis	68

5.3.3 Percent Sand by Weight	71
5.3.4 Core Descriptions	72
5.4 $^{210}\text{Pb}/^{137}\text{Cs}/^7\text{Be}$ Sediment Ages and Deposition Rates	78
5.4.1 Age Dating Sand Signals	79
5.4.2 Age Assignment Between Glew Cores	84
5.5 Relationship between Sand Percent and Climate.....	87
5.5.1 Visual Comparisons	89
5.5.2 Correlations and Regressions	91
5.6 Summary	94
6 Discussion	96
6.1 Introduction	96
6.2 Infilling of the Kalamazoo River Mouth	96
6.3 Sand Percent and Climate	99
6.4 Application of Results	102
6.5 Sources of Error	103
7 Conclusions	106
7.1 Infilling of the Kalamazoo River Mouth	106
7.2 Sand Percent and Climate	107
7.3 Future Work	108
References	110
A Historic Maps and Images	115
B Raw GPR Data	117
C Sediment Analysis Data	124

D ^{210}Pb Error Calculations	137
E Climate & Sand Concentration Correlation	140

List of Tables

4.1 GPR lines: location, direction run and length	49
5.1 Sediment Core Locations	63
5.2 Udden-Wentworth Grain-size Classification	68
5.3 Calculated sediment ages with depth	83
5.4 R ² values between Climate, Wind, and Sand Percent	93

List of Figures

1-1	Relative lake level curve for Lake Michigan	2
1-2	Historical annual average lake level for Lakes Michigan and Huron	3
1-3	Schematic diagram of a coastline	4
1-4	Map: National and state view of Michigan	9
1-5	Geomorphic features of the coastline from the Saugatuck 7.5' Quadrangle	10
1-6	Photograph: Dune ridge separating Oxbow Lake from Lake Michigan	11
1-7	Saugatuck quadrangle map and corresponding satellite image	12
1-8	LIDAR hillshade of Oxbow Lake	13
2-1	Oxbow Lake with locations of Livingstone and Glew cores	17
2-2	Photograph: Glew coring device and accessories	19
2-3	Photograph: Glew corer with full core	19
2-4	Photograph: Glew core extraction device	21
2-5	Photograph: Intrinsic germanium well model gamma spectrometer	24
2-6	Photograph: Mastersizer 2000 system	28
2-7	Photograph: Ground penetrating radar	35
3-1	Archived maps of Allegan County for the years 1873 and 1913	36
3-2	Photograph: Kalamazoo River mouth through time	38
3-3	Topographic 7.5 minute map of the Saugatuck Quadrangle	39
3-4	Time lapse trace of infilled Kalamazoo River mouth and Oxbow Lake coast ...	42

3-5	1867 map with shoreline of Lake Michigan	43
3-6	1895 map of shoreline of Lake Michigan	44
3-7	Longshore transport sediment load averages at Saugatuck Harbor	47
4-1	Map: GPR lines and approximate pier locations	49
4-2	GPR – SAUG-01	52
4-3	GPR – SAUG-02	55
4-4	GPR – SAUG-03	56
4-5	GPR – SAUG-04	57
4-6	GPR – SAUG-05	58
4-7	GPR – SAUG-06	60
5-1	Livingstone core lithology and sand percentages with depth	65
5-2	Glew Cores: LOI _{Org} (550 °C)	67
5-3	Graphs A-E: Grain-size distribution for all Glew cores	69
5-4	Graph: Sand percentage with depth	72
5-5	Lithostratigraphic core logs of all sediment cores	74
5-6	Core lithostratigraphy with sediment examples from core OL-L1	75
5-7	Age-depth model of core G3 (²¹⁰ Pb, ¹³⁷ Cs, and ⁷ Be)	81
5-8	A) Dated OL-G3 sand percentages; B) Monte Carlo calculated age error	82
5-9	LOI _{Org} Correlated sand percent	85
5-10	Constant sedimentation rate correlated sand percent	86
5-11	“Wiggle Matched” correlated sand percent	86
5-12	Map: Locations of wind stations	88
5-13	Visual correlations: Sand percentage and lake level, PDSI, wind data	90

6-1	Range of wind headings and sand sources for study site	105
-----	--------------------------------------------------------------	-----

Chapter 1

Introduction

1.1 Introduction

The east coast of Lake Michigan boasts some of the largest and most extensive freshwater dune fields in the world. The development of dunes provides a means of tracking climatic history if the drivers of dune activity can be accurately determined. Studies of Lake Michigan's complex coastline have aided the understanding of lake level using beach ridges, which in turn has acted as a proxy for dune activity extending beyond historical records. Dunes along the western coast of Michigan continue to be studied to infer past climate based on periods of dune activation and stagnation (Hansen et al., 2010). This study explores links between dune activity in the last 100 years and climatic factors, to find causality with such mechanisms as lake level, storminess, and drought through time. If evidence for causality is found, these mechanisms will allow for more accurate reconstructions of past climate, and possibly lake levels from eolian records greater than 200 years old.

1.2 Lake Michigan Fluctuations

Studies of beach ridges around Lake Michigan have produced the standard record for high stands of Lake Michigan for the past 4,700 years. High lake levels created beach ridges along the Lake Michigan coast, marking temporary maximum elevation at a point in time. Organics found in swales between beach ridges were dated to determine the times of high stands, with high stands recorded by foreshore sediment. Studies by Thompson and Baedke (1997) and Baedke and Thompson (2000) produced four relative lake level curves (RLLC) from five sites surrounding Lake Michigan, with each curve corrected for isostatic rebound. The data were merged to create a 4,700 year record of lake level highs. Their record shows long-term, non-periodic highs, and short-term quasi-periodic (~33 year and ~160) year trends (Figure 1-1). Historic records from lake level gauges around the Great Lakes have been recorded (Figure 1-2) from 1860 to present with some scattered lake level data before this (Bishop, 1990).

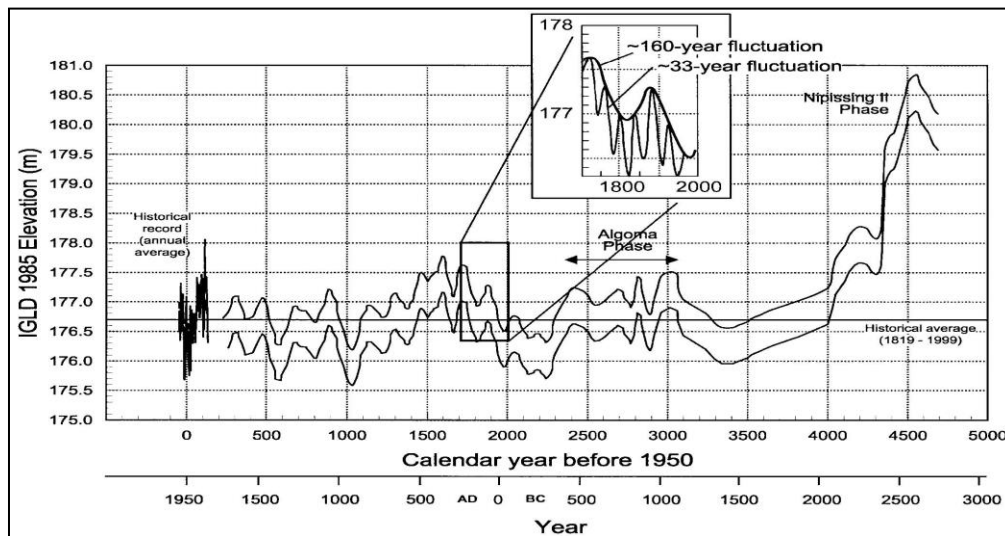


Figure 1-1 Relative Lake Michigan lake level curve from Baedke and Thompson (2000)

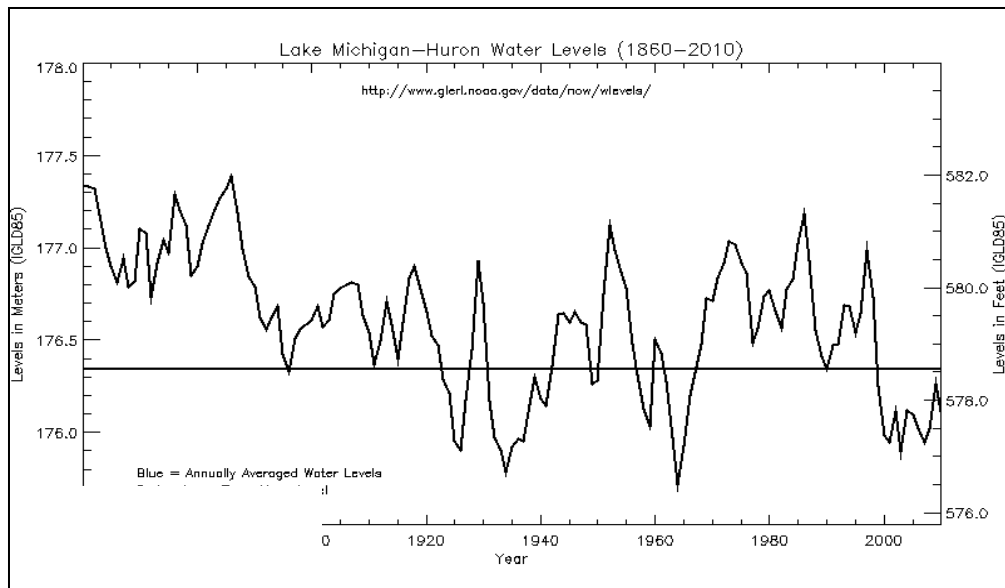


Figure 1-2 The historical annual average lake level for Lakes Michigan and Huron between the years 1860 and 2010. Chart from GLERL through NOAA (2011).

Records of lake level derived from beach ridges have been correlated with paleo-dune activity from records older than 200 years (Olsen, 1958). As lake level fluctuates, it changes the shape of the coastline. Rising lake levels cause shoreline transgression, where previously exposed beach becomes submerged and beach width decreases. Regression with lowered lake level exposes previously submerged shorelines and existing beaches grow wider. Foreshore elevation, indicated by gravel deposits, is a clear gauge of lake level highs (Figure 1-3). As lake level rises, it erodes beach ridges. The removal of vegetation destabilizes the lakeward side of the dunes, making the sand susceptible to winds and mobilization. If lake level were to drop, a new beach ridge would form lakeward of the previous one, preserving stratigraphy beneath it and extending the beach lakeward. Beach ridges form following high-stands and preserve foreshore gravel deposits from which past lake level highs are determined (Thompson and Baedke, 1997). Based on the work of Thompson et al. (1997), the sequence of lake level highs are as

follows, in calendar years before present (1950 AD): the Nipissing phase (4,700 – 4,000 ca BP) (Thompson et al., 2011) – highest recorded lake level; Algoma Phase (3,100 – 2,300 ca BP) – second oldest high stand; unnamed high stand (2000 – 1200 ca BP); Medieval Warm Period (1000 – 600 ca BP); and Little Ice Age (500 – 200 ca BP).

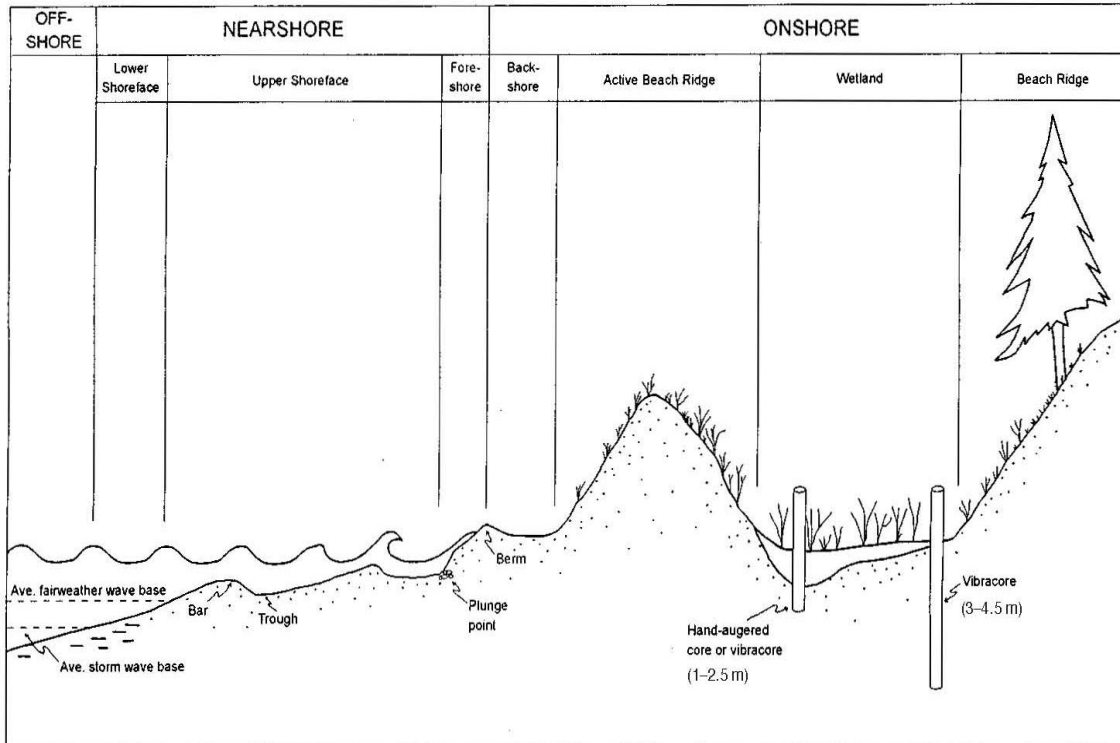


Figure 1-3 Schematic diagram of a coastline showing depositional environments for the Lake Michigan coastline (Thompson and Baedke, 1997).

Quasi-periodic fluctuations in lake level have been explained using climatic factors (temperature and precipitation), with perpetually higher and drier periods associated with lower lake levels (Croley, 2006). Colder, wetter times were linked to high lake level, (Fraser, 1990), and any prolonged anomalous change in climate and the amount of water supplied to the drainage basin would alter lake level (Bishop, 1990; Argyilan, 2003). Modeling by Croley (2006) for the Great Lakes under extensive drought

conditions, predicts the lakes becoming terminal. Bishop (1990) used the location and damage caused by flooding of settlements, before lake level records were systematically kept, to determine lake elevation and signs of flooding for past climate trends further into the past than is recorded by NOAA.

Argyilan (2003) compared lake level trends to known climate variables between 1860 (first recorded lake levels) and 1995. She found that highs and lows shift temporally based on increased surface temperatures in winter and decreased longevity of snowpack, leading to earlier melt runoff. The overall seasonal shift in lake level through the year is a clear sign of climate change. Shorter seasonal transitions and increased temperatures are projected to lead to more dramatic lake level changes through time.

1.3 Michigan Coastal Dunes

Lakes are dynamic bodies of water that transport and deposit sediment over time to create beaches and coastal dunes. A clearer understanding of drivers of lake level is achieved by taking a closer look at events affecting the lake during periods of lower lake level. Fraser (1990) reconstructed coastal erosion and signs of coastal inland flooding using evidence from aggraded streams, marshes, and soils in eolian sand. Soil formation in dunes record dune stagnation; accompanied by signs of flooding, soil formation would be linked to lake high stands. Such inferences permit correlation between prominent datable paleosols found along the western Michigan coast (Arbogast et al., 2004) and lake level. Michigan coastal dunes form in response to coastal regression as prograding shorelines introduce more sand to the beach when lake levels fall (Thompson and

Baedke, 1997). Thus, it is expected that excess sand during regressive trends in lake level supplies sand for dune formation.

Hansen and colleagues assembled a brief history of dune formation spanning deglaciation to present for the southeastern coast of Lake Michigan has been summarized by Hansen et al. (2010). The timeline can be referenced to time periods in Figure 1-1, showing corresponding lake level highs and lows. Six stages are described: Stage 1) Pre-Nipissing (deglaciation – ca. 5.7 ka) – dunes formed from ancestral lake level highs after deglaciation; 2) Nipissing (5.7 - 3.8 ka) – dune growth and migration due to Nipissing transgression and fall from the Nipissing peak; 3) Post-Nipissing interlude (3.8 - 3.3 ka) – stabilized dunes during a period of low lake level; 4) Algoma (3.3 - 1.6 ka) – episodic activation of dunes during a time of lake level rise and the formation of large parabolic dunes along the coast; 5) Holland paleosol interlude (1.6 - 0.5 ka) – slowing of dune activity marked by a spodic paleosol within dunes along the coast (Arbogast et al., 2004); and 6) Modern (0.5 - present) – resurgence of dune growth and migration that predates European settlers. The history outlined by Hansen et al. (2010) illustrates a suggested relationship between lake level highs and lows and their effect on dune formation and times of migration.

As lake level rises, the erosion of coastal dunes by wave action destabilizes them by removing vegetative cover. Other causes of dune activation: 1) loss of dune vegetation due to drought or exceptionally cold temperatures; 2) anthropogenic disruption, or organisms compromising the health of the native flora that stabilize the dune surfaces; and 3) increased storminess that transports more coastal [or dune] sand due to its disruptive forces (Donnelly et al., 2001; Scileppi and Donnelly, 2007). The

destabilization of dunes triggers dune activation and increases sand transport. Scileppi and Donnelly (2007) found strong correlations between sand deposits in marshes along the Atlantic Northeast coast of the US, and arrival of hurricanes to the coast. They remark how sand deposits in organic mud contain denser mafic grains, showing signs of rapid deposition through density displacement. Climate, such as drought and storminess, has been correlated in multiple studies with lake level and dune activation (Arbogast et al., 1999; Fisher et al., 2012) but equivocal in Timmons et al. (2007).

Small lakes separated from Lake Michigan by dune complexes contain detailed records of dune mobility in their sediment records. Dune activation causes increased sand transport, and thus eolian input to lakes, recording times of dune activation along the coast of Lake Michigan. The benefit of studying these lake sediments is based on their high-resolution record of dune activity, greater than that of OSL (optically stimulated luminescence) dating of dune sand and radiocarbon dating of paleosols within the dunes (Timmons et al., 2007). Increased sand concentrations in lakes adjacent to Lake Michigan caused by dune activation were coined “sand signals” by Fisher et al. (2012). The purpose of sand signal research is to decipher whether climatic trends correlate to patterns in sand concentrations from limnologic records of small lakes in the path of migrating coastal dunes. Determining the climatic drivers behind dune activation allows for further connections to be made to climatic drivers of lake level, and climate of the distant past.

So far, publications have had contradictory results as to whether connections can be made between lake level and dune activation (Timmons et al., 2007). It is known from modern process studies that Great Lake coastal dunes are more active during winter

(Marsh and Marsh, 1997). Fisher et al. (2012), documents sand and snow transported together creating alternating laminations on dunes and lake ice, as well as sand traveling far onto lake ice where it would not otherwise reach during warmer months. At the end of cold periods, accumulated sand is deposited en masse into lakes when ice thaws (Fisher et al., 2010). Eolian sand signals in the limnologic records may not all be from eolian processes, with each coastal lake having its own history. Nevertheless, understanding eolian sedimentation into coastal lakes gives researchers a better understanding of paleo-dune activity and perhaps paleoclimate history from sediment cores.

1.4 Study Site Overview

Oxbow Lake is a body of water located west of Saugatuck, Michigan in Allegan County (Figure 1-4). It formed after the Kalamazoo River was rerouted to the north, by a man-made channel, and the former mouth of the river infilled with littoral sediment. Subsequently, dunes accreted on top of the closure, separating the former channel from Lake Michigan. The Kalamazoo River is presently surrounded by dunes, both new and old, with a large dune complex that predates foredunes and dune ridge in front of Oxbow Lake (Figure 1-5). Infilling of the Kalamazoo River mouth started in 1906 when water was diverted from the Kalamazoo River to an artificial channel 3 km up the coast from the natural mouth (Figure 1-7). The study site trends west-east, and is located where the old Kalamazoo River mouth, approximately 2 km long, emptied into Lake Michigan. Stable 30 m high dunes surround the study site to the south and east. To the west is a recently formed (>100 years) dune ridge complex with swales and blowout dunes behind

it (Figure 1-5 and 1-6). The north is bounded by the rerouted river bend and artificial channel.

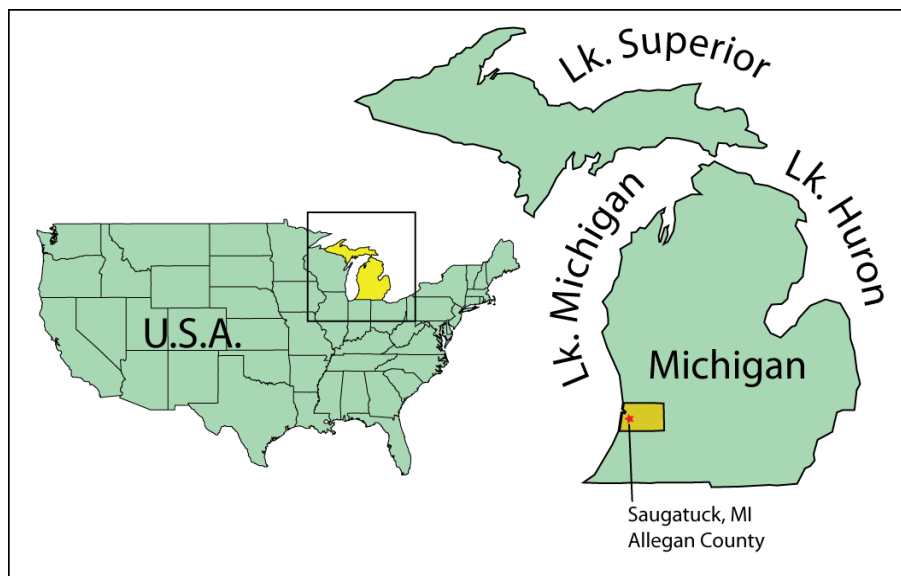


Figure 1-4 A national and state view of Michigan, the yellow square highlights the study site in Allegan County, MI.

The dune ridge separating Oxbow Lake from Lake Michigan averages 10 m high and spans the distance from just south of the former river mouth to approximately the artificial channel (Figure 1-6 and 1-8). Both vegetated and non-vegetated (blow out) dunes exist in this area, as well as swales in which water accumulates seasonally (Figures 1-4 and 1-7). The water surface in Oxbow Lake is at approximately the same elevation as Lake Michigan. The recent formation of the dunes in the mouth of this abandoned channel provides a rare opportunity to explore: 1) sedimentation styles within a small lake with good chronologic control along the coast; and 2) driving forces behind the formation and activation of dunes over a 100-year period using climatic records.

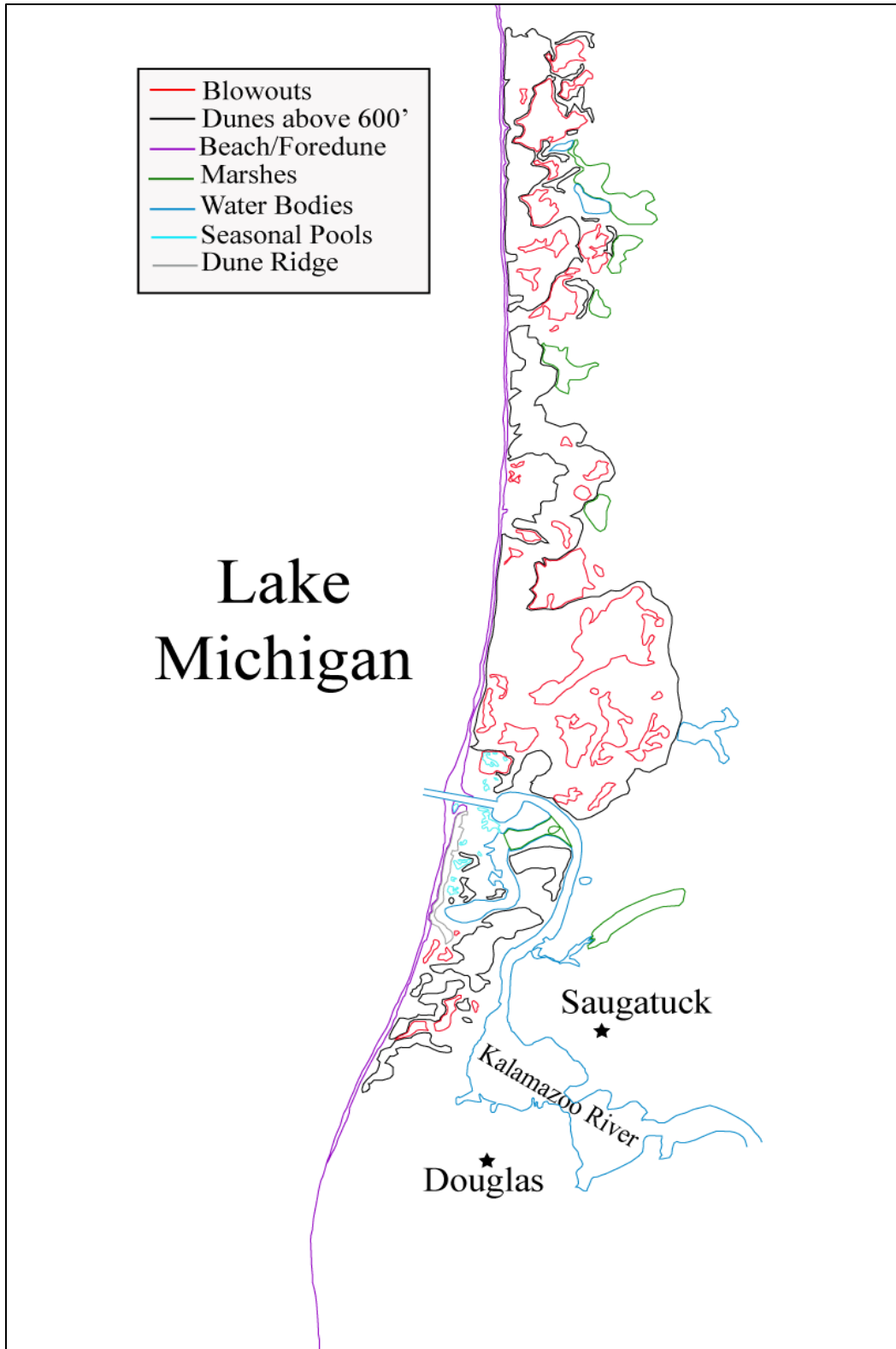


Figure 1-5 Geomorphic features of the coastline from the Saugatuck 7.5' Quadrangle map shown in Figures 1-7 and 3-3.



Figure 1-6 Photographs of the dune ridge (arrow) that separates Oxbow Lake from Lake Michigan. A) View southwest from above Oxbow Lake, in the foreground; B) Looking west from Oxbow Lake towards the 10 m high dune ridge separating the two lakes. Aerial photograph from Norm Deam.

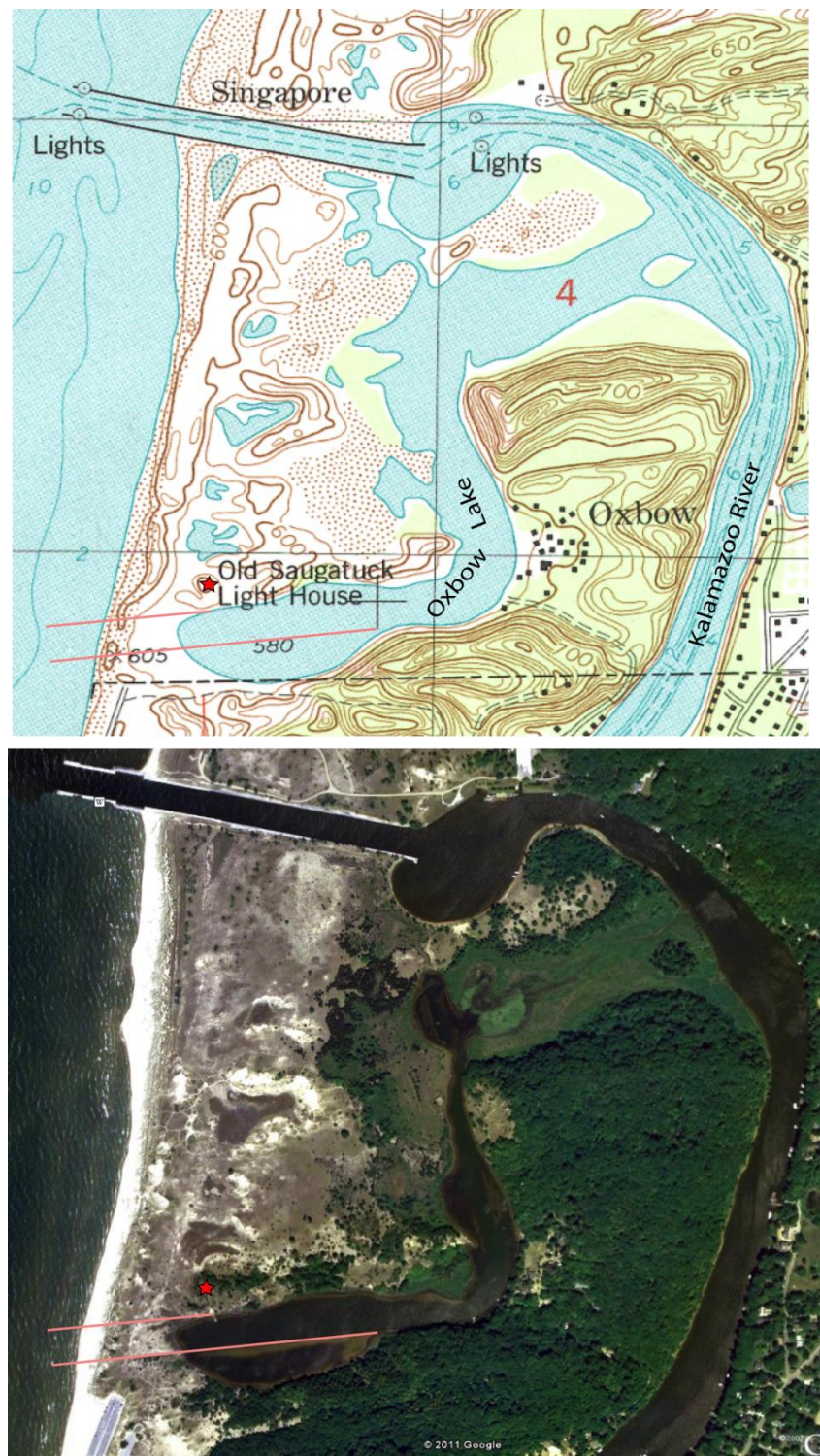


Figure 1-7 7.5 minute Saugatuck quadrangle map (1981) and corresponding satellite image (2010) courtesy of Google Earth™. Red star shows position of Old Saugatuck Lighthouse and pink lines show historic channel for reference.

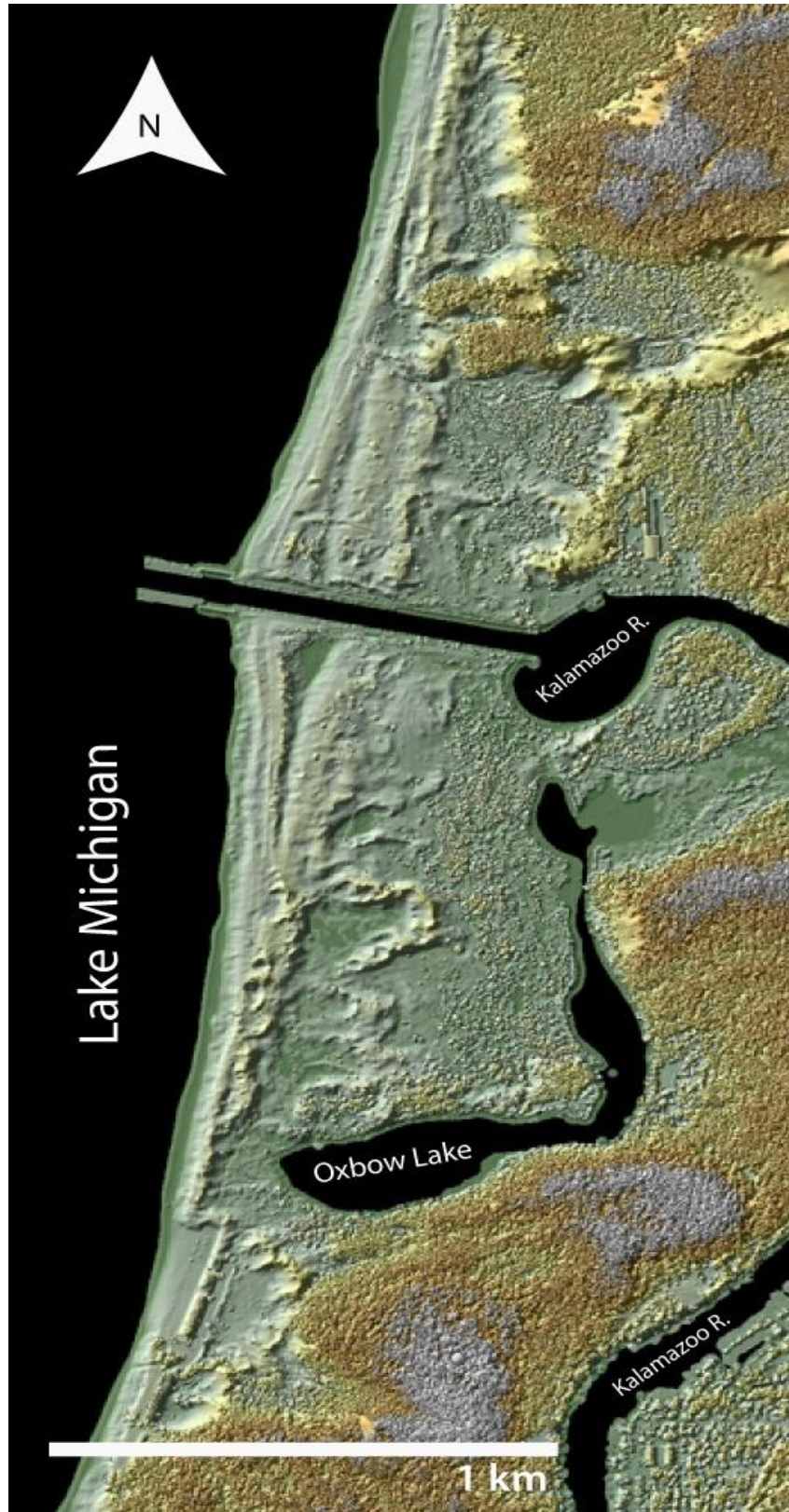


Figure 1-8 LIDAR hillshade of Oxbow Lake, study site, and surrounding area.

1.5 Hypothesis and Objectives

The purpose of this research is to determine whether there are correlations between climate and dune activity. This hypothesis is testable using sediment cores from Oxbow Lake correlated with climatic conditions for the last 100 years. The first objective is to find correlations between climate and eolian activity on cores with well constrained chronologies, and to apply those findings to analogous research of sand signals from sediment cores dating from the mid-Holocene to present. A second objective is to create a modern analog of coastal processes at the study site using ground penetrating radar and historical photographs to document coastal change for the last 100 years, and reconstruct the stages of infilling.

The working hypothesis is that eolian sand concentrations in the sediment cores (sand signals) from Oxbow Lake will correlate with trends in climate (drought [aridity], storminess [high winds that precede precipitation], and high lake level [leading cause in dune de-vegetation]) through time. The importance of this study is the direct comparison between sedimentologic records and known climate variables, a uniformitarianism approach to understanding paleo-coastal dune activity. The second hypothesis is that historical photographs, dated core lithology, climate records, and ground penetrating radar can be cross-referenced, and used to reconstruct the process of infilling of a channel mouth within the time of photographic evidence to model processes along the Lake Michigan coastline.

Chapter 2

Methodology

2.1 Introduction

This chapter summarizes the steps taken to attain data, including the retrieval of cores, processing and sampling of cores, and procedures used to examine the cores. The steps taken to acquire and process ground penetrating radar data are also explained. Methodology of ground penetrating radar used to image subsurface accretionary features of the channel mouth and subsequent dune formations are covered.

2.2 Historical Data

Historical data for this study was gathered with the aid of residents from the area including the owner of the Old Lighthouse, Norm Deam, and the contributions of the Saugatuck Douglas Historical Society. These contributions include historical maps, photographs, newspaper clips, and anecdotes from locals and historians on the closing of the Kalamazoo River mouth. Data from the U.S. Army Corps of Engineers (USACE) was used on currents and sand load transported via long shore transport.

2.3 Sediment Cores

Sediment cores were taken from Oxbow Lake in both winter and summer using Glew and Livingstone coring devices. A modified Livingstone square-rod corer with a two inch diameter steel barrel (Wright, 1984) was used to collect sediment cores at one-meter intervals. The Livingstone corer was chosen for its ability to collect the uppermost sediment with relatively minimal disruption, as well as to take multiple deeper thrusts to retrieve a deeper stratigraphy. After retrieval, the cores OL-L1-1 and OL-L1-2 were described and logged.

Cores have the following labeling system: Lake Name - Type of core & Core number - Thrust number. An example: OL-L1-1 stands for Oxbow Lake– Livingstone Core #1– Thrust 1. Glew cores lack thrusts; they only penetrate the sediment once. Core locations were recorded using a Garmin handheld GPS unit. Optimal locations were determined to be in the deepest portion (center) of Oxbow Lake, and were distributed across the lake in an east-west orientation to capture change in sedimentation with distance from the coastal foredune (Figure 2-1). Winter cores were taken in February 2011 at five places across the lake through lake ice. Four Glew cores and one Livingstone core (2 thrusts) were retrieved. Due to loss of sediment moisture during storage, the Glew cores were not used; however, the Livingstone cores were logged as OL-L1-1 and OL-L1-2. In June 2011, seven Glew cores and three Livingstone cores were retrieved aboard an anchored platform atop two canoes. Due to the soupy nature of the uppermost organic sediment, the Livingstone cores from the summer were not preserved. The six Glew cores, OL-G1 through G6 were brought back to the lab and refrigerated, and G3-D was

sectioned at centimeter intervals on site, placed into Zip-Loc bags, and chilled on ice to preserve the sediment for ^{210}Pb age dating.

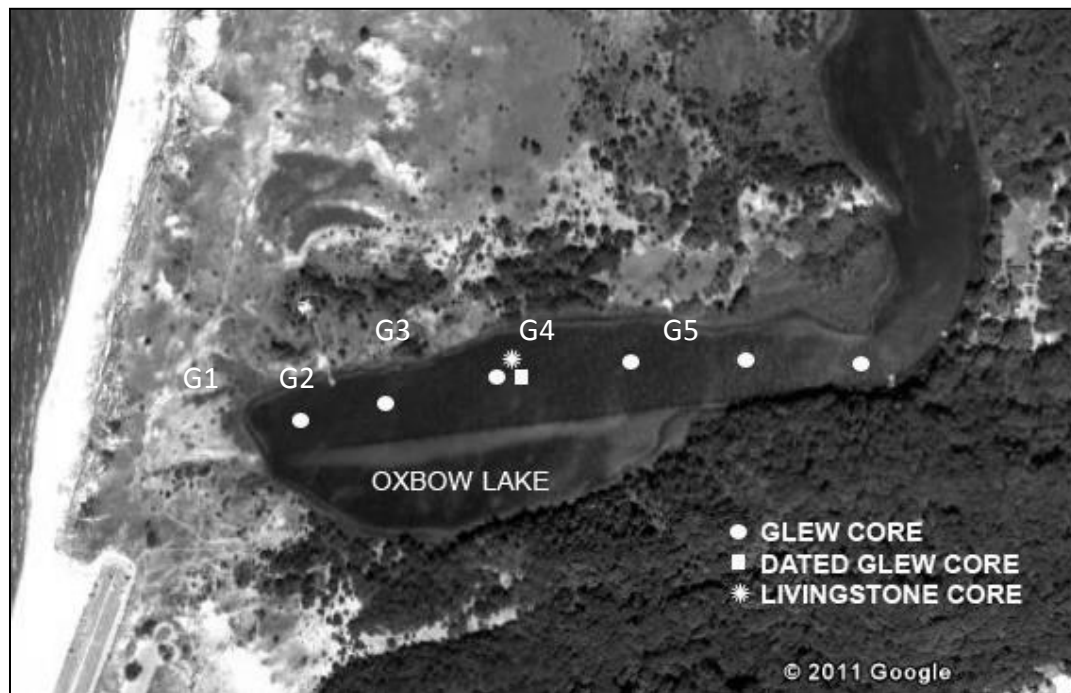


Figure 2-1 Oxbow Lake with locations of Livingstone and Glew cores. Satellite image from Google Earth, 2011.

2.3.1 Core Retrieval

The Glew coring device is used to collect the uppermost sediment while leaving it relatively undisturbed. The Glew corer consists of white plastic tubing, a black rubber ring surrounded by three metal brackets for secure attachment of the coring tube, and a rubber piston that is released at the top of the apparatus to create suction (Figure 2-2). Depending on the depth of the water, rods can be attached to the top of the device to allow for more leverage during deeper core retrieval. During collection, the clear plastic

tube is firmly attached to the Glew corer and is pushed into the sediment, perpendicular to the sediment surface. Water depth is taken, and then the tube is inserted into the sediment and core length is determined by subtracted total depth by depth of water. When the tube ceases downward penetration, or the length of the tube has been filled by sediment, a brass messenger attached to a rope sets the rubber stopper and the suction keeps the sediment in the tube until a water-tight plug is placed in the bottom of the tube and capped. The plug is inserted while the sediment core is underwater to prevent sediment loss.

When the core is out of the water and the bottom capped securely, a small hose is used to siphon off the water to within 1 cm of the sediment surface (Figure 2-3). Methods for preserving water-sediment interfaces were used to stabilize sediment and reduce mixing of the uppermost sediment during transport. Tomkins (2007) devised a method using Zorbitrol® Plus Superabsorbent Polymer, which absorbs all remaining liquid at the water-sediment interface and creates a gelatin. The capacity of Zorbitrol® (sodium polyacrylate) to absorb water was measured as 100 mg for every 25 ml of water, to maintain a thick consistency once water is absorbed. Based on the dimensions of the core tube, the volume of water left inside and the absorptive capacity of Zorbitrol®, 160 mg was calculated to be the minimum amount of sodium polyacrylate needed. To reduce the potential for field use error and maximize stability of the uppermost sediment layer, 200 mg of Zorbitrol® was measured into prepared vials and used before capping cores. Cores were capped, sealed with duct tape, labeled and positioned vertically for storage in a refrigerated area. The positioning of the Glew cores is essential. An upright position must

be maintained at all times or sediment mixing will occur, especially with sediment cores high in water content or low in density.

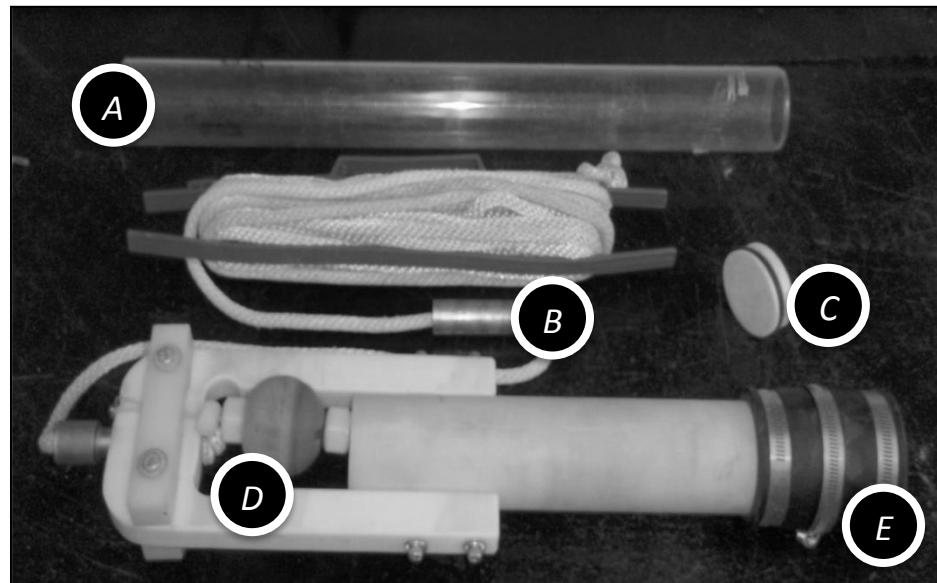


Figure 2-2 Glew coring device and accessories: A) core tube; B) brass messenger; C) watertight plug; D) suction ball; and E) tube attachment.



Figure 2-3 Glew corer with full core (left), water being extracted to 1 cm above sediment (center), and corer in image with thrust rods (right).

2.3.2 Core Processing

Glew cores were sectioned into centimeter discs using equipment shown in Figure 2.4. The watertight plug inserted at the base of the core during collection is used as a guide for the extrusion of the core. Plugs are made of solid discs of plastic and soft rubber outer rings for a watertight seal. When uncapped at the bottom and top, the core is lowered onto a second plug that is used as a plunger. When both plugs are inserted at the base, the core is lowered onto a rod anchored by a platform. The crank-operated lowering device descends one centimeter of the rod for every four full rotations of the handle. The core is pushed downward, stopped by the handle below it, every centimeter after rotating the crank. Once a centimeter of sediment is pushed out of the tube, it is emptied into a petri dish using a wide flat tool to guide it across the stage placed at the top of the core tube. Each petri dish is labeled with the core name and depth, sealed, then refrigerated at 4° C.

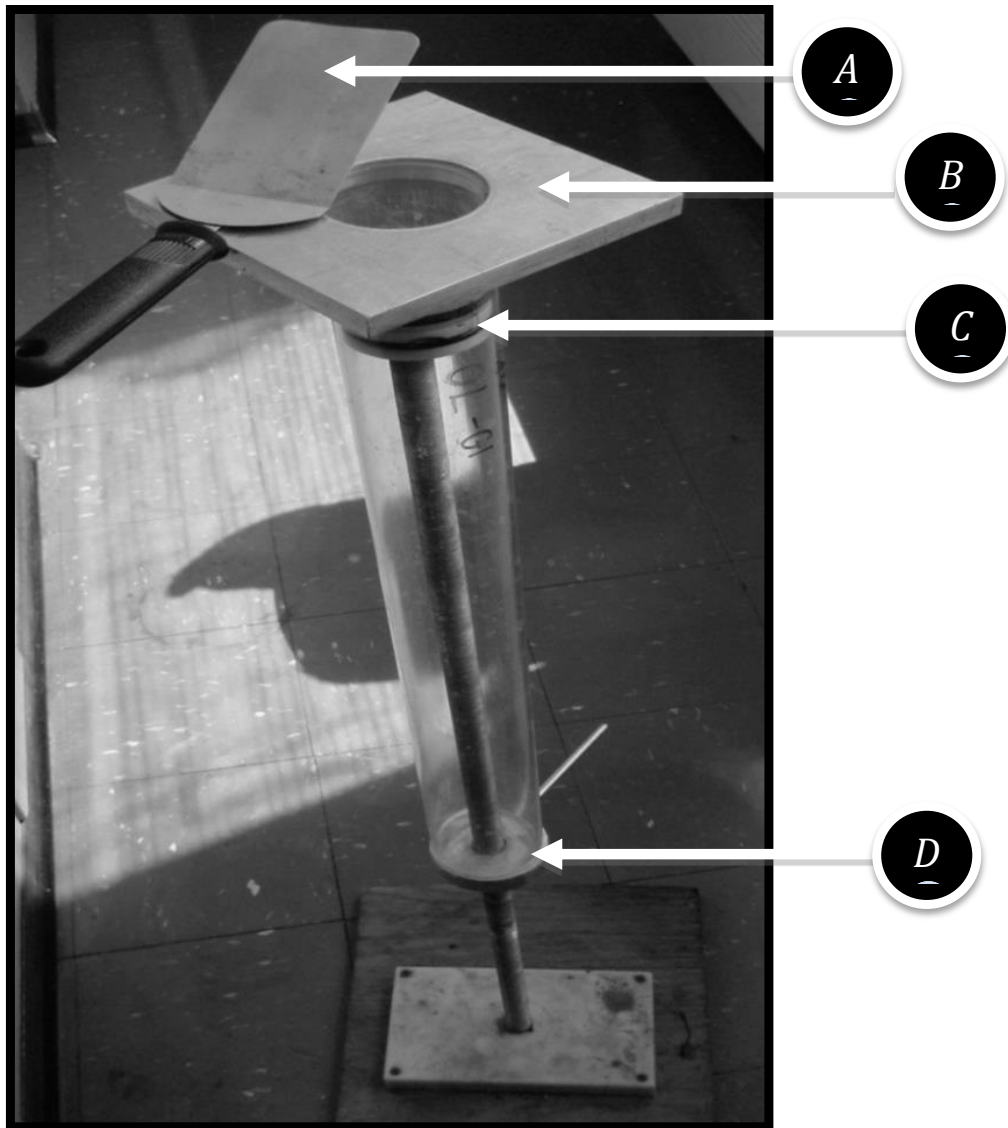


Figure 2-4 Glew core extraction device. A) Spatula for dividing core into centimeter thick discs; B) Stage for catching sediment as it is being extracted; C) core tube plugs for air tight seal as core is being pushed up the tube; D) crank-operated system that allows the core to be extruded centimeter by centimeter.

2.3.3 Core Sampling

The following sections describe sampling of the Glew cores for analysis, including ^{210}PB dating, loss on ignition, percent sand by weight, and grain size analysis.

2.3.3.1 $^{210}\text{Pb}/^{137}\text{Cs}/^7\text{Be}$ Dating

The protocol from Gottgens (1996) was used to process the cores, and is briefly summarized. Following field collection and sectioning of core OL-G3-D, empty crucibles were weighed in the lab and 1 cc of each centimeter section was placed in a crucible and reweighed. Samples were dried at 100° C for 24 hours, and reweighed to record dry sediment weight for calculation of bulk density. The same procedure was followed for samples to be run through the gamma spectrometer. Samples were pulverized using a ceramic mortar and pestle into a fine powder and emptied back into their crucibles for reweighing and subsequent placement into a labeled plastic vial. Note that 2 cc of dried pulverized sample is needed. Filled vials were tapped down to account for compression, and more of the sample was added if it fell below the 2 cc line drawn on the vial. A volume of 2 cc was required to maximize readings, allowing little gamma reabsorption and for all sediment to sit within the germanium crystal. Once complete, the cap was placed on the vials and plastic adhesive was applied lightly to the cap/vial contact to seal the capsule. Prepared samples were stored 21 days to allow the sediment inside to equilibrate radon (^{222}Rn) with radium (^{226}Ra).

The age of sediment for this study is based on the concentrations of ^{210}Pb , ^{214}Pb , ^{214}Bi , ^7Be and ^{137}Cs emitted from each sample over a 24-hour period, under the assumptions of the CRS (constant rate sedimentation) model. ^{210}Pb from within the earth's crust (supported) is a decay product of ^{226}Ra . ^{210}Pb originating from the atmosphere (unsupported) also appears in sediment and must be separated from the supported ^{210}Pb using a set of equations. Isotopes ^{214}Pb (295 and 352 keV) and ^{214}Bi (609 keV) are used to calculate supported ^{210}Pb based on the uranium-series decay products,

and total ^{210}Pb is counted by the gamma spectrometer. The gamma spectrometer counts the number of individual gammas that pass through the germanium crystal for each type of isotope, based on its individual energy signature (Figure 2-5). The germanium crystal is kept cold using liquid nitrogen and shielded from outside gamma background by a virgin lead shield. Results are collected as spectra after gamma signatures are counted, amplified and converted to digital format. Peaks of individual isotopes are delineated to account for noise below the spectral curve and regions of interest on the curve are specified. Once spectra are delineated, both net and gross count values for ^{210}Pb , ^{214}Pb , ^{214}Bi , ^7Be and ^{137}Cs are recorded into a spread sheet which calculates the age of the sediment based on the concentrations of isotopes and daughter products.

The following equations are used in this study (Gottgens, 1996): The activity equation that measures gamma energies of interest [Equation 1].

$$[1] \quad C = (P_c - B_c) / (E \cdot I \cdot t \cdot g)$$

Where C is activity in bq/g, P_c is peak counts, B_c is background counts, E is a measure of efficiency (counts/ γ), I is a measure of intensity (γ /disintegration), t is time, and g equals sample weight in grams.

The second equation is one of Efficiency, E, [Equation 2]. Where A represents the activity of the standard.

$$[2] \quad E = (P_c - B_c) / A \cdot I \cdot t$$

The next step is finding unsupported ^{210}Pb . Total ^{210}Pb activity is determined with [Equation 1] for ^{210}Pb gamma peak (46.5 keV) and Supported ^{210}Pb activity by using [Equation 1] for ^{214}Pb (295 and 352 keV) and ^{214}Bi (609 keV), then subtract Total and Supported ^{210}Pb , for a difference equal to the Unsupported ^{210}Pb activity.



Figure 2-5 Intrinsic Germanium Well model Gamma Spectrometer (left) used to date sediment from core OL-G3-D to create a dated sedimentation chronology.

The same procedure is followed to calculate the activity of ^{137}Cs (662 keV) using [Equation 1]. ^{137}Cs is used as a dating marker for the years 1959-60 A.D. and 1963-64 A.D., when significant nuclear weapons testing occurred, the fallout from which shows up in sediment of that time period. With a half-life of 53 days, ^7Be (477 keV) was used as age control on the uppermost sediment. The short half-life of ^7Be makes it a good dating isotope for the uppermost sediment; in turn, the presence of ^7Be indicates the uppermost sediment was preserved.

The calculation of ^{210}Pb dates was done in three stages (Gottgens, 1996), starting with finding cumulative residual unsupported ^{210}Pb , A_t , below sediments of age t [Equation 3],

$$[3] \quad A_t = A_0 e^{-kt}$$

where A_0 is total unsupported ^{210}Pb (bq/cm^2), and k represents the radioactive decay constant for ^{210}Pb (0.03114 yr^{-1}). The age of sediment at a given depth is calculated using [Equation 4],

$$[4] \quad t = (1/k) \cdot \ln(A_0/A_t)$$

To calculate sedimentation rate, r ($\text{g}/\text{cm}^2 \text{ yr}$), [Equation 5] was used, where C is the concentration of unsupported ^{210}Pb (bq/g).

$$[5] \quad r = (k \cdot A_t) / C$$

Results of this three-step calculation are recorded in years to depth for further use in relating sedimentation to age.

The following methods and explanations for calculating error are from Gottgens et al. (1998). Gamma emission counts follow a Poisson distribution, allowing for standard deviation to be determined using the square root of the mean of the count values. Therefore, larger sample size or longer count time can reduce error associated with the method. Radionuclide activity, bq/g , is expressed as \pm one standard deviation (68.3% confidence limits) from the mean; this includes total, supported and unsupported ^{210}Pb . Counting errors in the calculation of net isotope activities can be estimated using the square root of the sum of the variance of the gross and background count rates. Error associated with the Constant Rate Sedimentation (CRS) model using ^{210}Pb for age-dating

and sedimentation rate was calculated using a Monte Carlo simulation. Normal distribution with the mean equal to measured activity and range equal to that of the counting error are used to simulate a probability density function for radionuclide activity. Values for the isotope activities are randomly chosen from this distribution and carried through the calculations of predicted age and sedimentation rate. After a large number of iterations, a distribution of predicted values results, representing combined uncertainty.

2.3.3.2 Loss on Ignition

Procedures used for loss on ignition (LOI) are outlined by Heiri (2001), and discussed in this section. LOI was calculated for each centimeter of all six Glew cores. Testing was done one core at a time. Labeled empty crucibles were dried and weighed. A volume of 1 cc of sediment was used from each centimeter section from cores G1–G6, and placed into individual crucibles. These samples were weighed in the crucibles, and then subtracted from the empty crucible weight for a wet sediment weight. Wet samples were dried in an oven at 100°C for 24 hours, and then reweighed after cooling to attain a dry weight for the sediment. Water content was calculated by subtracting wet and dry sediment values. Organic matter in the sediment was burned off at 550°C for 4 hours, followed by reweighing after time for cooling is allowed. The burning off of carbonates was achieved by placing samples in the oven at 950°C for 2 hours, and then weighed for a final weight free of carbonates and organics.

The percentage of organic and carbonate matter lost on ignition were calculated using Eq. 6 and Eq. 7, respectively (Heiri, 2001).

$$[6] \quad LOI_{550} = ((DW_{100} - DW_{550}) / DW_{100}) * 100$$

$$[7] \quad LOI_{950} = ((DW_{100} - DW_{950}) / DW_{100}) * 100$$

LOI_{550} and LOI_{950} represent the percentage of weight lost at 550 and 950°C respectively from the original dry weight (100°C). DW is the dry weight measured at the subscripted temperatures of 100, 550 and 950°C.

2.3.3.3 Particle Size Analysis

Approximately 1 cc of sample for every five centimeters or ten centimeters (20, 25, 30, 35, 45, 50, 60, 70, 80, 90, 100, 110, 120, 130, 140, 150) were placed into 50 ml plastic centrifuge tubes. Depths were chosen based on the concentration of visible sand, and the variability of the sedimentology where the samples were taken. The cores were comprised entirely of clean sand below 70 cm.

Organic matter was removed using a 30 percent solution of hydrogen peroxide, added slowly until the reaction ceased. The dispersant, sodium hexametaphosphate was added to the samples, stirred and left to sit overnight. Before running samples the following day, it was agitated once more using a tabletop stirring device.



Figure 2-6 A) Mastersizer 2000 and B) dispersal attachment for small volume samples shown.

To determine the particle size distribution (percent by volume) of terrestrial sediment for all centimeter sections of the Glew cores retrieved, a Malvern Mastersizer 2000 and Malvern dispersion unit for small sediment samples (Figure 2-6) was used. The dispersion unit was set to 2800 rpm to effectively distribute the sandy sediment, and the system was flushed using distilled water between samples. To begin, backgrounds for clean water were read and sample added slowly to allow for even distribution and checked to make sure enough sample had been added. Sample data from the Mastersizer 2000 is expressed as percent by volume value that was exported in Wentworth, USDA, and ASTM formats. Samples were repeated twice and results averaged for each centimeter section. Wentworth format for grain size distribution data was used for further analyses.

2.3.3.4 Percent Sand by Weight

Percent sand by weight was determined as a means for comparison with LOI in order to be unbiased when correlating Glew G1, G2, G4, and G5 cores to the dated core, G3. Similarities between cores resulted in the use of dated core G3 to date all the rest of the Glew cores comparatively. Different methods leading to the same end result (silica left over) were used as a means for gauging concentration of sand in each centimeter. Empty crucibles were dried and weighed. Sediment was taken from each petri dish section of cores G1-G6, and placed into individual crucibles. Samples were weighed in the crucibles, and values subtracted from the crucible weight for a wet-sediment weight. Wet samples were dried in an oven at 100°C for 24 hours, and reweighed after cooling for a dry sediment weight. Water content was calculated by subtracting wet and dry sediment values.

Organic matter in the sediment was burned off at 550°C for 4 hours, and then reweighed after cooling. Carbonate in the sediment was removed using ten percent concentration hydrochloric acid (HCl), which was added slowly as needed until the reaction ceased. Once there was no reaction the crucibles were filled with water and covered until all sediment had settled to the bottom. Water was siphoned off the top until most water was removed from the crucibles without disturbing the sediment, dried at 100°C for 24 hours, and then weighed for a weight free of carbonates and organics.

The final step was to run the sediment through a 63- μm sediment sieve to remove all sediment smaller than sand based on the Wentworth sediment grain size scale, and weigh the final product. Percent sand was then calculated using total dry sediment weight and final dry sediment weight.

2.4 Aligning Sand Percent Data

Correlations of sand percent were based on core OL-G3, which was age-dated using ^{210}Pb , ^{137}Cs , and ^7Be isotopes. The ages were used to assign dates to the other four cores from Oxbow Lake in three ways. Sand percent values were plotted against time on a scatter plot with a moving average line applied to illustrate trends for the sand percent points.

2.4.1 Comparison of LOI_{Organic} Trends

LOI values were determined for the cores OL-G1 through G5 at centimeter intervals. The trends were plotted on a scatter plot. Specific patterns of variability in LOI values for all cores were observed. Ubiquitous LOI trends were used as time markers to correlate the absolute ages of OL-G3 to the rest of the cores. Depth values for the LOI data set were used to identify sand percentages of equal depth for the corresponding cores. A timeline was created from 1929 to 2011, and sand percent values corresponding to marker years were placed along it. The remaining sand percentage values were evenly distributed between the key years. This method assumes variability in sedimentation rate throughout the lake. A source for error in this method is the different rates of decomposition of organics across the lake based on oxygen content, depth and temperature. The lake depth was not highly variable, reducing this error.

2.4.2 Constant Sedimentation Rate

The organic-rich silt unit was age-dated from OL-G3. The age spans from 1943 to 2011 and acts as an age bracket for the undated cores. The variable unit thickness was divided by 68 years to determine a constant sedimentation rate with the results for each core plotted on one graph. A constant sedimentation rate was assumed for this method.

2.4.3 Aligning of Sand Percent Trends

This direct correlation method matches corresponding sand percent variability (wiggles), of OL-G3 through time with the undated cores. Ages were assigned to peaks and valleys on OL-G3, and transferred to the corresponding highs and lows on all other cores. A timeline from 1934 (last years with a marker) to 2011 was set and the sand percent values for cores OL-G1 to OL-G5 marker years were placed along it. The sand percent values between the marker years were evenly distributed based on the span of years and the number of values occurring in that time. This method assumes a variable sedimentation rate of sand through time.

2.5 Correlating Sand Percent & Climate

Correlations between sand percent and climate data were completed using simple Pearson's correlations in Microsoft Excel. Sand percent values were compared annually

to wind, lake level, precipitation, temperature, evaporation, and Palmer Drought Severity Index (PDSI). Each core, G1-G5, differs in sand concentrations with depth. Thus, each core has different trends that were correlated individually to each of the aforementioned climate data sets. Off-setting data by varying numbers of years was not possible in these tests due to the nature of the sand percent data used. There were not sand percentage assigned to every year and so there are gaps in time between values of sand percentages. Only climate variables for those specific years were used as well; for this reason problems of autocorrelation are not likely. Regressions were run to determine if the correlations were significant. Unless otherwise noted, distributions of sand and climate data are assumed to have a normal distribution.

Wind data obtained through the USACE, thanks to personal communication with Robert Jensen, was correlated using cumulative hours per year above 6.5 m/s for wind station data 1979-2009, and above 7 m/s for older data from 1956-1997. The threshold of wind speed for moving eolian sand at an elevation of 10 m (height of dunes) between 1956 and 2009 was determined using equation $V_z = 5.75 V^* \log(z/k)$ from Bagnold (1941), assuming that wind velocities of 5 m/s moves sand at 1 m height. Wind speed calculated to move sand at 10 m elevation was 6.4 m/s. The data spanning 1979-1997 was recorded to 0.1 m/s, and the data from 1956-1997 was rounded to the nearest whole number. Therefore, 6.5 m/s was used for correlations from 1979-2009, and 7 m/s was used between 1956 and 1997. Another facet of the wind correlation was cumulative annual hours and cumulative fall and winter hours blowing above 6.5 or 7 m/s between the NW and SW directions. Wind direction was chosen based on wind rose data from the USACE and continuing coastal dune research done by Deanna van Dijk on the

southeastern coasts of Lake Michigan. She found the strongest winds blow in fall and winter, and in those seasons the predominant wind direction is SW (225°) to NW (315°) (Deanna van Dijk personal communication, 2011). Wind data was organized into different subsets to compare to sand signals through time. These subsets consisted of: cumulative annual hours of wind above 6.5 or 7 m/s (based on the station used), cumulative annual hours of wind above 10 m/s, the ratio of winter and fall hours to annual hours of winds 6.5 m/s or stronger, and cumulative annual hours offset by one year with respect to sand signals through time.

Lake level was correlated using average annual lake level of Lake Michigan. Lake level is controlled by prolonged change in climatic factors. To have a large change in lake level would signify a long-term change in various factors in the environment such as precipitation, temperature, evaporation (wind + temperature), and drought (precipitation + evaporation). The annual average lake level was used to show the integrated yearly trends in climate and their relationship to annual trends in sand concentrations.

The Palmer Drought Severity Index is a measure of drought developed in the 1960s. The index is calculated from precipitation and temperature data; index values of -4.0 or lower represents extreme drought conditions, and values of +4.0 or higher indicate extremely wet conditions (Alley, 1985). PDSI was correlated to sand percent to determine if there is any relationship between dune activity and aridity of the region.

Lake Michigan buoy and South Haven temperature and precipitation data, as well as buoy evaporation data were correlated with annual sand percent. Annual, maximum fall, and maximum summer average evaporation trends (mm) were correlated to sand percent to test for connections between the amount of ground moisture evaporated and

movement of dune sand. High levels of evaporation during fall and summer is likely to lead to dry sand and sand mobility. Dry sand during the summer could lead into the windy fall season allowing for more dune activity; similarly, dry sand in fall and the coming of the windy winter months would have a similar effect.

Both land based and over-lake precipitation (mm) and temperature were correlated to sand percent to see: a) if there is a difference between land based and over-lake precipitation or temperature; and b) to run linear regressions between amount of rainfall or temperature, and the movement of sand into Oxbow Lake. For similar reasons, average summer, fall and winter precipitation/temperature, as well as annual average precipitation/temperature were used. All averages (summer/winter/fall/annual) were correlated to G1-G5 individually to determine if there is a connection between specific seasonal conditions, or annual averages, and sand percentages.

2.6 Ground Penetrating Radar (GPR)

Ground penetrating radar creates cross sectional images of the subsurface, based on the differences in dielectric properties of sediment (Jol, 2003). The reflection profiling mode of ground penetrating radar measures in two-way travel time of a radar signal from the transmitter to the receiver after interacting with the subsurface. Data was collected along six lines covering an area between the westernmost edge of Oxbow Lake and Lake Michigan. Procedures and field methods followed those described by Jol (2003) and Dr. David Krantz of the University of Toledo.

The console, battery and laptop were carried in a large daypack with separate compartments for each with a tray for the laptop, and kept ~5 m from the antennas to

reduce noise. One hundred megahertz antennas running parallel-broadside (Jol, 2003) were separated by a 1 m wide frame and moved in quarter-meter steps to maximize resolution and imaging depths of ~10 m (Figure 2-7). The time interval between measurements was 2 seconds.

Topographic relief was measured using a laser level. Locations of GPR lines were recorded using a GPS in UTM coordinates. Elevations of GPR lines were calculated in reference to Lake Michigan lake level for that day, which was 176.3 m above sea level. GPR data was corrected for elevation using the laser level data and GPS coordinates. Ekko View Deluxe and Corel Draw were then used to process and filter the data, then add topography.



Figure 2-7 Ground penetrating radar in area separating Oxbow Lake from Lake Michigan with 100 MHz antennas. Photograph by Jim Traub.

Chapter 3:

Historical Background & Saugatuck Harbor

3.1 History of the Kalamazoo River at Saugatuck

The town of Saugatuck had its beginnings deeply rooted in the fishing and boating industry. Through time they encountered many difficulties with the meandering and periodically infilling natural Kalamazoo River's final lengths, at times losing vessels to its shallow mouth.

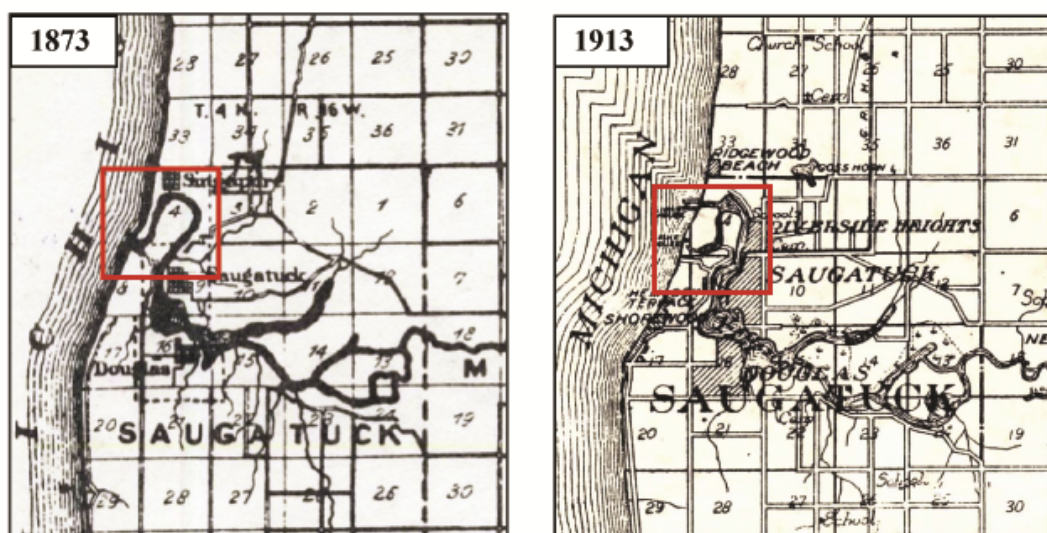


Figure 3-1 Archived maps of Allegan County for the years 1873 and 1913.
Courtesy of: Saugatuck Douglas Historical Society (SDHS)
<http://sdhistoricalsociety.org/SDHSWeb/maps/maps.htm>

HISTORICAL BACKGROUND:

Historical records indicate plans for the construction of a more direct channel a few years before the project was begun in 1904. By 1906 the artificial channel was constructed and in use, proving to be more accommodating to larger ships that could no longer pass through the natural Kalamazoo mouth and the Old Lighthouse was put out of commission. With the Kalamazoo River's water redirected and little to no flow, the natural mouth rapidly infilled. By 1912, the Kalamazoo River had separated from Lake Michigan (Lane, 2006) (Figure 3-1).

Photographic evidence, between the years 1890 and 1920, documents the infilling of the Kalamazoo River mouth (Figure 3-2). In 1905, before the use of the artificial channel, the mouth was open and sediment accumulated only occasionally. Conversation with local historians told of periods of time when the mouth would be deeper or shallower depending on the year, but sand accumulation stayed well below the water surface. Note the small amount of accumulation on the right (north) side of the channel. Approaching the sixth year of the artificial channel (1912), the accumulation of sand in the former river mouth becomes clear on the right side, unfettered by lake-bound water. Upon close inspection of the historical photograph from 1912, it can be assumed that the offshore currents are coming from the north and breaking on the northern jetty and depositing within the mouth on the same side. By 1920 the mouth was completely closed by a barrier bar. With sand accumulation above lake level, the formation of the dunes that now separate Oxbow Lake from Lake Michigan begins.

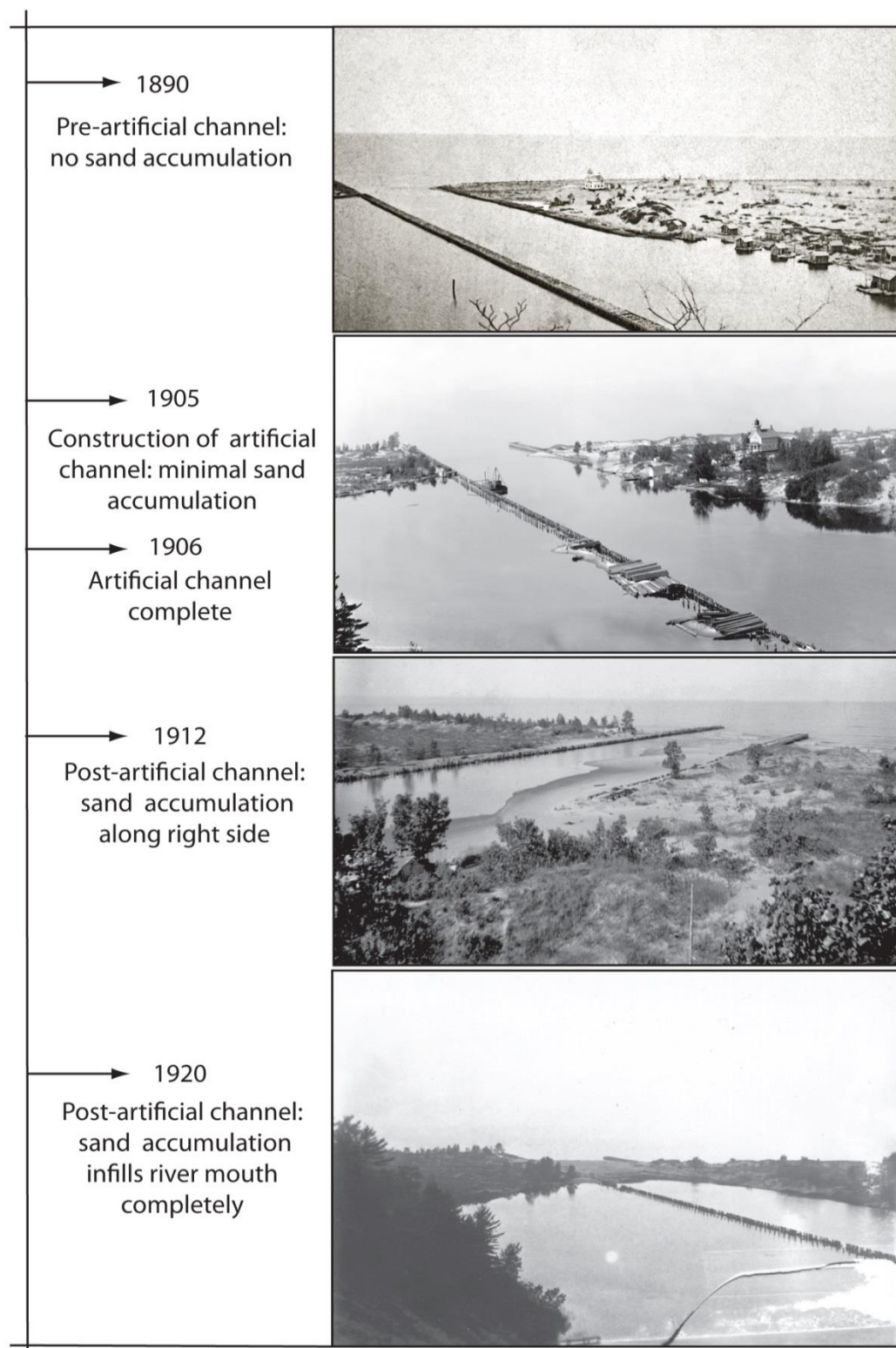


Fig. 3-2 Kalamazoo River mouth, North (right) & South (Left). Photographs/dates by SDHS. Courtesy of: Saugatuck Douglas Historical Society (SDHS)
<http://sdhistoricalsociety.org/SDHSWeb/maps/maps.htm>

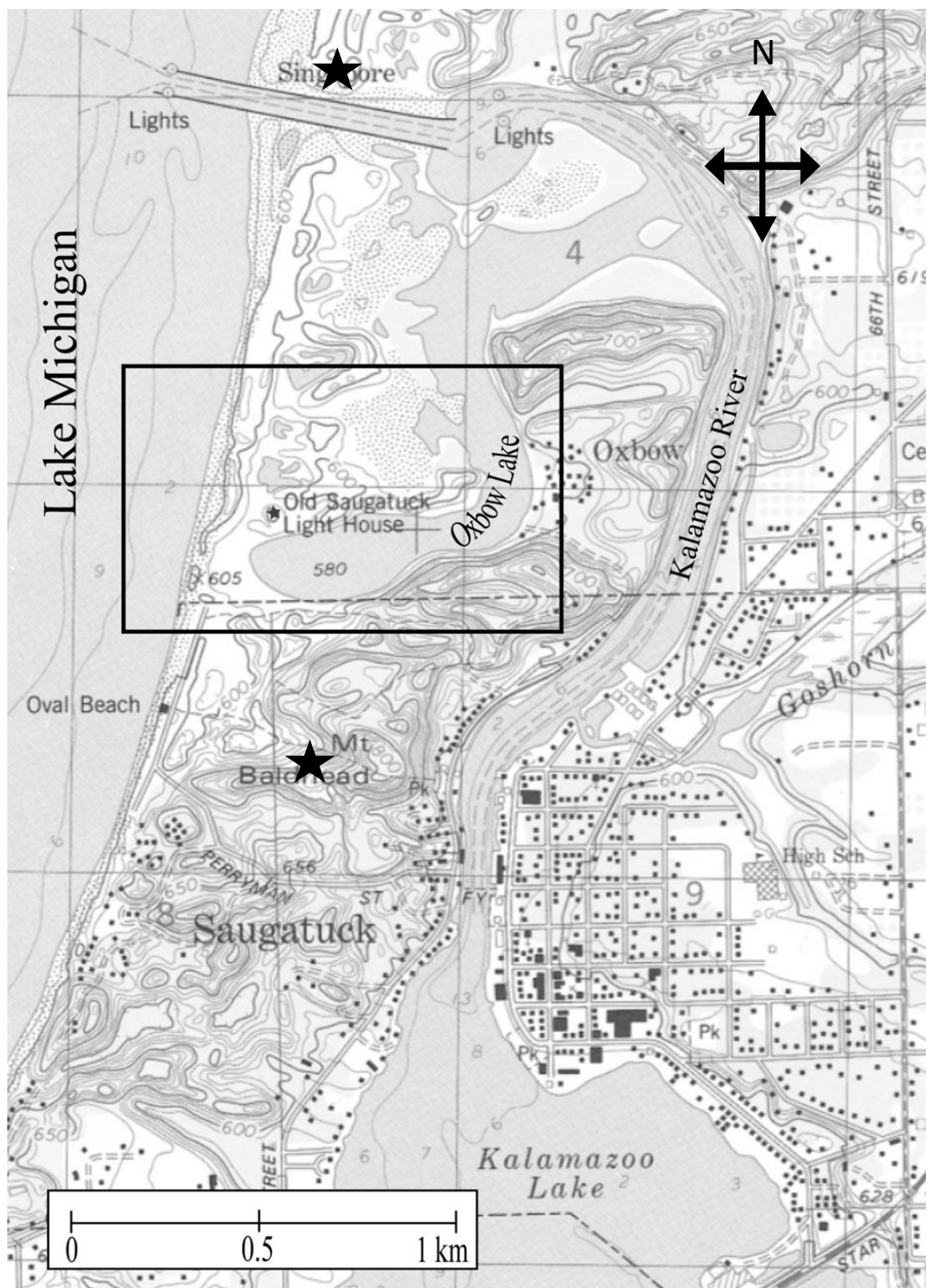


Figure 3-3 Topographic 7.5 minute map of the Saugatuck Quadrangle, Michigan - Allegan County (1981). The square designates the study area. Singapore and Mount Baldhead are marked (stars).

SHIFTING SANDS AND THE CHANGING COAST:

Old newspaper articles, archived by the Saugatuck/Douglas Historical Society, document dune movements in the historical town of Singapore and Mount Baldhead (Figure 3-3). These regions had experience with “shifting sands” as early as 1884, with older reports cited in newspaper articles dating to the early 1800s. Conservation efforts began as early as 1895 using sand fences, and in 1905 to 1932 by using vegetation to stabilize the large Mt. Baldhead dune. The town of Singapore was abandoned and covered by dunes (Lane, 2006). Historical newspaper clippings record sand infilling the Kalamazoo River mouth, and noted it as “shifting sands.” This is interpreted as eolian in origin. At present, land conservancies for the protected dune areas and Oxbow Lake area recognize the importance of vegetative cover on the dunes. Public access is restricted to trails to cut down on degradation of important dune-stabilizing plants, such as dune grass.

Large quantities of littoral sand are transported along the southwestern coast of Michigan via longshore transport. Historical maps and photographs document dunes that formed as barriers along the coast, and that in the last 100 years, sand infilled the mouth of the Kalamazoo River. Historical photographs show progradation of the beach through time in 1890, 1905, 1912, and 1920 (Figure 3-2). The amount of sand transported via longshore transport is reported in the next section, however an inspection of historical maps and photographs concludes that by 1950 the beach and dune system as we know them today were in place and the abandoned channel had become a lake. Progradation of the shoreline and infilling of the river mouth is illustrated in Figure 3-4 (original map: APPENDIX A), spanning the natural Kalamazoo in 1831, after the installation of jetties in 1893, and the near-present state of Oxbow Lake in 1950.

The foredune ridge separating the Lake Michigan coastline from land, between Oxbow Lake and the artificial Kalamazoo River mouth, had developed before 1950 and after the construction of the Old Lighthouse. The Old Lighthouse was constructed in 1859 and in 1867 was 300 feet due east of the Lake Michigan shoreline (Figure 3-5). The mouth of the Kalamazoo River at that time was reinforced by wooden slab piers on the north and south sides of the channel. The jetties constructed in 1893 are shown in Figure 3-6, a map created in 1895. Two years after the installation of jetties, sand had accumulated along the coast against the structures, causing progradation. By 1895 the Old Lighthouse was 700 feet due east of the shoreline; indicating 400 m of progradation in 28 years. By 1905 (Figure 3-6) low foredunes had begun to form.

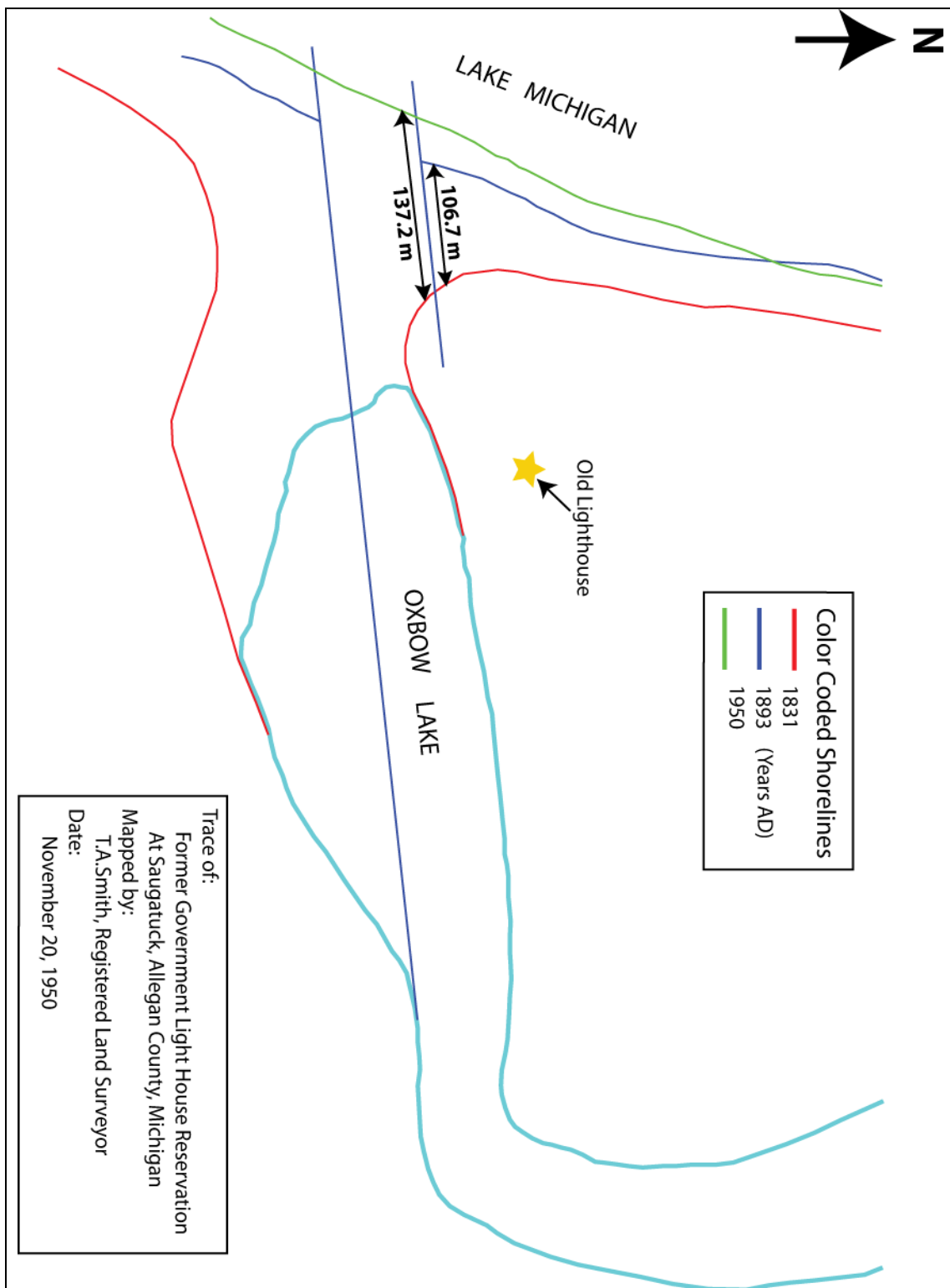


Figure 3-4 Trace of infilled Kalamazoo River mouth and Oxbow Lake coast for years 1831, 1893, and 1950. Jetties are lines running roughly perpendicular to coast in 1893. Map courtesy of Norm Deam, owner of the Old Lighthouse property.

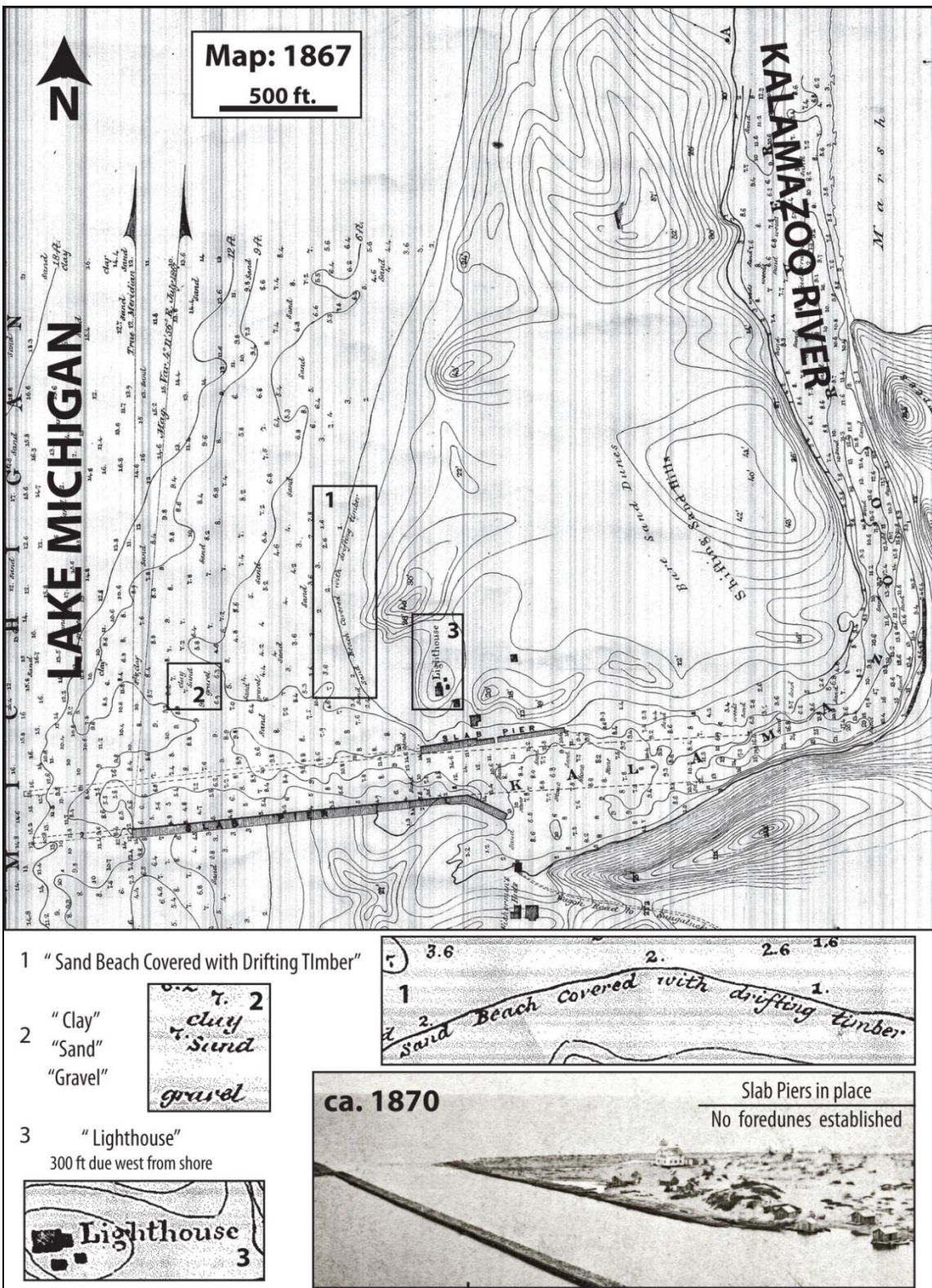


Figure 3-5 1867 map with shoreline of Lake Michigan surrounding the former Kalamazoo River mouth, with key elements numbered below. A photograph shows the coastline as it was during time of map's creation. Map and photograph courtesy of Norm Deam.

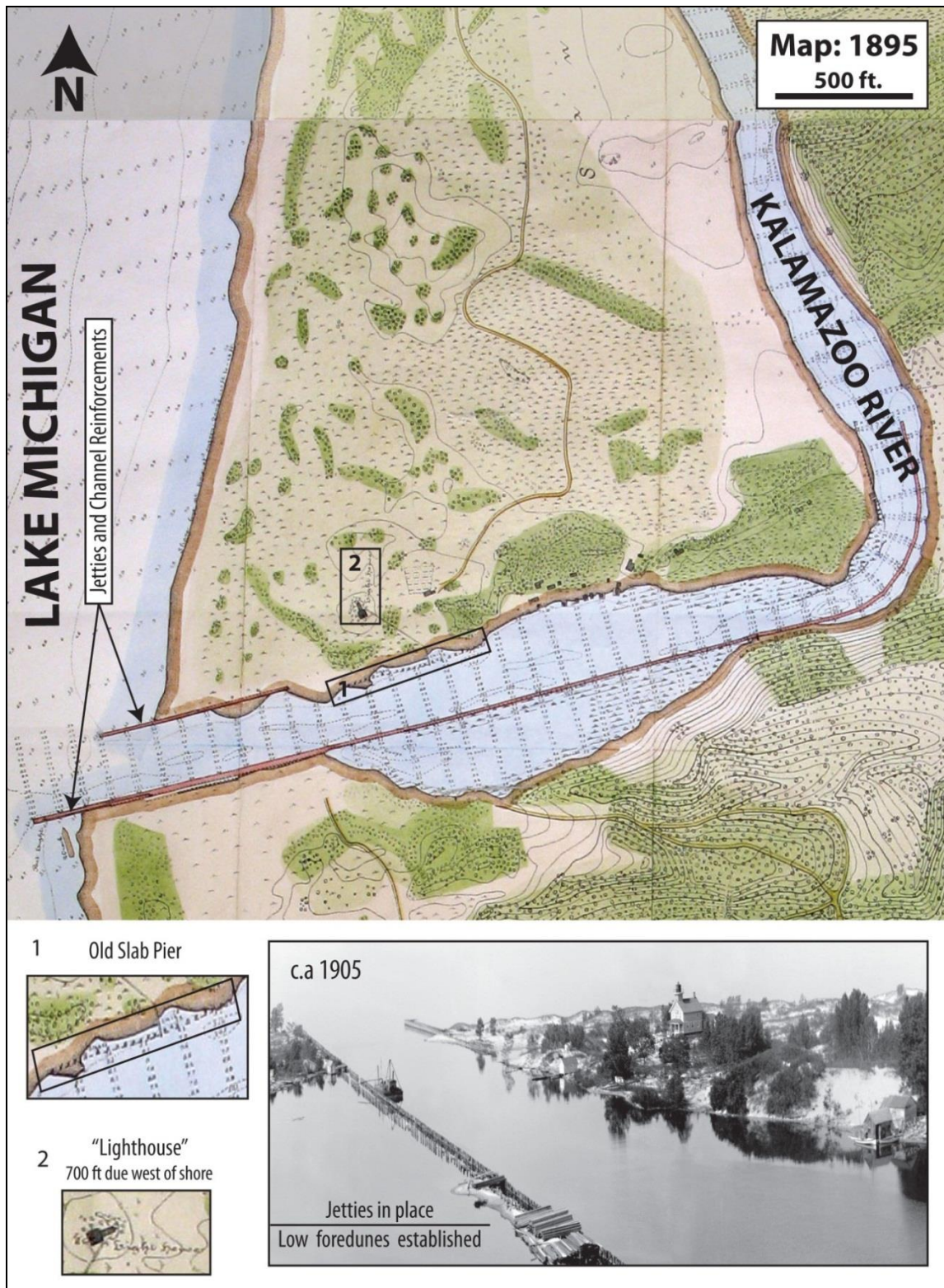


Figure 3-6 1895 map of shoreline of Lake Michigan surrounding the former Kalamazoo River mouth, with key elements numbered below. A photograph shows the coastline as it was during time of map's creation. Map and photograph courtesy of Norm Deam.

NATURAL DISASTERS:

Floods along the Kalamazoo River are reported in the local newspaper, dating back to 1854. Floods occurred in the years 1854, 1855, 1858, 1868, 1869, 1883, 1887, 1896, 1901, 1904, 1908, 1916, 1937, 1947, 1950, and the most recent large flood occurred in 1975. Documentation of tornados at or near Oxbow Lake comes from newspaper clippings, residents' stories, and physical evidence. The town of Saugatuck was affected by a tornado in 1896, then the old lighthouse was demolished by the tornado of 1956 and on its foundation a new building was constructed in its likeness. During this episode, vegetation was uprooted and the dunes destabilized, exposing sand for eolian transport.

3.2 Saugatuck Harbor Research

The U.S. Army Corps of Engineers recorded environmental and climatic changes, as well as sediment transport in the Saugatuck Harbor area in an impact assessment, that is briefly summarized (Baird, USACE). Baird and associates found that dunes surrounding the north and south jetties advanced significantly during the record low lake level of 1955 to 1968, and suggested a relationship between low lake level and dune activation. Observations of peak storm wave direction are from the northwest and west-southwest, with stronger northwest storms on average. Extra Tropical Cyclones (ETC) were found to have east-west periodicity of 10 years and north-south of approximately 30 years (half of a North Atlantic Oscillation period).

Maximums for northward long shore transport (LST) were in 1958 and southward LST in 1992. Northward LST trends were recorded between the years 1956 and 1961.

These trends show a periodicity of approximately 10 years. The average net LST for both north and southward LST is 20,000 m³/yr and 40,000 m³/yr, respectively; where the north shore is not deprived of sand, the south shoreline receives the 55% of the net LST bypassing the jetties amounting to 18,000 m³/yr it should be receiving. All values calculated for long short transport (LST) sediment load are based on availability of sediment from 1904 to 1938.

Values shown in Figure 3-7 are average values for LST sediment load for the 34-year span, between 1904 and 1938. Baird and associates calculated an average southward LST sediment volume of 134,000 m³/yr, of which 64,500 m³/yr bypasses the jetties; 69,500 m³/yr is caught behind the jetties, carried by northward waves to the north shoreline, or deposited in the northern fillet. An average northward LST sediment volume of 115,000 m³/yr was calculated, of which 52,000 m³/yr bypasses the jetties amounting to 63,000 m³/yr caught behind the jetties. Of the 63,000 m³/yr, 46,500 m³/yr are carried by southward waves to the south shoreline, and 14,000 m³/yr is deposited in the southern fillet.

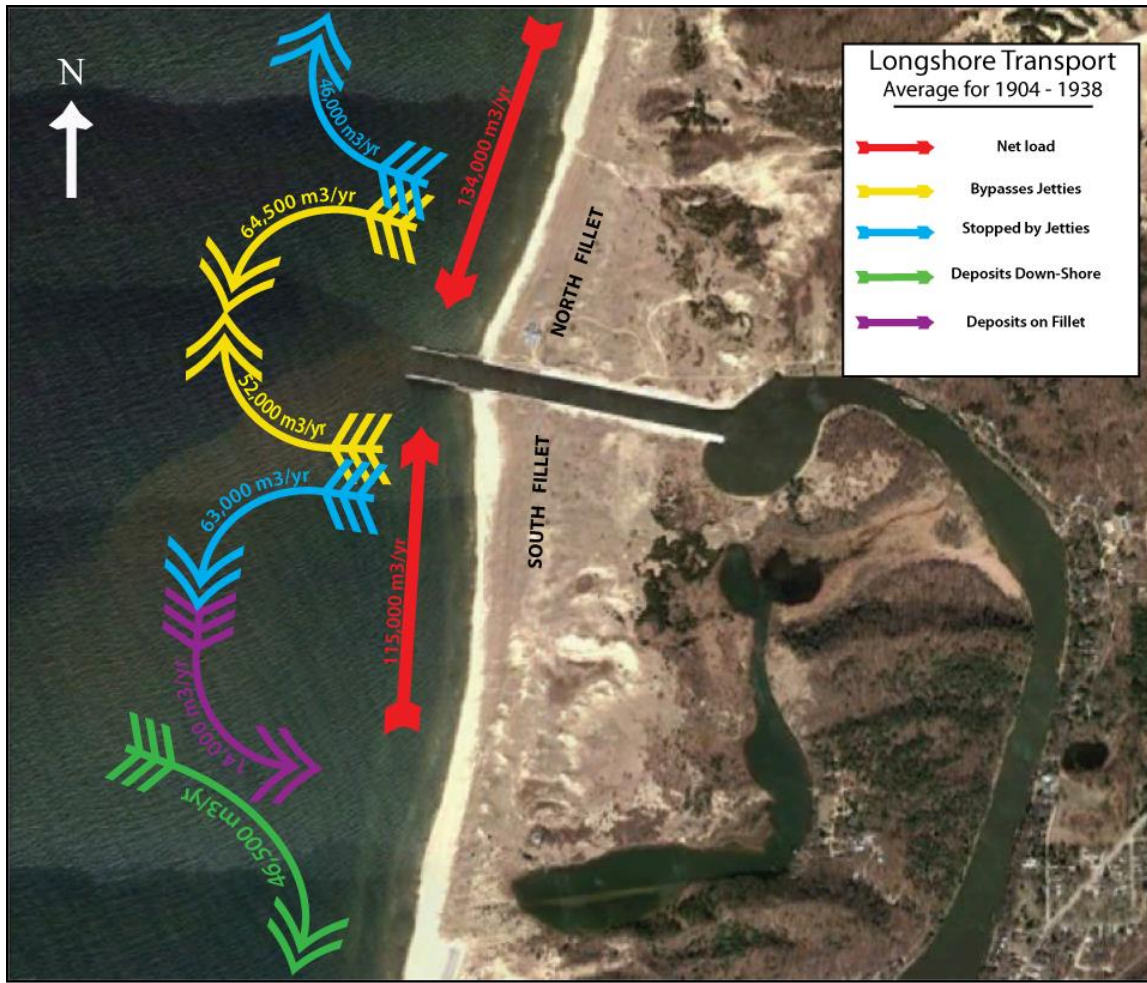


Figure 3-7 Average annual longshore transport volumes at Saugatuck Harbor based on data from Baird, USACE. Black dotted line represents pre-artificial channel coastline.

Chapter 4

Ground Penetrating Radar Results

4.1 Introduction

Ground penetrating radar (GPR) results and interpretations are presented in the interpretations, black lines highlight major reflections and colored regions highlight packages of sediment assumed to represent common depositional environments. Transect locations were chosen to image the outline and infilling of the abandoned Kalamazoo R. channel (lines 1-4), the structure of the current dune ridge (line 5), and more recent beach structures (line 6) (Table 4.1).

4.2 Ground Penetrating Radar Results

GPR LINE SAUG-01

GPR line SAUG-01 is a 244 m profile, running south to north across low-relief dunes in the infilled region of the old Kalamazoo River mouth that was collected north of Oval Beach (Saugatuck, Michigan) (Figures 4-1 and 4-2). The line runs perpendicular to the old channel, extending beyond the preexisting river mouth on both sides. Line

SAUG-01 is approximately parallel with the Lake Michigan shoreline and the dune ridge immediately to the west.

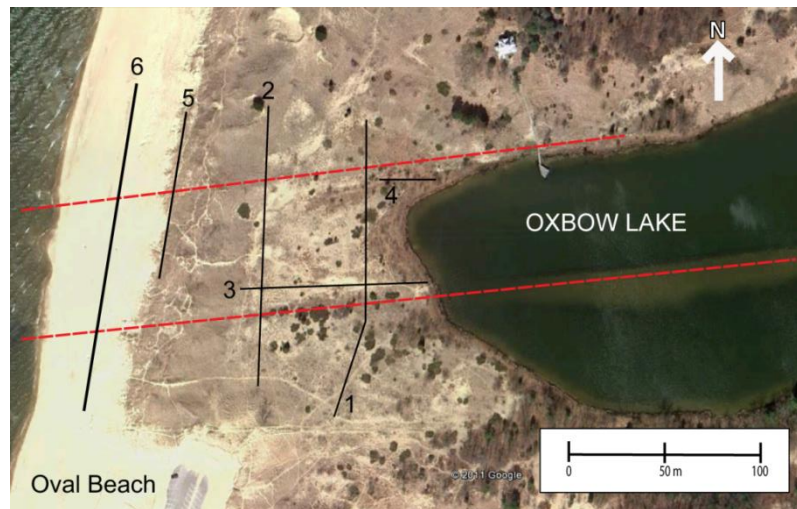


Figure 4-1 GPR line (black lines) and approximate pier locations (red dashed lines). Satellite image of Oval Beach and study site from Google Earth, 2011.

Table 4.1 GPR lines: location, direction run and length

Ground Penetrating Radar Locations, Lengths and Directions				
Line	Start UTM	End UTM	Length	Run
1 (A)	16T 0564399m E 4723886m N	16T 0564440m E 4724102m N	247	S to N
2 (B)	16T 0564444m E 4724149m N	16T 0564358m E 4722934m N	242	N to S
3 (C)	16T 0564361m E 4724001m N	16T 0564472m E 4724002m N	111	W to E
4 (D)	16T 0564378m E 4724060m N	16T 0564450m E 4724053m N	73	W to E
5 (E)	16T 0564343m E 4724063m N	16T 0564317m E 4723965m N	96	N to S
6 (F)	16T 0564288m E 4724210m N	16T 0564265m E 4723931m N	280	N to S

Prominent reflections are highlighted with black lines, and nearly continuous reflections are used as boundaries for the various color-coded sediment packages. These reflections show widely varied geometries in an older sediment package (paleo-sediment); elevations for sediment are below 177 m. Strong reflections are recorded down to 170-172 m elevation where the signal fades quickly. A weak reflection at 167 m elevation suggests a boundary between two units and the curved portion of the older sediment, unit A, has a lower transparent appearance and an upper unit, unit B, has both continuous and discontinuous undulating reflections. The top of unit 1B is marked by a strong continuous reflection appearing to cross-cut reflections of unit 1A. Unit 1B appears to have a channel-like geometry between 100 and 190 m distance, and the overlying reflections at 175-176 m elevation dip toward the channel, and lay parallel to the underlying reflection. The southern portion of unit 2 extends to the south edge of the survey line, but fills the channel cut into unit 1B between 165-190 m distances. The uppermost unit, unit 3, appears to follow the underlying contours of unit 2. The dune that is imaged at the north end of the transect consists of continuous and discontinuous reflections with an apparent dip to the south, and directly overlies unit 1B.

Radar interpretations were aided with the knowledge that the uppermost unit (unit 3) is eolian sand from dunes at the surface, and that GPR transects were run across the infilled river mouth known from historical photographs, maps, and the position of remnant piers from the old channel of the Kalamazoo River. Unit 1B is interpreted as an older surface that the Kalamazoo River may have incised into. The lower, transparent unit 1A may record organic-rich sediment, such as a marsh deposit. Unit 1B may represent older fluvial deposits. Unit 2 is interpreted as a fluvial deposit, and the southern

end may record the former position of the Kalamazoo River before it was narrowed by the installation of wooden piers to the northern side of the channel, causing scouring and deepening of the channel between 100 and 190 m distance along the GPR line. The channel fill of unit 2 will include both fluvial and littoral sediments, especially the dome-shaped deposit and overlying south-dipping packages in the bottom of the channel. The sequence of infill may be recorded in the ca. 1912 photograph in Figure 3-2. Once the channel was infilled, the low-relief dunes of unit 3 formed on its surface.

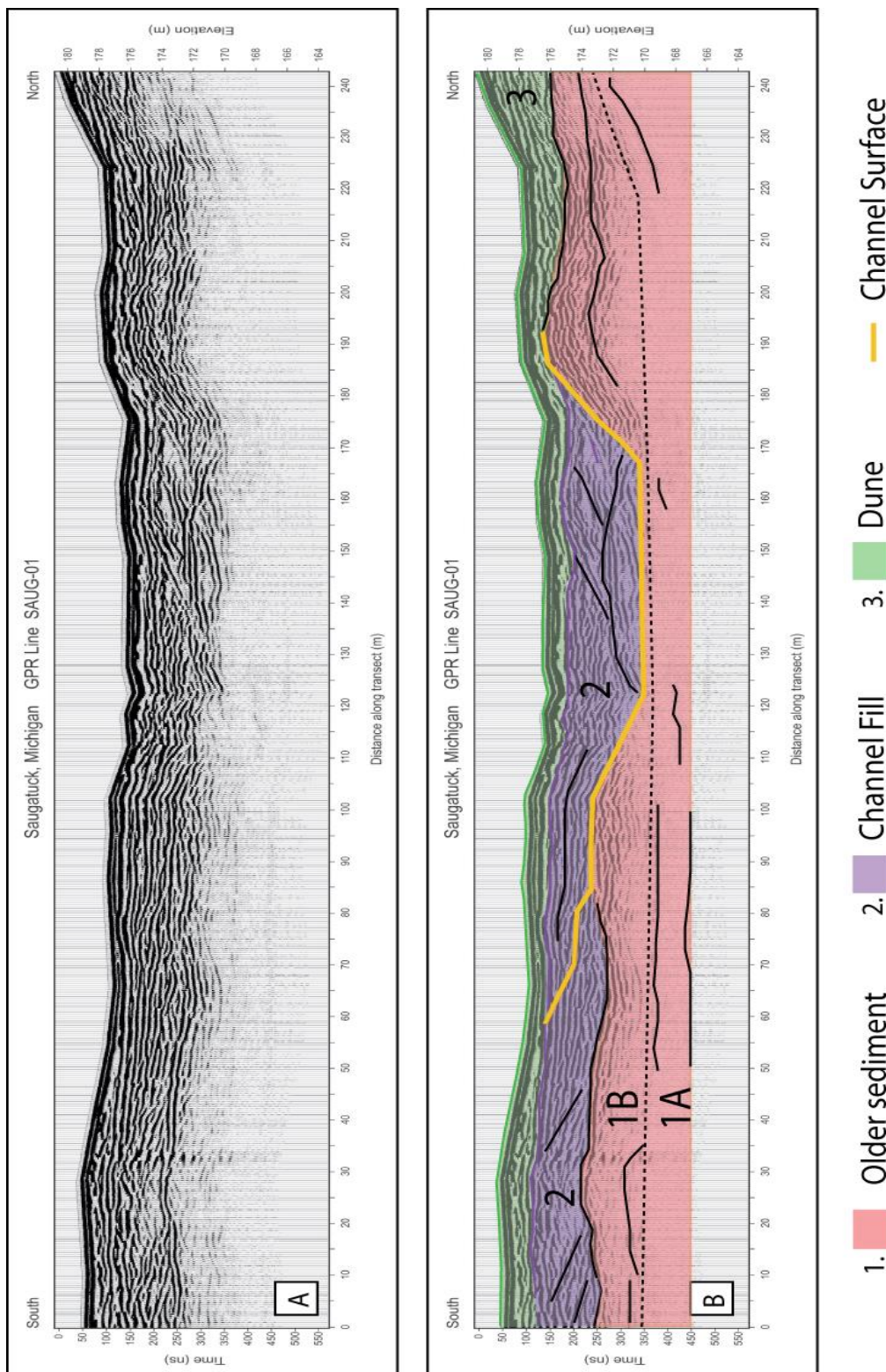


Figure 4-2 The original (A) and interpreted profiles (B) for GPR line SAUG-01 corrected for elevation, oriented south to north, between 25 and 100 m from the western edge of Oxbow Lake (Figure 4.1)

GPR LINE SAUG-02

Line SAUG-02 is a 241 m GPR line (Figure 4-3) that was collected parallel to SAUG-01, approximately 50 m further west (Figure 4-1). The stratigraphy strongly resembles that of SAUG-01, with the same four units (1A, 1B, 2, and 3) identified. The boundary of the channel surface is not as evident and the position of unit 1B between 140 and 200 m distance is uncertain. Due to the proximity of the former Lake Michigan shoreline at the northern edge of this GPR line (indicated by a red line in Figure 3-4), it is reasonable to infer that the northern half of unit 1B and overlying unit 2 are littoral in origin. The portion of unit 2 between 75 and 140 m distance is characterized by short, discontinuous reflections with many concave and inclined reflections. This section of unit 2 is interpreted as channel fill, consisting of mostly littoral sand deposits. The parallel reflections of the south end of unit 2 are also interpreted as littoral in origin. Channel infill is overlain by dune sediment (unit 3) spread evenly over the underlying topography.

GPR LINE SAUG-03

A 111 m GPR line, running west to east across low-relief dunes in the infilled region of the old Kalamazoo River mouth was collected perpendicular to lines SAUG-01 and SAUG-02 (Figures 4-1 and 4-4). The profile is parallel to the old channel, and north of the southern wooden pier (Figure 4-1).

Similar to the other GPR lines, the signal begins to fade at approximately 8 m depth. At this depth, the lower reflections, especially on the west side, are concave to the east. Like the other lines, a faint reflection appears at 166 m elevation. Above the inclined reflections, the stratigraphy consists of low-relief, discontinuous, undulating reflections

until approximately 2 m from the surface; there, the reflections become more continuous and parallel. The top few meters in this transect encompass the local topography, and is interpreted to represent dune sand, the same as the last two interpretations.

The deepest reflections are interpreted as deposits that infilled the mouth of the channel, transitioning to more horizontal beds of littoral sediment as the channel shallowed. Thus, the channel infilled in two stages; the first episodes of infill were migrating bar forms, followed by planar deposits in shallow water. The bars accreted eastward, and were possibly controlled by storm events supplying large packages of littoral sediment.

GPR LINE SAUG-04

A 16 m GPR line, running west to east across a vegetated low area in the infilled region of the old Kalamazoo River mouth, was collected just south of the northern pier (Figures 4-1 and 4-5) and runs parallel to SAUG-03. Numerous sediment packages were evident from this short transect, which closely mirrors the stratigraphy interpreted in the other profiles. Below 170 m there are inclined reflections dipping east, similar to the basal unit in SAUG-03. Between 170-172 m elevations, there are channel infill sediment packages, also similar to those seen in SAUG-03. Above two very strong horizontal reflections are eastward dipping reflections. Parallel reflections around 174 m elevation are interpreted as the dune sequence. The lower three units (1B, 1A, and 2) are interpreted as littoral bars deposited as sand infilled the channel mouth where the Kalamazoo River was cut off, mirroring the channel infill of SAUG-03.

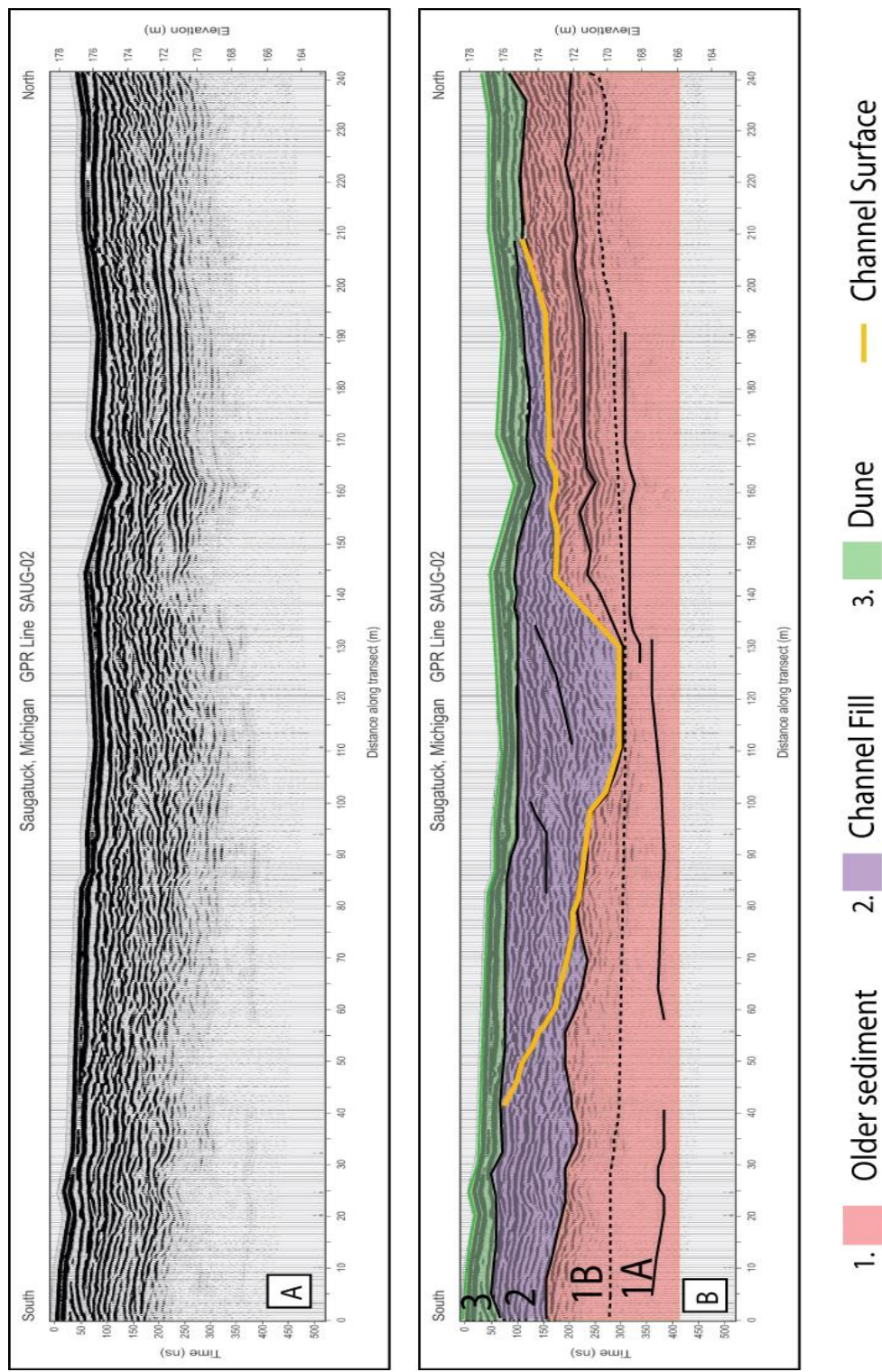
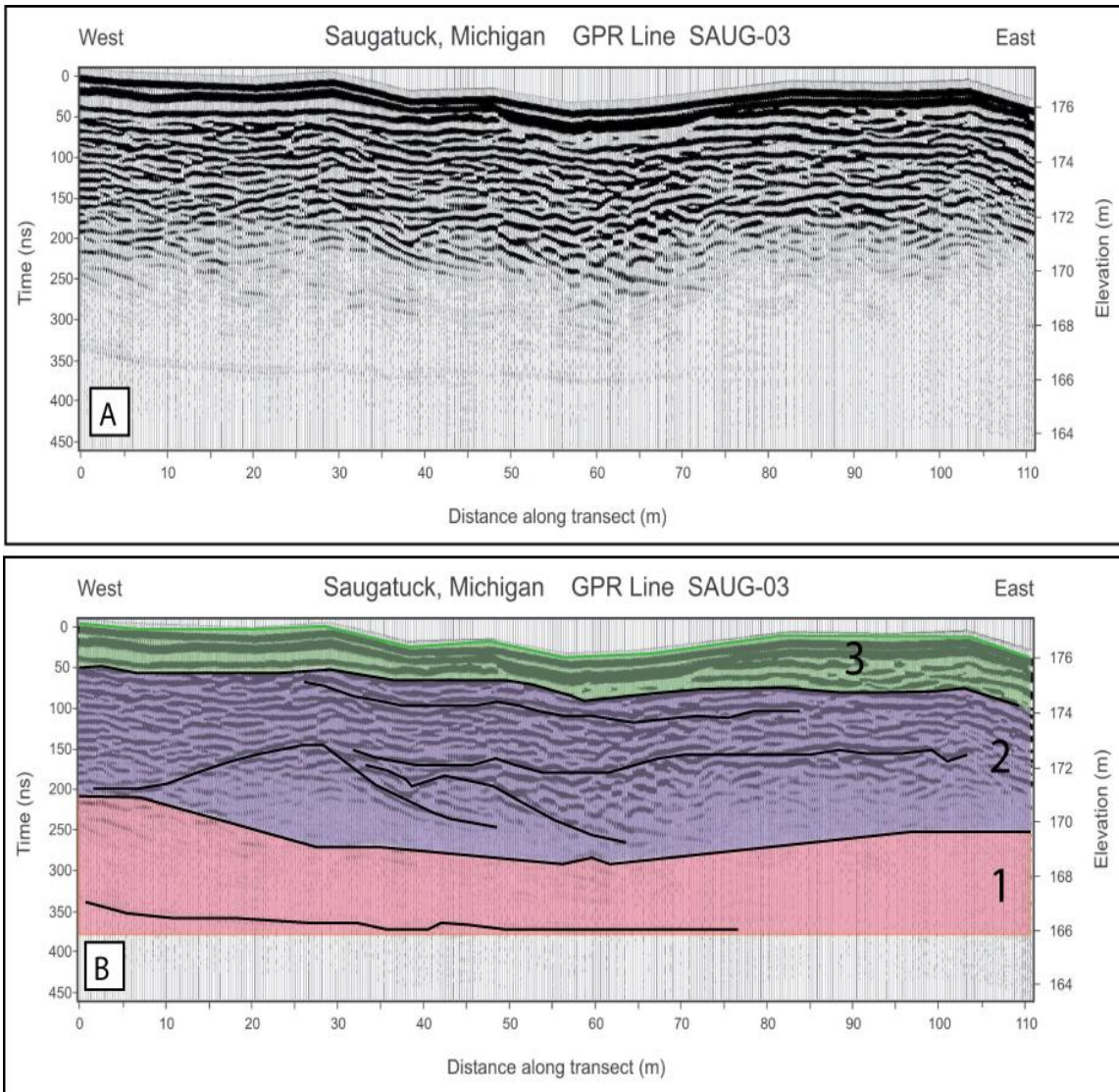


Figure 4-3 The original (A) and interpreted profiles (B) for GPR line SAUG-02 corrected for elevation. This line is between Oxbow Lake and the foredune along Lake Michigan, west of GPR line SAUG-01.



- 1. Older sediment
- 2. Channel Fill
- 3. Dune

Figure 4-4 The original (A) and interpreted profiles (B) for GPR line SAUG-03 corrected for elevation, and oriented west to east. This line was run from the foredune bordering Lake Michigan to the shoreline of Oxbow Lake (Figure 4.1)

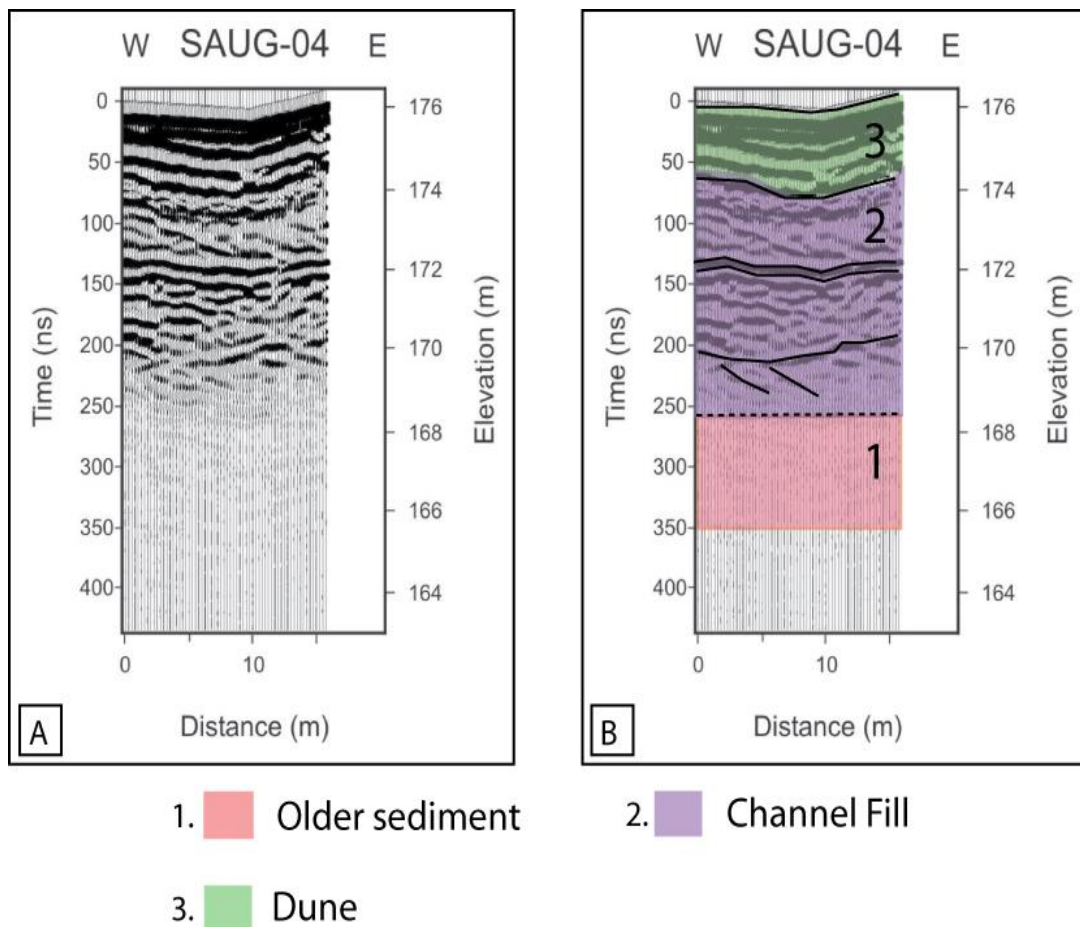


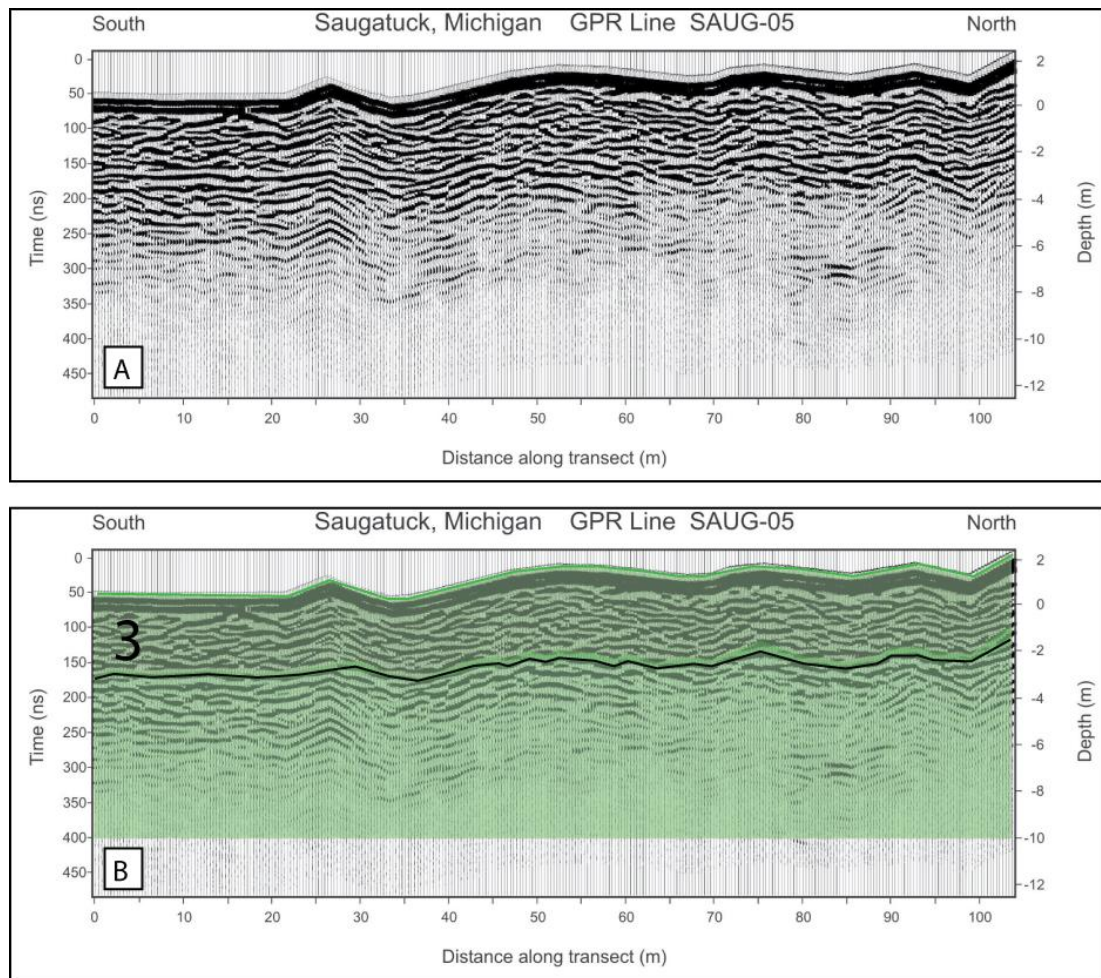
Figure 4-5 The original (A) and interpreted profiles (B) for GPR line SAUG-04 corrected for elevation, oriented west to east. This line was run slightly west of Oxbow Lake, and is the shortest line, at 16 m (Figure 4.1)

GPR LINE SAUG-05

A 104 m GPR line, running south to north along the top of a dune ridge (± 10 m high), dividing the old Kalamazoo River mouth and Lake Michigan, was collected parallel to SAUG-01 and SAUG-02 (Figures 4-1 and 4-6). The line runs perpendicular to the old channel and along the foredune ridge beginning to form in ~ 1920 (Figure 3-2).

The reflections are mostly low amplitude, and increasingly discontinuous with depth. Gradual disappearance of signal indicates loss from increasing depth rather than

dielectric properties. There is one strong reflective surface within this unit at a depth of 4 m from the surface sediment. Considering the dune sequence in this location is ~100 years old, this stronger horizontal reflection could represent either a soil horizon or the water table.



3. Dune

Figure 4-6 The original (A) and interpreted profiles (B) for GPR line SAUG-05 corrected for elevation, and oriented south to north., This line runs along the crest of north-south oriented foredune separating Lake Michigan from Oxbow Lake (Figure 4.1)

GPR LINE SAUG-06

A 141 m GPR line, running south to north on the modern beach was collected ~20 m lakeward from the shoreline (Figures 4-1 and 4-7). The GPR profile extends both north and south of the wooden piers bracketing the former channel mouth. No corrections for elevation were needed along the flat beach. Three units (1, 2, and 4) were observed. The lowest unit, unit 1, has gently dipping reflections on the south and north sides of the GPR line. Unit 2 has reflections that cross-cut those of unit 1B, and have been marked as the channel surface. Reflections fluctuate between continuous and discontinuous, many with cross-cutting geometries. Flat lying beds overlie unit 2, which are interpreted here as swash deposits on the beach. Because some of the unit 2 channel fill sequences are flat-lying and continuous, they likely consist of littoral and fluvial deposits.

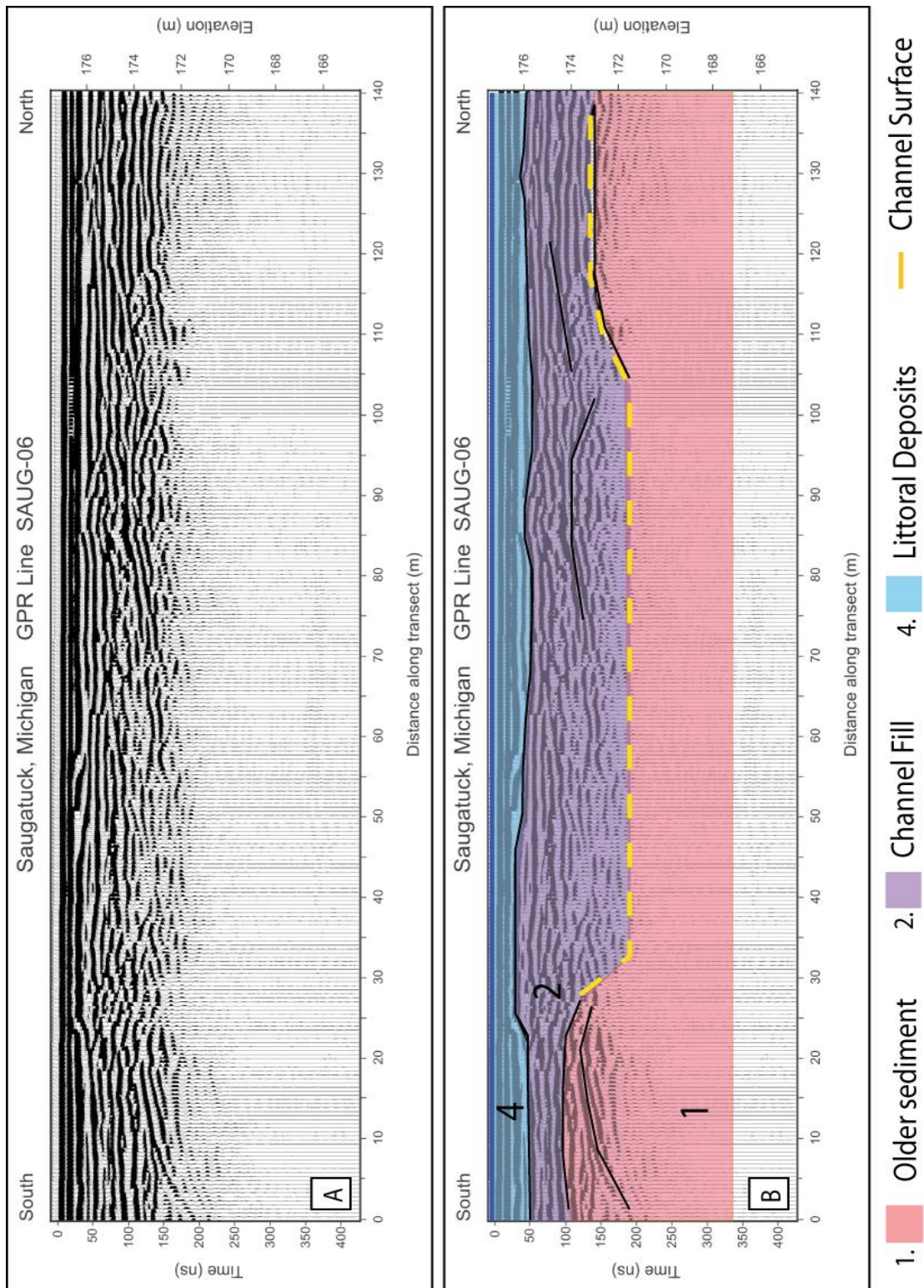


Figure 4-7 The original (A) and interpreted profiles (B) for GPR line SAUG-06 not corrected for elevation, and oriented south to north. This line runs parallel to Lake Michigan on the western side of the foredune separating it from Oxbow Lake (Figure 4.1)

4.3 Summary

The GPR profiles record older sediment of unknown origin (unit 1A and B) underlying all other units and cross-cut by the Kalamazoo River channel. This channel was at first broad and shallow, deepening upon installation of wooden piers. First, the portion of the channel south of the piers infilled from packages of littoral sediment in the form of bars coming from the west, and southward-dipping sediment infilled the channel from the north side once flow was cutoff in 1905 (seen in the 1912 photograph in Figure 3-2). As the channel shallowed, the deposits became more bed-like. After the channel had closed and a beach had formed (consistent with 1920 photograph from Figure 3-2) between the Kalamazoo River and Lake Michigan, eolian deposits began accreting to form a foredune ridge that continues to grow due to the constant supply of sand from the Lake Michigan coastline.

Chapter 5

Sand Percentage and Climate Results

5.1 Introduction

This chapter includes analyses from the Glew and Livingstone cores, $^{210}\text{Pb}/^{137}\text{Cs}/^{7}\text{Be}$ dated sediment using an age model equating years to depth, and the correlation of climatic factors, such as temperature, precipitation, evaporation, lake level, and wind to dated sand percentages to test for a connection between eolian activity and climate. Sample sites are listed in Table 5.1 and shown in Figure 2-1.

LITHOSTRATIGRAPHIC ANALYSIS:

A 1.5 m long Livingstone core was taken from Oxbow Lake, OL-L-1 and OL-L-2 (Table 5.1). The different sedimentary structures found in this core record a variety of depositional environments. Generally, basal pebbly sand is overlain by sand with interbedded organics (wood fragments) and silty sand (Figure 5-1)

Table 5.1 Locations of sediment cores taken west of Oxbow Lake, using Garmin handheld GPS unit.

Core Name, Type, Location, and Date Taken				
Core	Core Type	Date	UTM Coordinates	
OL-G1	Glew	6-30-11	16T	0564570m E 4723840m N
OL-G2	Glew	6-30-11	16T	0564580m E 4724041m N
OL-G3	Glew	6-30-11	16T	0564608m E 4724050m N
OL-G3-D	Glew	6-30-11	16T	0564608m E 4724050m N
OL-G4	Glew	6-30-11	16T	0564785m E 4724060m N
OL-G5	Glew	6-30-11	16T	0564925m E 4724096m N
OL-G6	Glew	6-30-11	16T	0565075m E 4724134m N
OL-L1-1	Livingston	2-10-11	16T	0564576m E 4724040m N
OL-L1-2	Livingston	2-10-11	16T	0564576m E 4724040m N

5.2 Livingstone Core Analysis

From 150 cm to about 70 cm depth, the lithology is massive pebbly sand with interspersed pebbles. Due to Livingstone coring procedures, there is a section of sediment without structural integrity at the top and base of the overlapping core segments between 97 and 99 cm (Figure 5-1). The pebbles periodically occur in clusters, and could be the result of storm events washing coarse sediment into the previous mouth of the Kalamazoo River, or fluvial deposits of the Kalamazoo River. Coarsening of the sand upward in the core is accompanied by an increase in dark (probably mafic) minerals within the sand, consistent with a high-energy, turbulent depositional environment caused by high-energy coastal processes and storm events (Scileppi, 2007). Before the installation of the jetties, the coast was 137 m east of its current position (Figure 2-4),

suggesting that the pebbly sand could be littoral deposits from storm surges, that may have been reworked by fluvial processes.

Between 60 and 70 cm depth, 1 cm thick rhythmic silty deposits alternate with sand in couplets. The couplets were separated by a thicker layer of sand, typically about 1 cm in thickness. Overlying these rhythmic deposits are finely laminated silt and sand deposits, though particle size analysis shows little silt present at that depth (Figure 5-1).

The fining of the interbedded deposits suggests a lower-energy environment with episodic changes. The laminated sediments lie below a thick layer of wood fragments/chips between 49 and 68 cm (Figure 5-1). A sawmill in the old town of Singapore, upriver of the former Kalamazoo River mouth, produced lumber for neighboring areas. This sawmill was in business between the years of 1837 and 1875 with its most productive years between 1871 and 1875 after the Chicago fire in 1871. Episodic deposits of wood chips (Figure 5-1) may have been from the Singapore sawmill area during its time of operation, or subsequent reworking by fluvial erosion of the land near it. The silt deposited with the upper woody deposits may be the result of erosion following high flow along the Kalamazoo River, possibly associated with storm events along Lake Michigan.

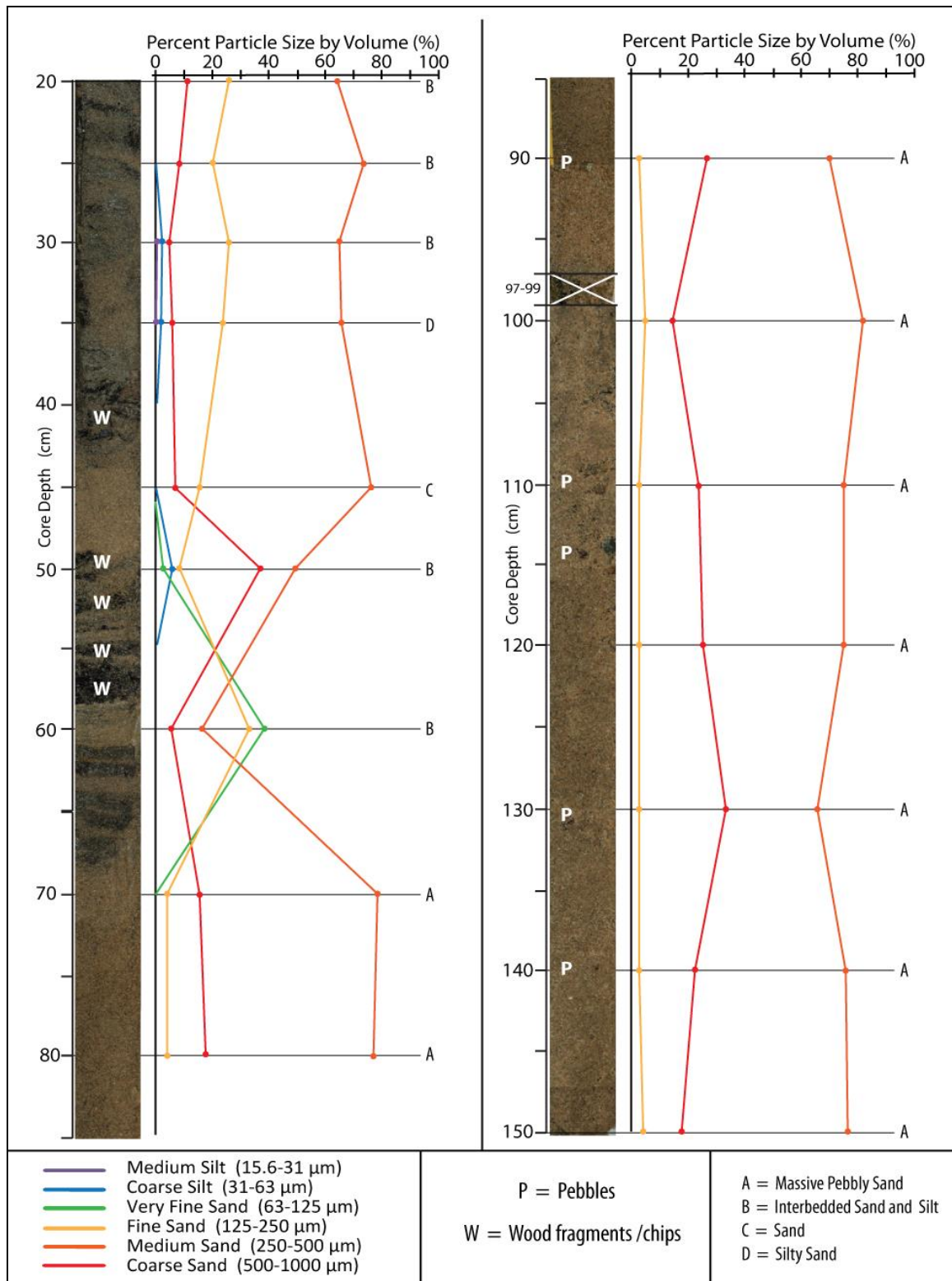


Figure 5-1 Percentage by volume of particle sizes from the Livingstone cores, OL-L-1 and OL-L-2, from Oxbow Lake. (Omitted first 20 cm of OL-L-1)

Between 44 and 49 cm is a massive sand deposit. This sand could represent the final years of water flowing through the Kalamazoo's natural mouth. After jetty installation in 1897, the jetties would have increased the flow velocity of the river, and the increased energy would have prevented the accumulation of fine-grained sediments. From 44 cm to the top of the core marks the transition from fluvial to lacustrine depositional environment, based on the transition from sand to silt and organics. Overlying organic sediments were not preserved in the top of the Livingstone core. The collected Glew cores recover the sediment missing from the top of the Livingstone core.

5.3 Glew Core Analysis Results

Six Glew cores were subjected to a series of laboratory analyses to determine their composition, and for one core, age of the sediment. The amount of sand introduced into the lacustrine system from surrounding land was compared to climate records, and the stratigraphy used to determine the timing of the transition from a fluvial to a lacustrine system. While it has been assumed in this study that deposition of organics is consistent across the lake, decomposition of those organics may not be. The thicknesses of organics layers in each core differ and this may be a factor of uneven distribution of organics throughout the lake or uneven decomposition due to differential temperatures or organic activity. Another factor would be compression of the sediment, either under its own weight or under the force of the core tube during collection of the sediment cores.

5.3.1 Loss on Ignition (Organics)

Loss on ignition (LOI) was used to assess the percent by weight of organic matter to total sediment sample weight in each centimeter of core for cores G1-G5 (Figure 5-2). The results were used: 1) to quantitatively show the mass of organics with depth in the cores; and, 2) as a proxy for correlating the dated core (G3) to the remaining undated cores. Organic matter generally decreased with depth in all cores, representing the transition from sandy fluvial (0-5% organics) to organic-rich lacustrine (up to 35% organics) depositional environment. Spacing of high and low organic content varied from core to core. Trends in organics were used to correlate sand percentages between the dated core (G3) and other Glew cores. Sand percent correlations will be discussed later in this chapter. Some decomposition of organic matter is assumed, and may differ across the lake based on a number of environmental factors (core depth being the main variable).

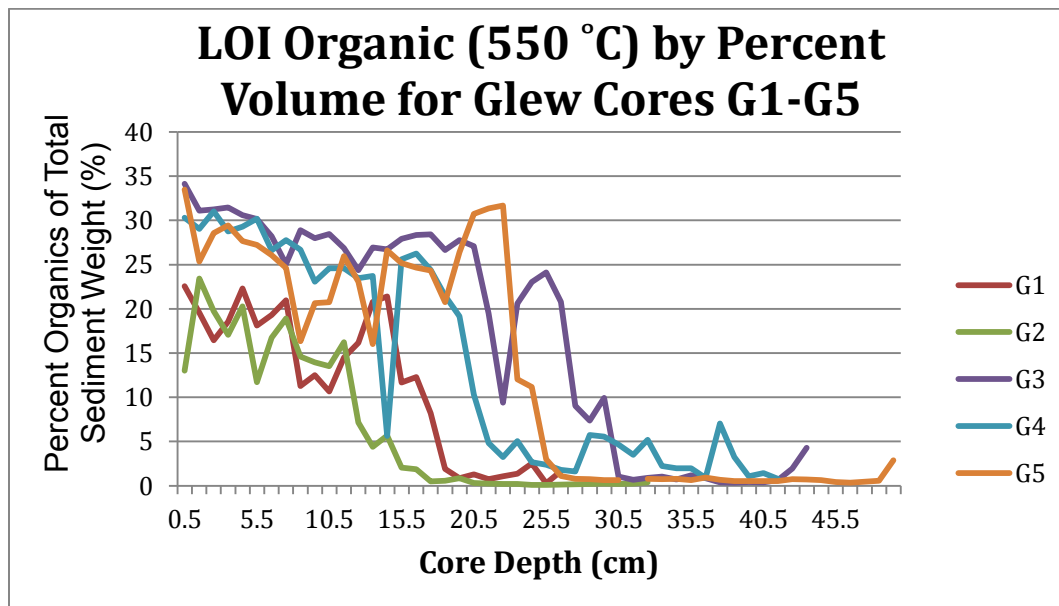


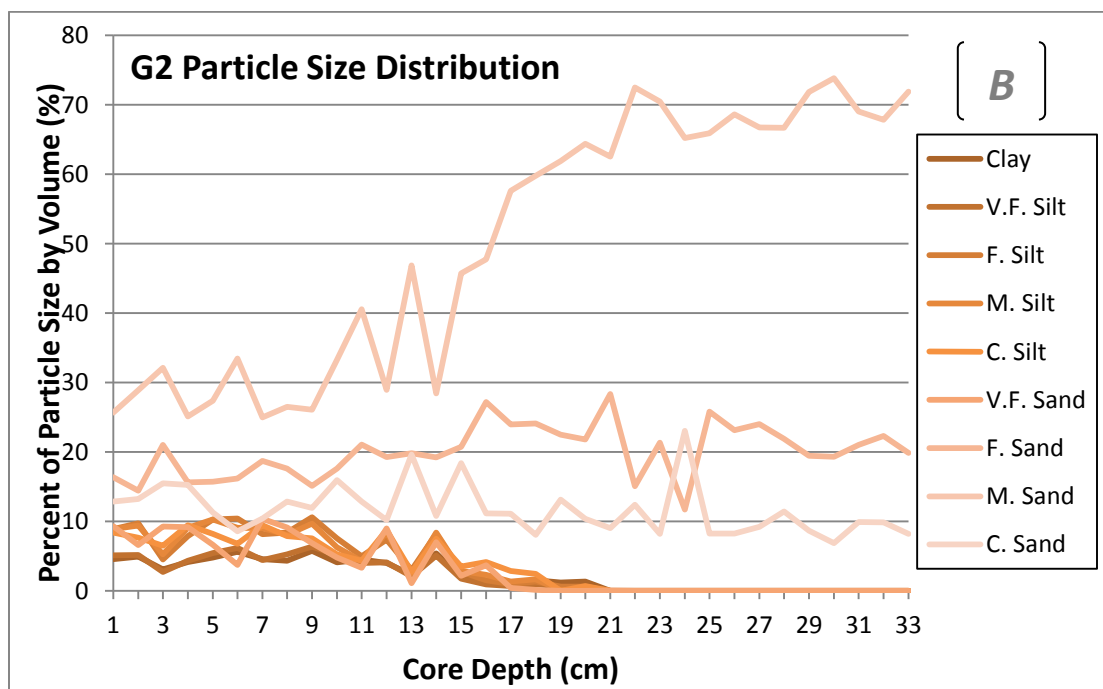
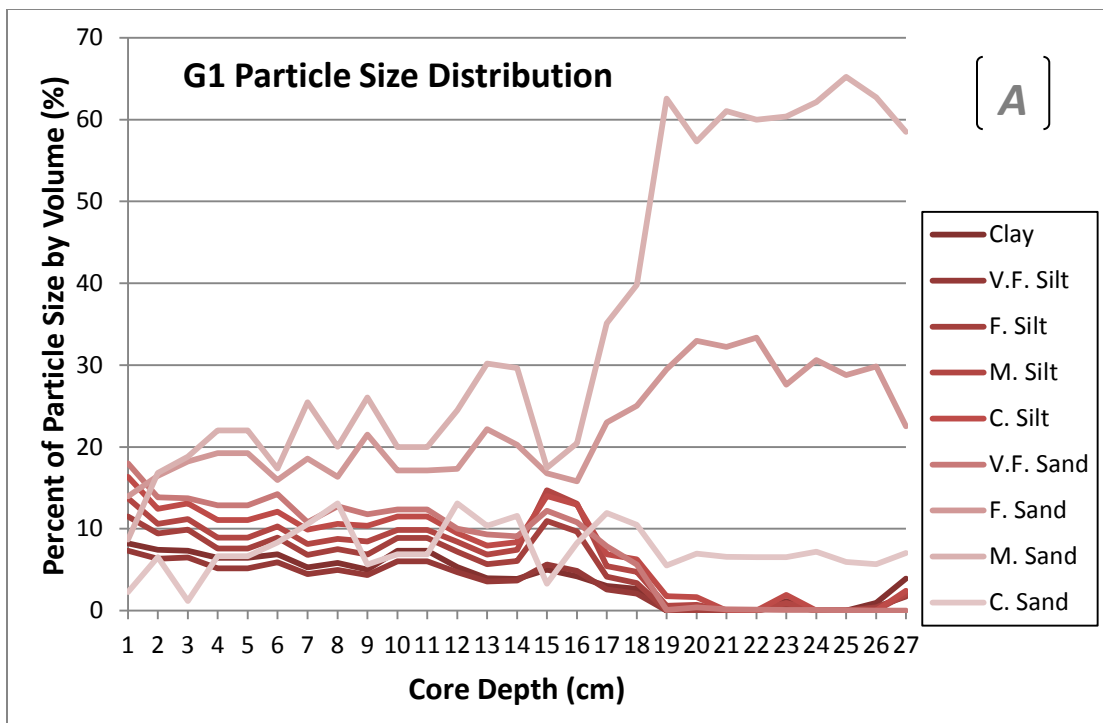
Figure 5-2 Organic loss-on-ignition for Glew Cores G1-G5. Raw data presented in Appendix C.

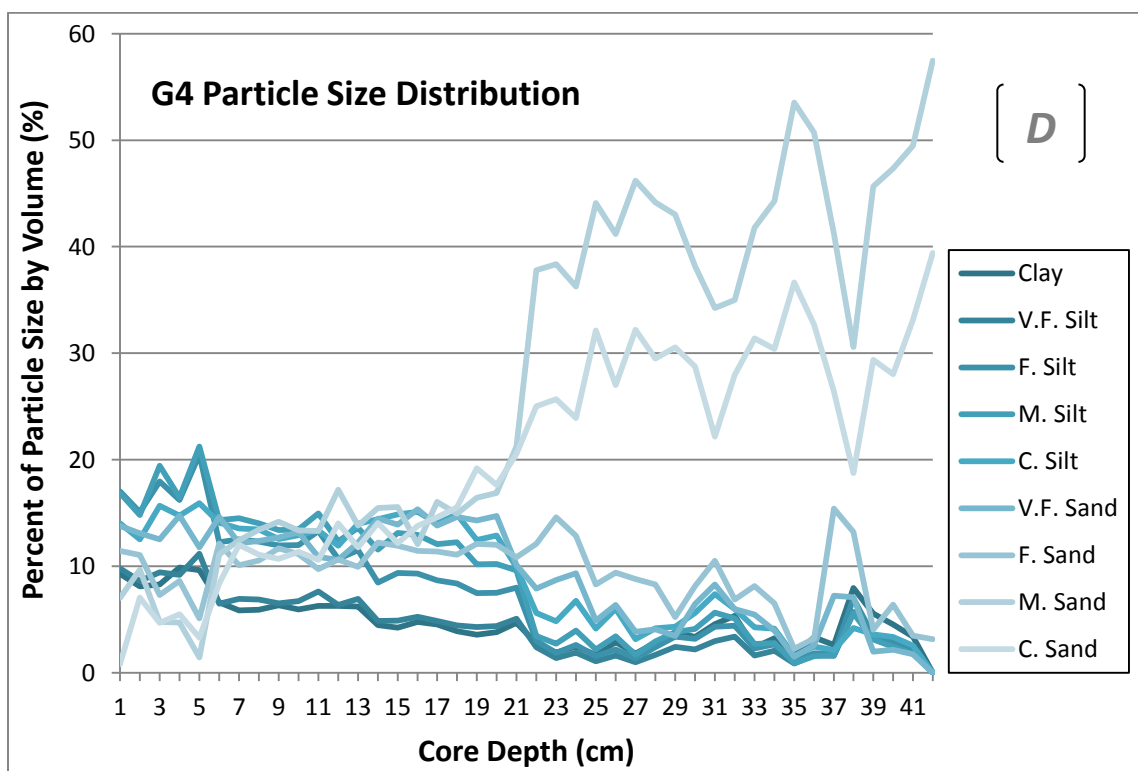
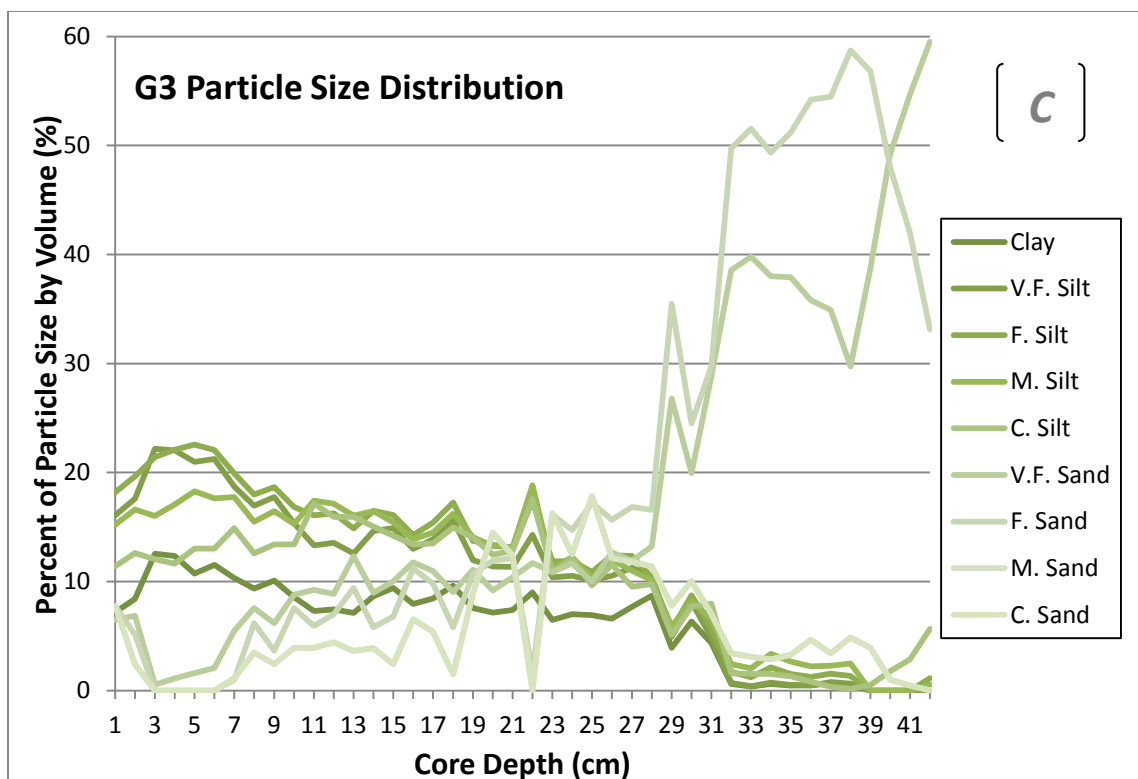
5.3.2 Particle Size Analysis

The distribution of particle sizes in each core shows a trend with depth (Figure 5-3, Table 5.2). Similar to the organic LOI data, these trends show similar spikes in sand percent by volume with increasing depth. This change in sediment size likely reflects changes in the energy system, such as from a fluvial channel to a lower-energy lacustrine system as recorded by increasing abundance of mud from the bottom to top of each core. One source of error in this procedure is the presence of shell fragments in the 250-500 μm and 500-1000 μm grain-size brackets, overestimating sand present. Hydrochloric acid was not used to avoid dissolving terrigenous eolian carbonate sediment; as a result, shell fragments were included in samples tested in the particle size analysis.

Table 5.2 - Udden-Wentworth grain-size classification of sediments.

Udden-Wentworth Grain-size Classification		
Wentworth Class.	Micrometers (μm)	Millimeters (mm)
V. Coarse Sand	1000-2000	1.0-2.0
Coarse Sand	500-1000	0.5-1.0
Medium Sand	250-500	0.25-0.5
Fine Sand	125-250	0.125-0.25
V. Fine Sand	63-125	0.0625-0.125
Coarse Silt	31-63	0.031-0.0625
Medium Silt	15.6-31	0.0156-0.031
Fine Silt	7.8-15.6	0.0078-0.0156
V. Fine Silt	3.9-7.8	0.0039-0.0078
Clay	0.06-3.9	0.00006-0.0039





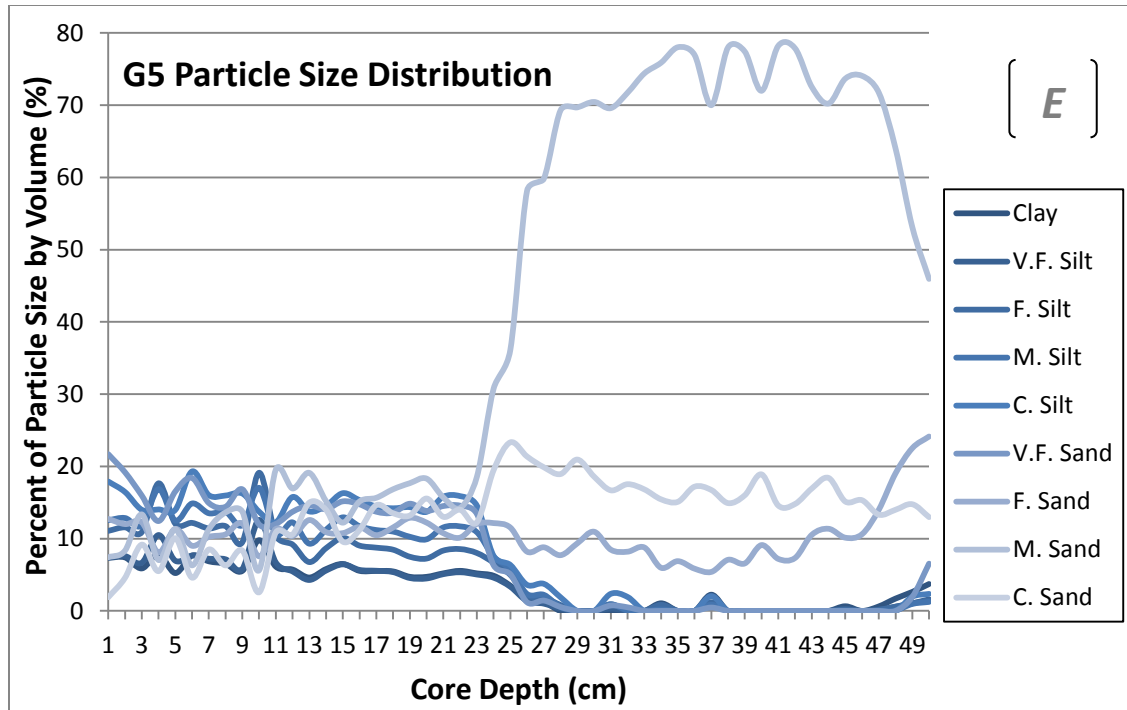


Figure 5-3 A-E Particle size analysis at 1 cm intervals down core for all Glew Cores from Oxbow Lake. Raw data presented in Appendix C.

5.3.3 Percent Sand by Weight

The sand percentage trends determined by weight in grams (LOI) were in tandem with both the organic LOI and particle size analysis results (Figures 5-2, 5-3 and 5-4). The depths where changes in sand percentages occur are different between cores; however, a rapid drop in sand content is observed in all cores. This evidence reinforces the interpretation that this study site has passed from a high-energy, fluvial and/or beach environment to a lacustrine one.

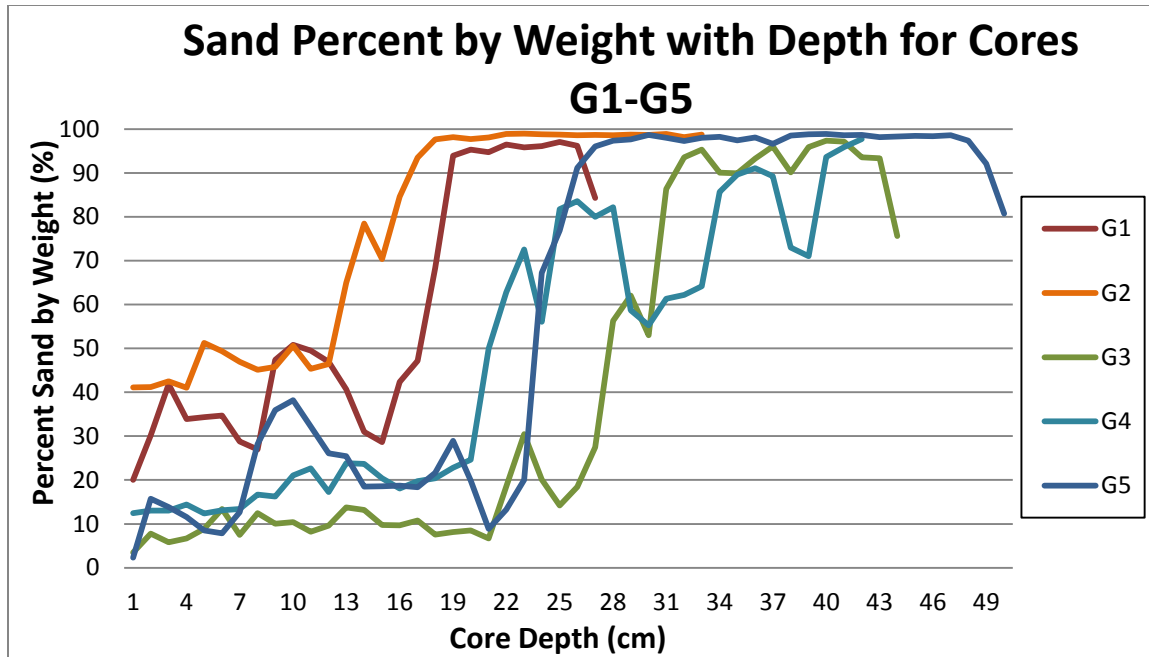


Figure 5-4 Sand percentages by weight for Glew Cores G1-G5 down core.

5.3.4 Core Descriptions

Sediment classifications are based on the criteria of Schnurrenberger (2003), and colors identified using the Munsell Color Chart. Sediments are described from the base to top of the core (Figure 5-5 and 5-6). Lithological descriptions are from sediment in both Livingstone and Glew cores, due to the loss of sedimentary structures after extrusion from Glew cores into 1 cm discs for analysis.

Unit A – Massive pebbly sand: Medium-to-coarse grained massive quartz sand light olive brown (2.5Y 5/3) in color. This unit is the lowest recovered with a unit thickness of ~1m. This unit contains interspersed granule and small pebble-sized grains towards the base, and occurs only in core OL-L1. Compared to other sandy deposits, this

unit possesses more mafic grains. This is the coarsest sedimentary unit, and is found only in the base of the Livingstone core.

Interpretation: Massive sand, thick deposits, interspersed mafic grains, and sparsely interspersed pebble clusters found within massive sand are indicative of a high-energy fluvial environment. This sediment unit is thought to have been deposited by the Kalamazoo River as alluvium, or littoral deposits making their way into the river mouth.

Unit B – Very finely-bedded sand and organic-rich silt: Fine-to-medium sand, light olive brown (2.5Y 5/3) color is interbedded with silt and organics, a dark, grayish brown (2.5Y 4/2) color. The organic rich silt is generally dark grey in color (2.5Y 4/1). The lower contact of this unit is abrupt with unit A in core OL-L1. Unit thickness ranges from 7-13 cm. Wood chips occur within this unit.

Interpretation: Due to the variability of sand and silt content, these deposits reflect the environmental instability due to closure of the Kalamazoo River mouth from Lake Michigan. While primarily a lacustrine environment after closure of the river mouth, storm surges could have introduced packages of sand into the system from the west (Lake Michigan), or these alternating beds could represent episodes of high and low fluvial energy, with wood chips transported from upriver from saw mills and the breakdown of wooden structures along the river and reworked into the sediment during high-energy events. Unit B-2, from Figure 5-6, has the thickest deposits of wood chips, possibly deposited during the years of sawmill operation upriver (ca. 1870s).

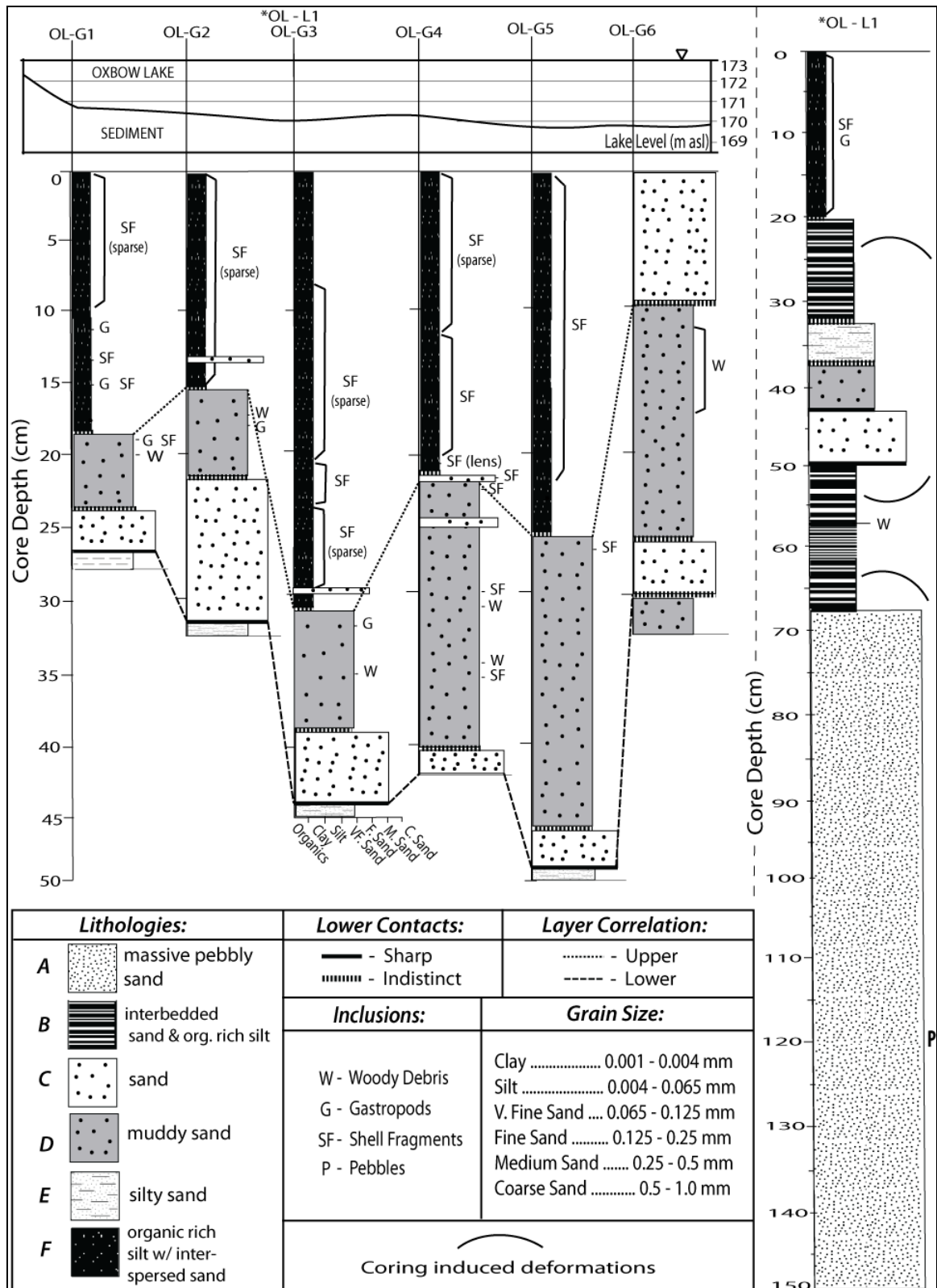


Figure 5-5 Lithostratigraphic logs of the sediment cores from Oxbow Lake, Saugatuck, Michigan.

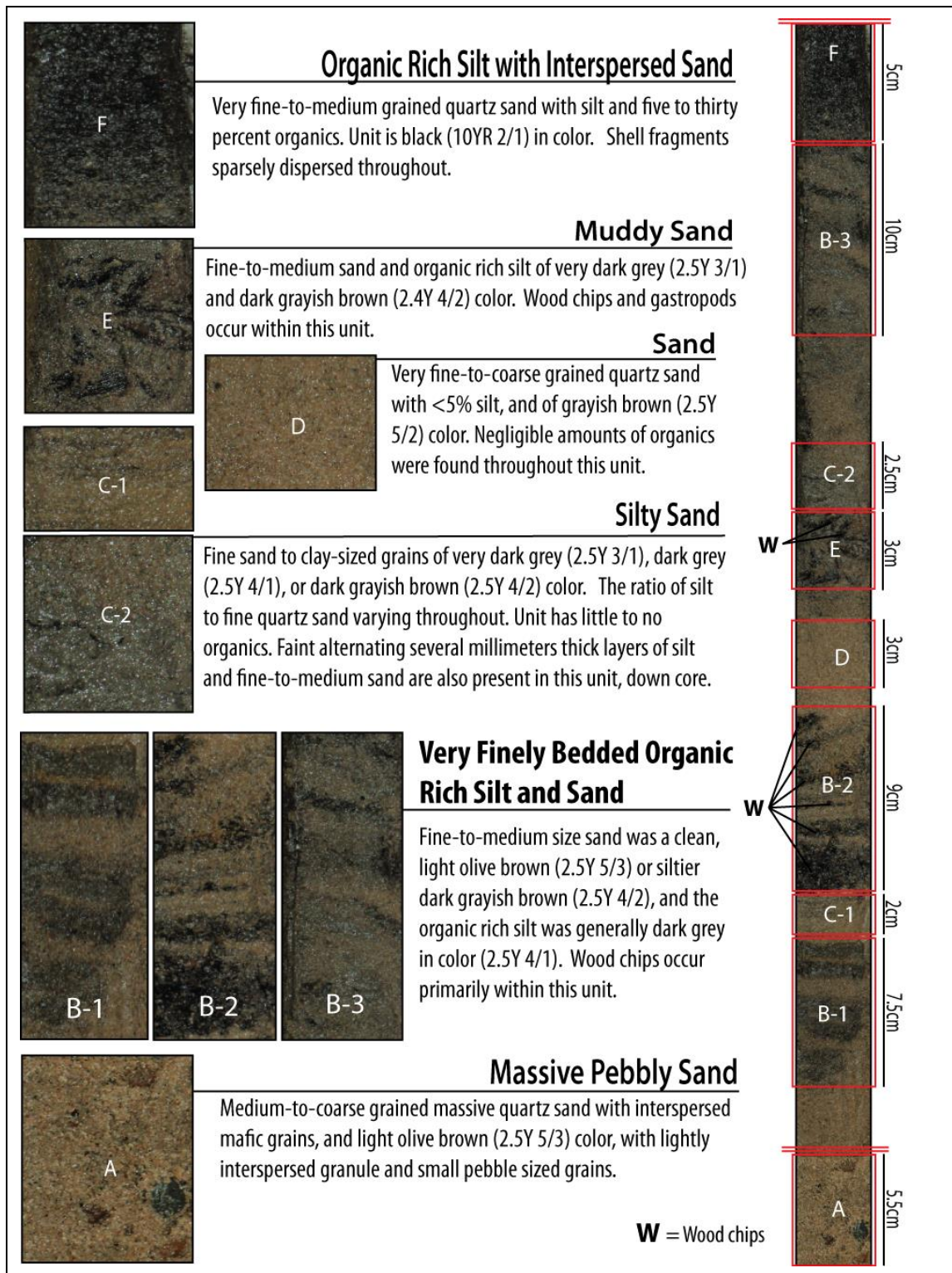


Figure 5-6 Photographs of core lithostratigraphy with sediment examples from core OL-L1. Measurements to the right of core represent thickness of example to scale on the left.

Unit C – Silty sand: Colors range between dark grayish brown (2.5Y 4/2) sand, and dark grey (2.5Y 4/1) silt, with a general blending of sand and silt throughout. Unit thickness was 5 cm for faint, alternating several millimeter thick laminations of silt and fine-to-medium sand at 63-58 cm. The laminated silt and sand has an abrupt upper and lower contact with the very thinly bedded sand and organic rich silt units. The upper portion of this unit, 33-37 cm in the Livingstone core, has an over-all Glew core thickness of 1-5 cm. This unit has variable concentrations of sand and silt, with little (B-1) to no structure (F) (Figure 5-6).

Interpretation: Alternating sand and silt with fine laminations may record episodes of closure of Oxbow Lake from Lake Michigan. The lack of strong structure higher in the core could represent sediment pulses into the developing lacustrine system.

Unit D – Sand: Very fine-to-coarse grained quartz sand with < 5% silt, of grayish brown (2.5Y 5/2) color, and thickness ranging from 1 to 7 cm. Negligible amounts of organics were found in this unit. The lower contact is abrupt, overlying silty sand in Glew cores G1-G5 and laminated sand and silt in OL-L1. Sand toward the top of the core was frosted.

Interpretation: The sand of this unit was found above the fluvial sand and between units of silt and organics. This signifies a high-energy event during the beginning of a closed lacustrine system. The frosted sand in the upper portions of the core are indicative of eolian sand, thus representing strong winds; however, the dune system surrounding the study site may be recycling eolian sand, which could get carried by littoral currents and redeposited by storm events.

Unit E – Muddy sand: Fine-to-medium sand and organic rich silt of very dark grey (2.5Y 3/1) and dark grayish brown (2.4Y 4/2) color. Unit thickness is between 5 and 20 cm in cores G1-G5. Wood chips and gastropods occur within this unit. It is very thinly bedded sand, and organic rich silt. There is a diffuse lower contact with the sand unit.

Interpretation: This unit was interpreted to be artificially produced due to disruption of the very thinly bedded sand and organic-rich silt unit, based on its occurrence in Glew cores at the same lithostratigraphic region one would expect to find very thinly bedded sand and organic-rich silt.

Unit F – Organic rich silt with interspersed sand: Very fine, fine or occasionally medium-grained quartz sand, with silt and 5-35% organic matter. Unit is black in color (10YR 2/1), has a diffuse lower contact of organic rich silty sand in Glew cores G1-G5, and very thinly bedded sand and organic rich silt in OL-L1. Organics are finely disseminated, assumed to be lake-based with the exception of the occasional oak leaf or dune grass from surrounding vegetated dunes. Unit thickness ranges from 15-30 cm. The quartz grains are frosted. This unit contained several layers of shell fragment hash, while interspersed gastropods and shell fragments exist throughout.

Interpretation: High organic content, accompanied by gastropods and rapid drop in sand suggests a completely closed lacustrine system. After the foredune formed between Oxbow Lake (old Kalamazoo River mouth) and Lake Michigan, a lacustrine system developed allowing for organics and gastropods to live and accumulate. The only sand evident from examination of the organics is eolian based on the frosted finish and general very fine-to-medium particle size.

5.4 $^{210}\text{Pb}/^{137}\text{Cs}/^7\text{Be}$ Sediment Ages and Deposition Rate

Gamma counts of $^{210}\text{Pb}/^{137}\text{Cs}/^7\text{Be}$ in centimeter-interval samples were used to date the sediment at depth in core OL-G3, assuming a constant rate of supply (CRS) of ^{210}Pb . The CRS model assumes that the rate of ^{210}Pb remains constant and the sedimentation rate changes, diluting the concentration of the radionuclide. Gamma counts of $^{210}\text{Pb}/^{137}\text{Cs}/^7\text{Be}$ in centimeter intervals were also used to create a sedimentation rate model. The equation generated by the sedimentation-rate curve calculates the age of the sediment based on its depth. Direct dating provided a date of 1897 for the lowest datable core sample ($>0.001 \text{ bq/g}$ activity for Pb^{210}). Based on the sedimentation-age curve in Figure 5-7 (based on direct ages calculated from sediment), between 1897 ± 20 years and 1929 ± 12 years there was little to no sedimentation followed by a sharp increase. This does not agree with the rapid sedimentation occurring in the mouth of the channel during this time. Therefore a discrepancy in the basal age may exist. A best fit curve to the age/depth model generates an equation that calculates the basal depth to be an age of 1929. Core G3 was then correlated to the remaining undated cores. Figure 5-7 illustrates the $^{210}\text{Pb}/^{137}\text{Cs}/^7\text{Be}$ gamma counts at depth for core G3, and the age model created to show deposition rate using depth versus core age to determine age at a specified depth using known gamma markers for constraint. Multiple examples include using ^7Be (~ 53 day half-life) and ^{210}Pb (~ 22 year half-life) to test the age of the sediment based on concentration of gammas emitted, as well as a spike in ^{137}Cs in 1964, marking the peak of atmospheric atomic weapons testing.

5.4.1 Age Dating Sand Signals

The ages for the dated core span from 1929 to 2011. The year 1929 represents the last year that unsupported ^{210}Pb gamma readings were reliably above zero (using depth and the age model equation), and 2011 was the year the cores were collected. Confidence that the uppermost sediment was preserved is strong based on the ^7Be gamma readings collected from the dating of OL-G3. Age assignments used in this study end at 1929, the year calculated using an age model for the last reliable depth in the dated core (34 cm) (Figure 5-7). Ages were assigned to sand percentages throughout the G3 core using this age model (Figure 5-8A).

Results from a Monte Carlo simulation for error using the age model show greater error with increasing age. The error associated with the age of the dated sediments is given as \pm one standard deviation (1σ) and consists only of the error associated with nuclear decay and the propagation of that error in the age calculation. These errors in years are \pm 1.2 years for sediments 1 to \sim 5 years old, \pm 1.5 at \sim 10 years, \pm 2 at \sim 20 years, \pm 2.5 at \sim 30 years, \pm 3 at \sim 40 years, \pm 4 at \sim 50 years, \pm 5 at \sim 60 years, \pm 7.5 at \sim 70 years, \pm 10 at \sim 80 years, \pm 15 at \sim 90 years, and \pm 20 at 100+ years. This error is related to the measurement of nuclear decay. These gamma count values are then used in the calculation of the ages. Error in the gamma counts are propagated by the CRS model and its assumptions. Histograms were plotted to illustrate the normal distribution of the results of Monte Carlo simulations for age using equation [4] (Chapter 3 section 2.3.1; Appendix D). Error bars were applied to the age model to depict the increase in error with increased age (Figure 5-8B). Based on the error associated with calculated age results, year-to-year correlations between sand percentages and climate data show both

strong and weak statistically significant correlations. Also, upon visual inspection, patterns among climate and sand percentage trends are found. These results for age-dated sand percent were compared to climatic factors discussed later in this chapter to determine any connections between environmental forcing and sand accumulation in the small lacustrine environment.

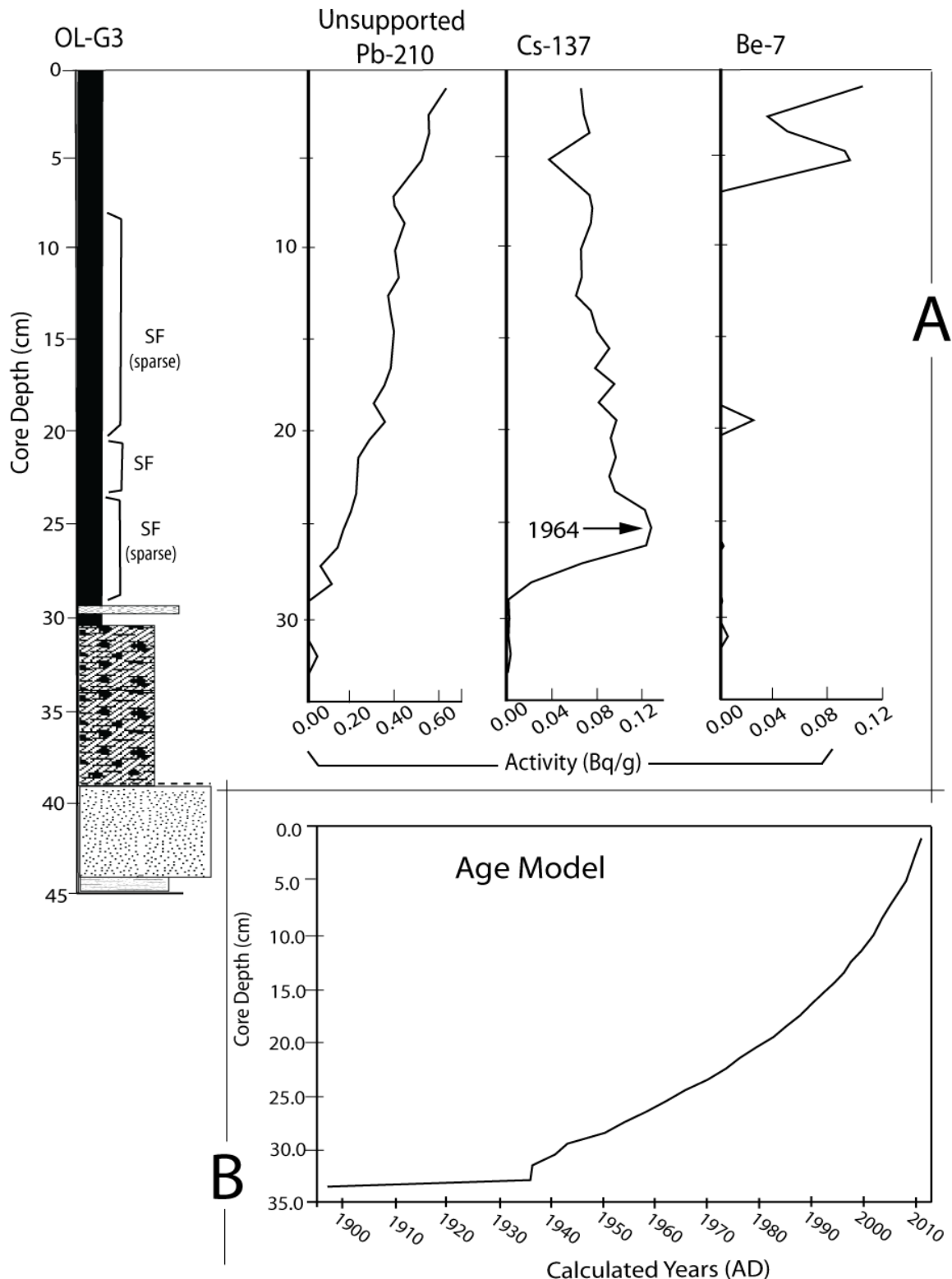


Figure 5-7 Age-depth model of core G3 using unsupported ^{210}Pb , ^{137}Cs , and ^7Be . Gamma readings used to determine deposition rate and age model. ^{137}Cs peak in 1964 is from atmospheric atomic bomb testing.

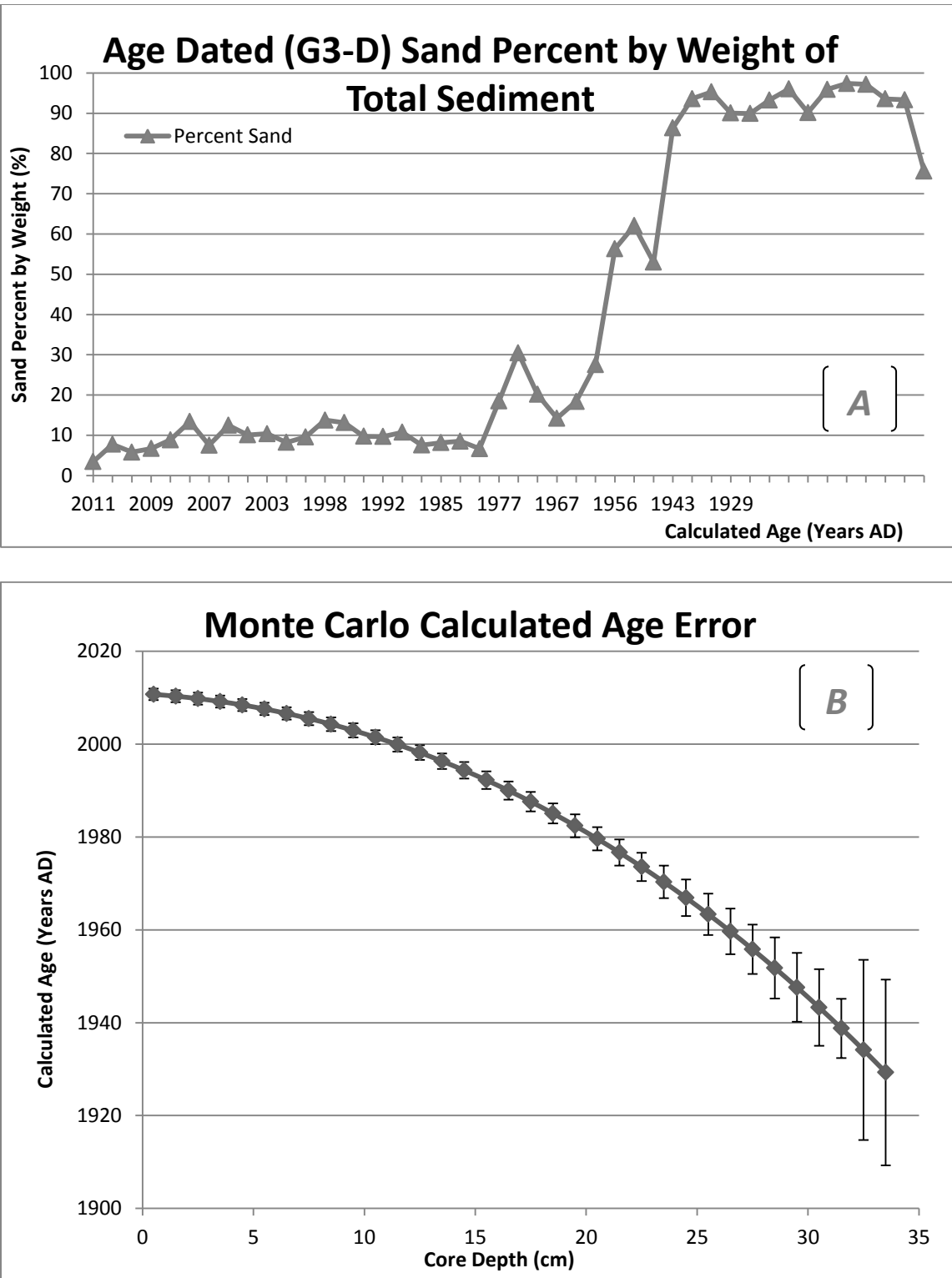


Figure 5-8 A) Age model used to date sand in core G3, and associated error in years. The age range is from 1929 to 2011. B) Error associated with assigned ages is one standard deviation.

Table 5.3 Sediment ages with depth, calculated using age model from isotopic dating methods.

Calculated Age with Depth - Ages and Calculated Error		
Depth	$y = -0.0003(x)^3 - 0.0538(x)^2 - 0.2971(x) + 2010.9$	Error: 1σ (\pm years)
0.5	2011	---
1.5	2010	1.2
2.5	2010	1.3
3.5	2009	1.3
4.5	2008	1.3
5.5	2008	1.3
6.5	2007	1.3
7.5	2006	1.3
8.5	2004	1.4
9.5	2003	1.5
10.5	2002	1.5
11.5	2000	1.5
12.5	1998	1.5
13.5	1996	1.6
14.5	1994	1.7
15.5	1992	1.8
16.5	1990	1.9
17.5	1988	1.9
18.5	1985	2.1
19.5	1982	2.2
20.5	1980	2.5
21.5	1977	2.5
22.5	1974	2.8
23.5	1970	3.0
24.5	1967	3.5
25.5	1963	3.9
26.5	1960	4.5
27.5	1956	4.9
28.5	1952	5.3
29.5	1948	6.6
30.5	1943	7.4
31.5	1939	8.3
32.5	1934	6.4
33.5	1929	19.4

5.4.2 Age Assignment Between Glew Cores

The results of three methods of correlating undated sediment cores to a dated core G3 are shown in Figures 5-9 to 5-11. By assuming that organic matter accumulation is constant in the lake, peaks in LOI are assumed to be the same age between cores; thus, LOI can be used to correlate ages from the dated core (G3) to undated cores. The LOI method was found to be the most robust of the three methods attempted, because the approach has the fewest assumptions, the longest reliable time span, and the use of a separate proxy to correlate horizons (Figure 5-9). The results show similar peaks in cores at approximately 1949 (G2-4), 1963 (G2, 5), 1974 (G1, 3), and 1979 (G2, 4). After 1979, peaks tend to occur separately of each other throughout cores G1-G5. There is a general rise in sand percentage in cores G1, G2, and G5 between 1999 and 2005; G3 and G4 stay relatively low with minor fluctuations occurring at unrelated times. G4 has peaks at years 1992-98, and 2002. G3 has low peaks in 1989, 1996-97, and 2005 (corresponds to spike in G2). Although the sand trends are not aligned throughout all cores, some peaks are shared by several cores at a time. This could be explained by numerous sand sources surrounding the small lake (explained in Chapter 6).

One explanation for weaker correlation between cores in the youngest sediment is the soupy consistency through which sand grains may settle. Because the top of the cores required combining multiple centimeters of sediment for a sample large enough to be tested, the resolution in the upper-most sediment is decreased.

The second method for correlating sand percentage values used the assumption of constant sedimentation rate of the entire core between 1943 and 2011. There is little agreement between the sand percentages for cores G1-G5 (Figure 5-10). The assumption

of constant sedimentation is likely incorrect for this environment, keeping in mind the numerous sources of sand surrounding the lake. Thus, this method is not used for correlating between cores.

The final method used is a wiggle-match method – aligning all cores using the peaks and valleys of sand percentage. Figure 5-11 illustrates the results, and while it appears to be the most correlated, it was highly subjective, and assumes that higher-magnitude fluxes of sand into the lake resulted in constant sand input. This assumption is unrealistic based on sampling data by Weyer (2005) in which sand was unevenly distributed on Silver Lake in wintertime ice and snow. Of the three models, the LOI method is considered the most robust and reliable.

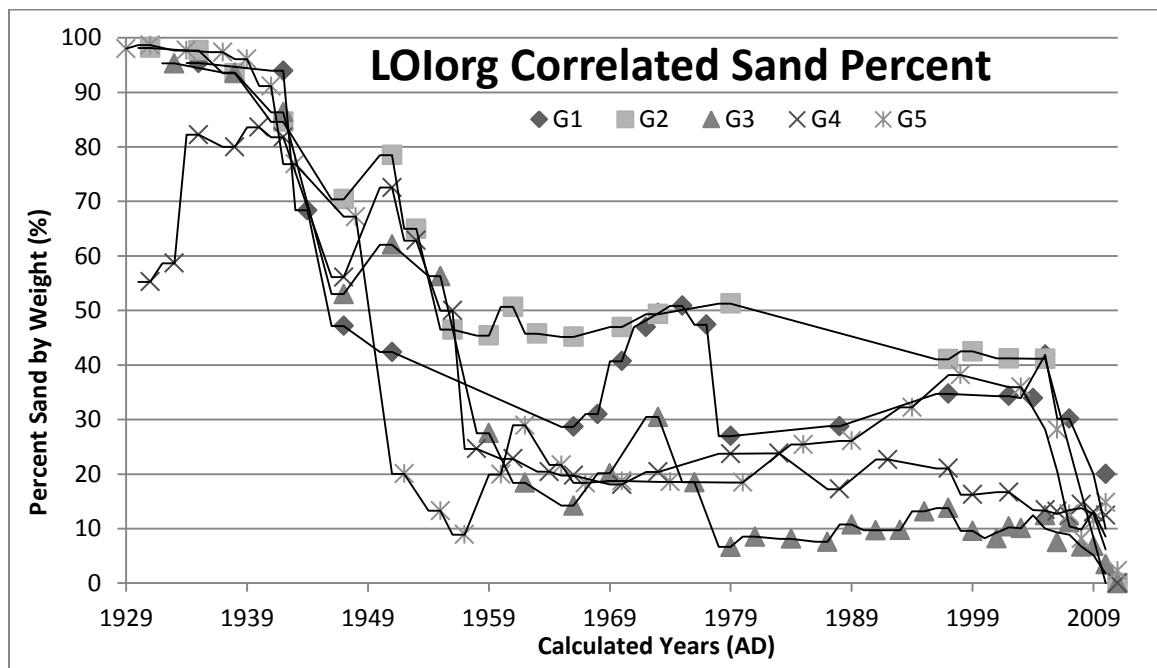


Figure 5-9 Age correlation between cores using LOI values between years 1929-2011.

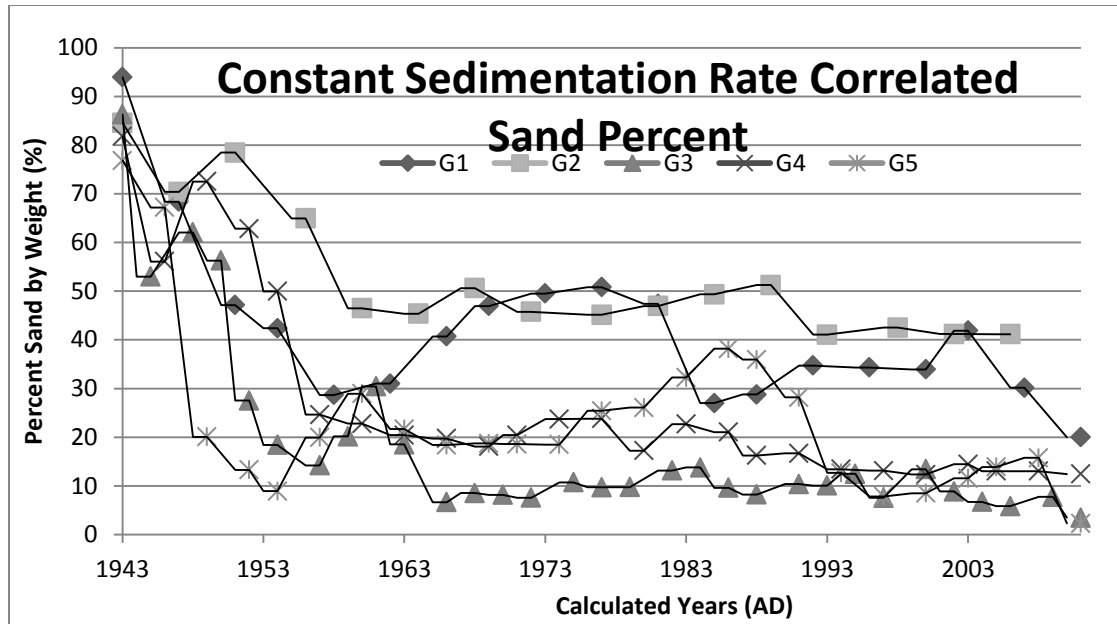


Figure 5-10 Age correlation between cores assuming a constant sedimentation rate through time between 1943 and 2011.

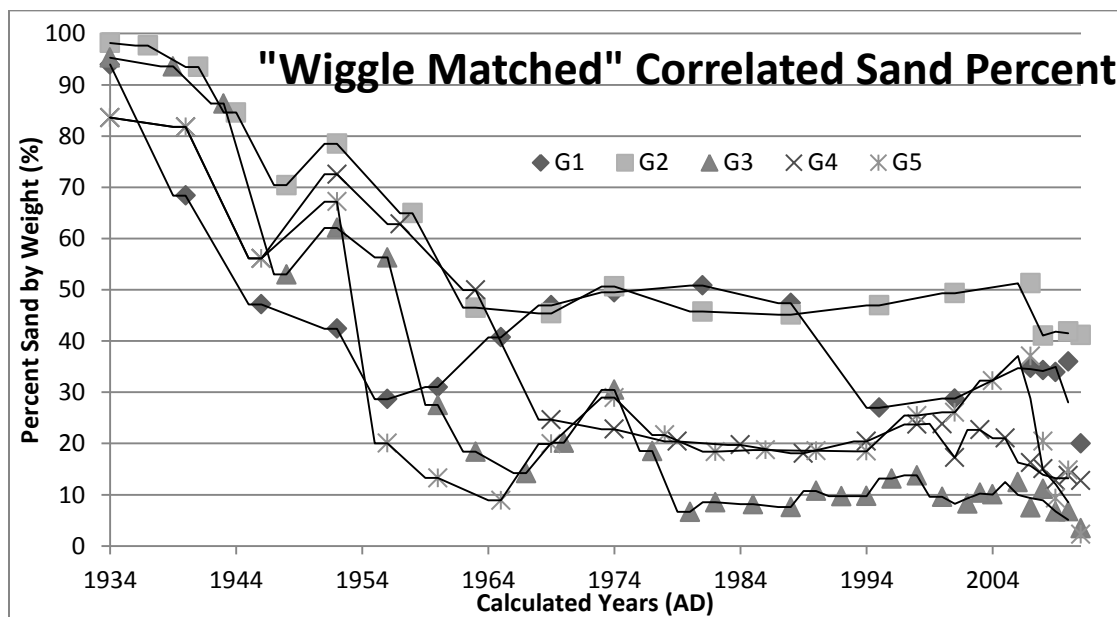


Figure 5-11 Age correlation between cores based on wiggle matching peaks and troughs in sand data with core G3 and cores G1-G5, from 1934 to 2011.

5.5 Relationships Between Sand Percent and Climate

Linear regressions, Pearson's correlations and visual comparisons are used in this study to test for year-by-year relationships between climate data and eolian sand in the lake cores. Climate data for these tests were obtained using databases from NOAA and USACE. The tests were done using wind data from buoys off the coast of Lake Michigan (Figure 5-12), as well as climate data from stations both land-based (South Haven) and over-lake (weather stations off the coast of Lake Michigan). The intention is to isolate one climatic factor at a time.

Visual correlations were done by matching trends of climate and sand percentage through time; relative similarities in trends were observed. Statistical correlations were run between climatic data and sand percentage; there were a broad range of correlation coefficients (r) values calculated; however, most results showed statistically significant low p values. High R^2 values fluctuated between positive and negative correlations, even between correlations of the same climate variable. Not all results for correlations were supported by the results of regressions with corresponding variables, and some residual plots suggest non-normally distributed data. Results in these sections are the highlights of the comparisons and correlations performed for this study.

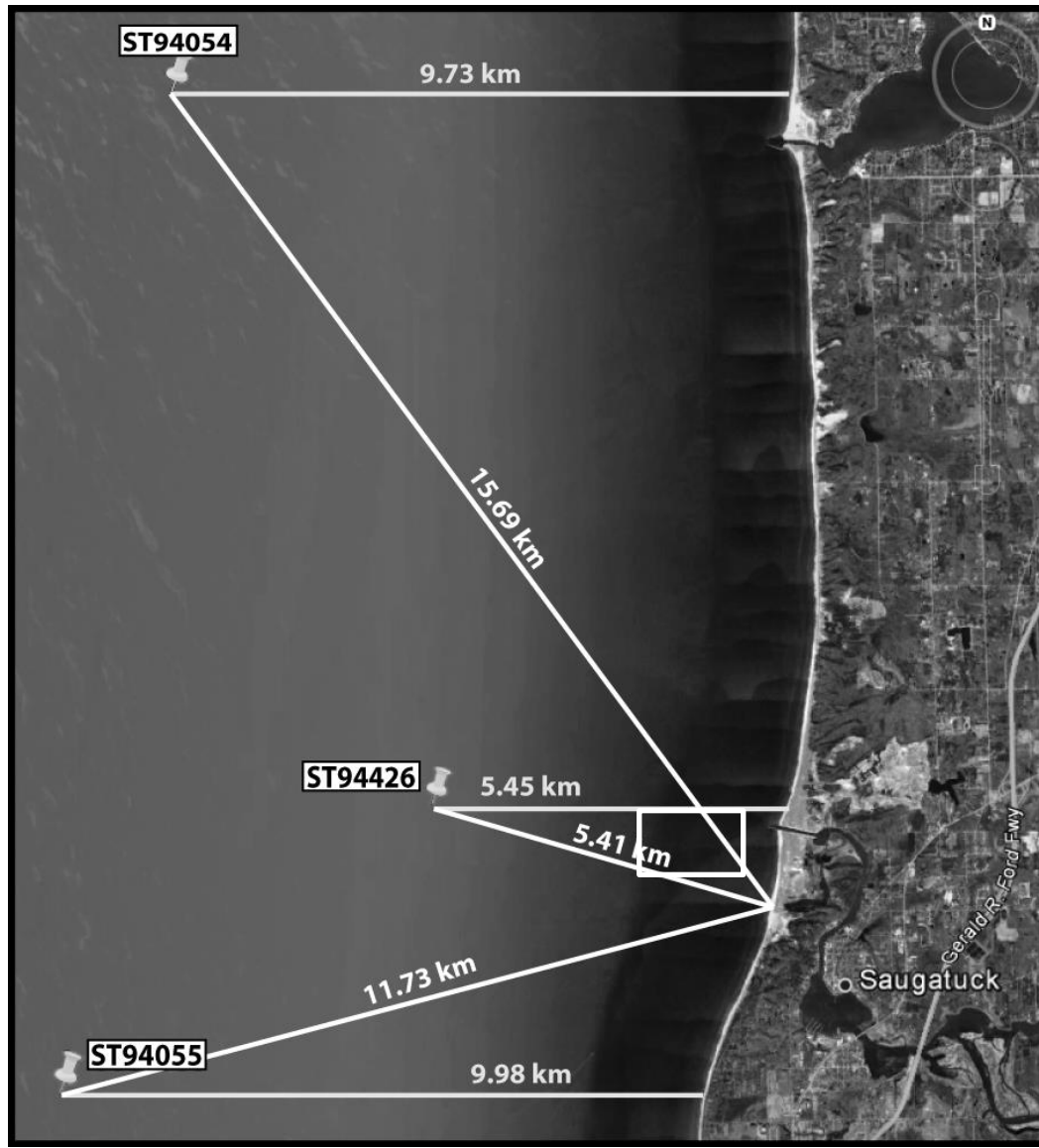


Figure 5-12 Locations of wind stations and their distance from shore and study site. Satellite image from Google (2012).

5.5.1 Visual Comparisons

Previous work suggests a relationship between lake level and eolian activity (Fisher and Loope, 2005; Fisher et al., 2007; Timmons et al., 2007; Fisher et al., 2012). Lake level, Palmer Drought Severity Index (PDSI), and wind data were visually compared; it was found that peaks in the sand data were aligned with peaks recording wet conditions in southwest Michigan, and peaks of high winds and water levels in Lake Michigan.

Lake level was used as a means of compiling multiple environmental factors at once because it integrates precipitation, temperature and evaporation. Lake level is a proxy for long term changes that only occur due to consistent environmental deviations from average. Initial comparisons of climate and sand percentage peaks show a commonality between lake level peaks for Lake Michigan and sand percentage peak values (Figure 5-13A). Making visual comparisons (wiggle matches) year-for-year between peaks in sand percentages and lake level show, within the first standard deviation error (error varies based on age of sediment), that there is a general agreement between peaks in lake level and peaks in sand percentage. Not all peaks are accounted for in the trends for the sediment cores, which means that lake level alone does not explain the movement of sand into the lake.

Relationships between PDSI and sand percentages were not as strong (Figure 5-13A). The PDSI peaks did not consistently match up to peaks in sand percent, but showed an off-set of peaks in which high winds occur right before a peak in sand percent. High PDSI signifies wet conditions, suggesting a connection between wetter (stormier) conditions and increased eolian activity. While initially this seems counterintuitive, dunes

along the vegetated coastline are only active during the storms that bring wind, and often rain (Hansen et al., 2009, 2010). Visual trends also suggest that increased sand percentages generally follow peaks in wind data through time (Figure 5-13B/C).

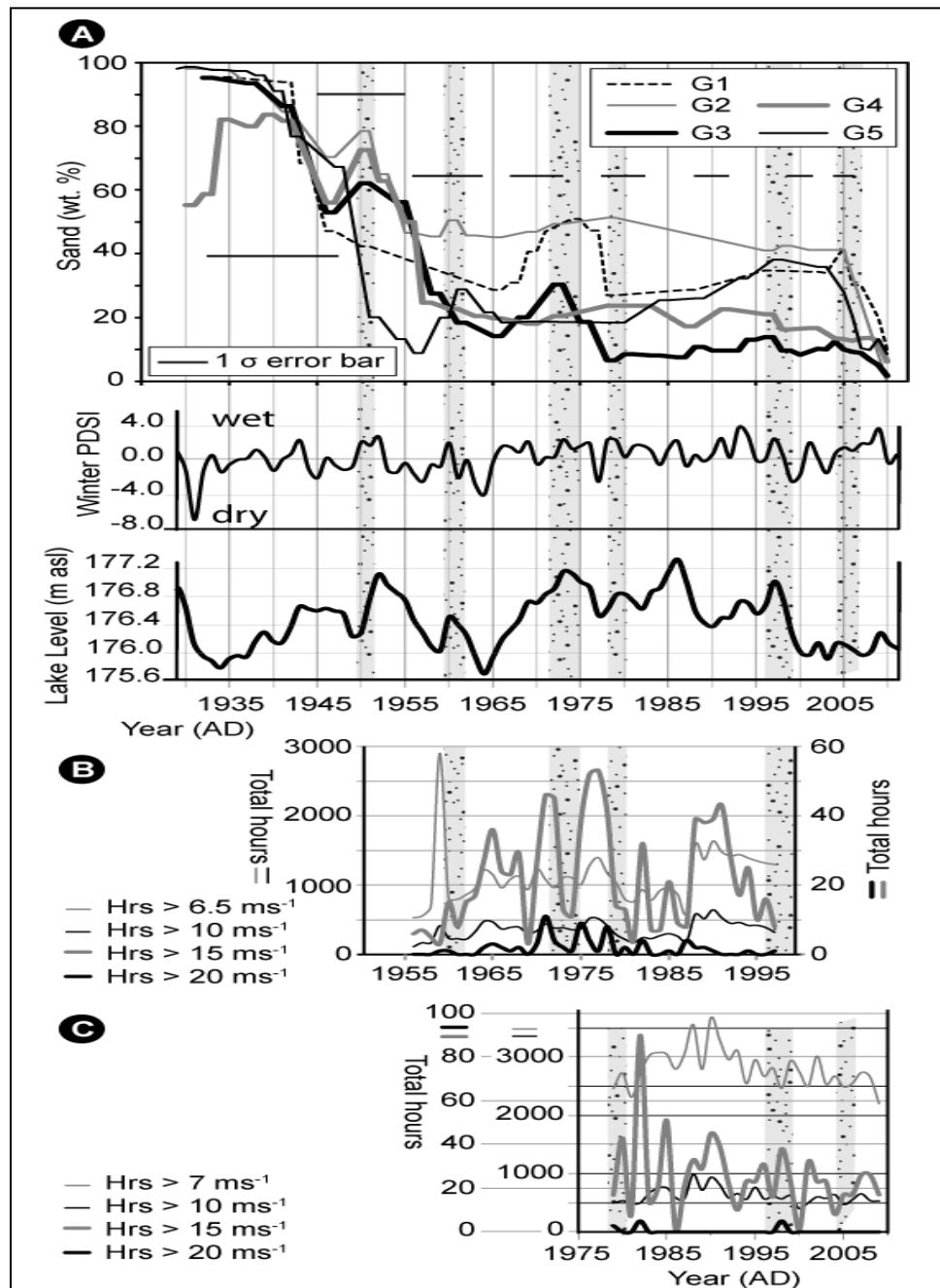


Figure 5-13 Visual comparisons between dated sand percentage peaks with average annual Lake Michigan lake level peaks, PDSI and wind data (A-C).

5.5.2 Correlations and Regressions

Based on suggested relationships between climate and sand percentages within lake sediment cores (Fisher and Loope, 2005; Fisher et al., 2007; Timmons et al., 2007; Fisher et al., 2012) correlations were examined between various climate variables and sand percentages. Table 5.4 displays the culmination of the correlation and regression results. Residual plots were examined for all statistically significant climate and wind regressions with sand percent Figure 5.14. The strength of the correlation coefficients varied; the highest calculated r value between climate and wind, with sand percentage being 0.71 and lowest is 0.06 (values rounded in Table 5.4). In general the strongest correlations were found between precipitation, evaporation, or wind station variables from Station 94055 on Lake Michigan when correlated to sand percent.

The weakest correlations with the lowest r values were between sand percent and lake level, PDSI, temperature, or wind station ST94426. While it is suggested in other studies, the connection between lake level and sand mobility (Fisher et al., 2012), this is not captured by the data from this study. Furthermore, aspects of climate linked to lake level, such as temperature and drought index (PDSI) also share the weak correlation to sand percent; while variables such as precipitation and wind have the strongest. Evaporation varies between strong correlations in summer and winter, but weak correlations in fall.

The strongest correlations were negative, and found between average annual and summer evaporation; wetter conditions would be associated with sand mobility in this instance. Significant negative correlations were calculated between sand percent and precipitation, and between sand percent and various wind variables from buoy ST94055.

Wind correlations with sand percent suggest that fewer cumulative hours of high winds in fall and winter are linked to increased sand concentrations in cores. Concurrently, a higher ratio of cumulative hours of fall and winter winds above 7 m/s to annual cumulative hours is linked to lower concentrations in sand percent. A strong negative correlation was found between evaporation and sand percent, suggesting that wetter conditions are associated with increased sand percentages in lake sediment. Residual plots done for all statistically significant correlation results display no plots with severe heteroscedasticity, due to the general lack of extreme outliers. Mild to no skew is detectable in residual plots of the climate and wind variables (Appendix E).

Table 5.4 Correlation coefficients, P values and R² values from Pearson's Correlations run between climate data and sand percentages through time, assuming unequal variance. Only strong statistically significant R² values are shown.

CORRELATION COEFFICIENTS FOR CLIMATE DATA and SAND PERCENT			
Climate Variable	Correlation Coefficient (r)	P	R ²
Annual Lake Level	0.14	0.429	
Annual Precipitation	-0.54	0.002	0.29
Summer Precipitation	-0.37	0.042	0.14
Fall Precipitation	-0.23	0.007	0.05
Winter Precipitation	-0.26	0.151	
Annual Evaporation	-0.62	0.001	0.39
Summer Evaporation	-0.71	0.000	0.50
Fall Evaporation	0.25	0.227	
Winter Evaporation	-0.22	0.269	
Annual Temperature	0.06	0.766	
Summer Temperature	0.15	0.471	
Fall Temperature	0.09	0.670	
Winter Temperature	0.12	0.580	
Annual PDSI	-0.09	0.605	
Winter PDSI	-0.06	0.740	
Fall PDSI	-0.15	0.419	
Summer PDSI	-0.08	0.682	
ST_94055 Hrs >7m/s	-0.20	0.446	
ST_94055 Hrs >10m/s	-0.51	0.052	0.26
ST_94055 Hrs >15m/s	-0.48	0.067	0.24
ST_94055 F/W	-0.45	0.094	0.20
ST_94055 Ratio	-0.65	0.008	0.43
ST_94226 Hrs >6.5m/s	-0.30	0.278	
ST_94226 Hrs >10m/s	-0.14	0.580	
ST_94226 Hrs >15m/s	-0.13	0.615	
ST_94226 F/W	-0.11	0.661	
ST_94226 Ratio	0.31	0.229	

5.6 Summary

Correlations show varied results between climate and sand percent. The strongest and most significant results were negative correlations between sand percent and precipitation, evaporation, and wind variables for years 1956-1997. These results suggest that wetter conditions (more precipitation) decrease sand transport into the lake, higher cumulative hours of strong winds lead to lower sand concentrations, and that more evaporation leads to less sand in sediment cores from within lakes downwind of dunes.

Results for linear regressions performed between climatic factors and sand percentages from core OL-G3, show that when correlating environmental forcing on dune activity, few correlations were statistically significant ($p > 0.1$, due to the random noise in environmental data), and positivity versus negativity was inconsistent throughout the correlations (Table 5.5). In summary, average precipitation (annual/fall), average evaporation (annual/summer), and wind (primarily concerning fall and winter winds) had moderate statistically significant relationship to sand percentages and ST94055 wind data found in sediment from lake cores downwind of dunes. An unexpectedly low r value was calculated between lake level and sand percentage ($r = 0.14$). Statistically non-significant correlations were calculated between PDSI and temperature, and sand percent (Table 5.4).

The results from visual correlations suggest stronger relationships between lake level and PDSI than the statistically generated R^2 values, while visual comparisons supported the statistical connections with wind. Lake level appeared to be important entering into or at high levels during times of increased sand percentages. Winter PDSI shows that wet conditions coincide with increased sand percentages. Results for wind

were positive, but off-set, showing increased sand concentrations in proximity to years with more cumulative hours of high wind conditions.

Chapter 6

Discussions

6.1 Introduction

The stages of closure of the abandoned Kalamazoo River channel are discussed first, and then, the links between climatic factors and the mobility of eolian sediment are explained. Lastly, the findings are compared to other regional studies and sources of error are considered.

6.2 Infilling of the Kalamazoo River Mouth

The channel's depositional history can be explained using historical photographs (Figure 3-2), grain size distribution (Figure 5-3), ground penetrating radar (GPR) (Figures 4-2 to 4-7), and lithology (Figures 5-1, 5-5 and 5-6), with assistance from the local Saugatuck residents. There is an increase in smaller particle sizes, and organic material from the bottom to the top of the Livingstone core (Figure 4-1) suggesting a transition from a beach/fluvial system to a lacustrine one. The base is composed of sand with interspersed pebbles, indicative of high-energy beach and fluvial environments. Particle size fines upward and organics become more abundant towards the top of the

core. Silt and organic-free sand records channel flow able to flush the channel of sediment smaller than fine and medium sand, while interspersed pebbles indicate episodes of storminess - energy high enough to carry littoral sediments into the river channel. The appearance of silt and organics represents a change in the type and energy of the depositional environment. The transition from fluvial sand to silty organics suggests a transition to a lacustrine environment.

THE CHANNEL:

The Kalamazoo River was diverted in 1906 and the mouth began infilling due to lack of outflowing water. The first accretionary features seen in historical photographs (Figure 3-2) are from 1905-1906 and GPR lines of the original Kalamazoo River mouth, that indicate sediment accumulating on the north side of the channel. This evidence is supported by analysis of GPR lines SAUG-01 and SAUG-02 (Figures 4-2 to 4-3), where infill packages appear to be dipping south and accreting against the north side of the channel. A subsequent photograph from 1912 shows extensive sand accretion against the northern side of the Kalamazoo River outlet, which is in agreement with GPR data collected across the abandoned river channel. Littoral sedimentation in the abandoned river mouth leads to closure of the channel by 1920. This process can be inferred from the interpreted GPR data where sediment packages accrete against the north side of the channel until a wedge of sediment created a level infill surface across the channel's length and width. Once the channel was cut off, the low-lying beach would have left Oxbow Lake susceptible to sediment influx via storm surge during times of increased wave height in the years following channel closure.

Old maps of the study area show different shorelines than today (Figures 3-4 to 3-6). Before jetties were installed in either the new or old mouth of the Kalamazoo River, the shoreline was ~140 m inland from its current position. The shoreline prograded 100 m in 60 years, this includes the infilling of over half of the original channel width after the installment of the first pair of piers in 1867 followed by extensions in 1897 (Figure 3-5 to 3-6). After installment of the jetties in the current Kalamazoo River mouth (1906), the coastline prograded another 30 m by trapping sand to the north and south of the new jetties.

The emplacement of the northern jetties in 1906 may have accelerated the infilling of the abandoned Kalamazoo River mouth by increasing rates of shoreline progradation through increasing the volume of longshore transported sand deposited along the shore.

THE FOREDUNE:

Dated sediment transitions and historical photographs record the period of transformation from the Kalamazoo River channel to the small lake formed when foredunes separated Oxbow Lake from Lake Michigan with both data sets showing channel closure in 1920 and foredune development until ca. 1945. With an age of ~1929 ± 10 years for the silty deposits at a depth of 34 cm, it is feasible that the presence of silt records closure of the river mouth by ~1920. Between approximately 1920 and 1943, a foredune separating Oxbow Lake from Lake Michigan developed, preventing storm surges from reaching Oxbow Lake. These dates correspond to dated sediment showing a transition from sand to silty organic-rich sand by ca. 1945. In the Livingstone core,

lacustrine sediment (silt and organics) occurs at a depth of ~30 cm, and based on the age model would have been deposited in approximately 1943, indicating the development of a lacustrine depositional environment, undisrupted by storm surges along the coast. The increase in organics to the top of the core suggests that the dune ridge continued shielding the developing lacustrine system from storm surges. The decreased sand concentration shows a transition from low to high energy with increased depth, and supports the transition from a channel to a lagoon system undisturbed by storm surges. Surfaces of the foredune ridge are illustrated in Figure 4-6, and show at least 8 m of eolian sediment accumulation in a span of approximately 23 years (1920-1943); a sedimentation rate of ~ 0.35 m/yr of sand for this sand dune. This rate of sand accumulation is normal for the southwestern Lake Michigan shoreline, with some foredune accretion rates exceeding 30 cm/year (van Dijk, 2004). Rapid accumulation is likely in response to broad sandy beaches with high littoral sand transport rates (Figure 3-7).

The agreement between core lithology, age model, and historical photographs supports the interpretations that after foredune development Oxbow Lake was undisturbed by storm surges and primarily silt and organics were deposited.

6.3 Sand Percent and Climate

VISUAL COMPARISONS:

By visually comparing climate and sand percentage data, there appears to be a positive association between them. Based on the results, wet conditions (positive PDSI), increased lake level, and prolonged periods of high winds are associated with elevated sand concentrations in lake sediment downwind of the dunes. An explanation for wet

conditions and increased eolian sand transport could be the presence of strong winds associated with low pressure systems (mid-latitude cyclones) increasing both storminess and bringing precipitation. This also explains the association of sand with wind data. Visual comparisons show that increases in cumulative hours of wind over 6.5 and 7 m/s share a relatively good connection to the increased presence of sand through time. It is likely that the wetter conditions could be a side effect of increased storminess, as are high winds.

High lake levels can be linked to various climatic factors, primarily increased precipitation and decreased evaporation. The increased presence of sand with increased lake levels could be from erosion of coastlines as lake level rises, making more sand available for transport (Anderton and Loope, 1995). This erosion has the potential to destabilize dunes along the coast and create more sand to be eroded by wind, thereby increasing eolian sand in downwind lakes. Blow-out dunes along the shoreline occur at this study site allowing coastal erosion to be a possible effect of higher lake levels triggering more eolian sand transport; however, during the lifetime of Oxbow Lake, a broad sandy beach with active foredunes has been available as a sand source.

STATISTICAL CORRELATIONS AND REGRESSIONS:

Correlations were run on sand percent against climate and wind data for years with sand percentage values. The results showed significant negative correlations between evaporation (annual/summer), precipitation (annual/fall), and wind data (ST94055 variables). The negative correlations found would suggest there is a strong connection between the appearances of sand in lakes downwind of dunes with wetter

(less evaporative) conditions. This may be due to several factors including, but not limited to, increased humidity during times of increased storminess and higher wind conditions.

The significant negative correlations between annual and summer precipitation could suggest that lower precipitation, which is linked to drier conditions, is crucial for sand mobility. An annual trend of low precipitation would allow the ground to dry, making the sand more susceptible to transport. Summer time would have strong winds coming off of Lake Michigan, as well as an increase in temperature creating drier conditions.

Wind impacts many of the other climatic forces correlated to sand percent. Alone, it too has a strong relationship with the appearance of sand percent in lakes downwind of dunes. The strongest correlation results for wind were found between the ratio of cumulative annual fall and winter hours to annual hours of wind blowing at velocities of >7 m/s and sand percent, as well as cumulative annual hours blowing >10 m/s. This was followed in significance by cumulative annual hours of wind >15 m/s. The first wind variable tested the proportion of fall and winter winds to the sum of all winds >7 m/s annually. The negative correlation between this ratio and sand percent suggests that a lower portion of cumulative annual hours in fall and winter, and perhaps a greater portion of wind in summer (speculation) leads to more sand. Based on these results, it is clear that there is a strong statistically significant correlation between less fall and winter winds, and sand percent. These results are not intuitive; especially when previous studies suggest that the strongest winds blow in fall and winter, and that sand-laden snow carries large amounts of sand greater distances as well as over lake surfaces in winter.

Varying wind speeds and their relationship to sand signals were tested, and of the calculations >10 and >15 m/s came up with the most significant correlations. The negative correlations initially seem counterintuitive; however, high winds are usually accompanied by storminess and precipitation. If this is the case, then the appearance of a windy cold front bringing precipitation along with strong and sudden high winds would result in less sand mobility upon the arrival of strong winds due to an increase in ground moisture. So the negative correlation is capturing, in essence, the correlation between precipitation with windiness, and sand mobility.

6.4 Application

Results and discussions are contrasted with past publications and previous research. The results argue against the position taken by Fraser (1990) that high lake levels lead to soil formation on dunes adjacent to the Lake Michigan shoreline. From statistical test done for this study, high lake levels are not associated with increased eolian activity, suggesting that dune stability and lake level highs are not strongly related phenomena. If such a connection could be made, it would redefine the environmental conditions that are suggested by paleosols in sand dunes along the coastline of Lake Michigan, such as the Holland Paleosol traced along the eastern rim of Lake Michigan (Arbogast et al., 2004).

The idea that low lake levels lead to increased eolian sand deposits is supported by Thompson and Baedke (1997), who also correlate high stands to beach ridges. The results of visual comparisons of lake level trends and sand percent trends through time in

this study favor high lake levels and increased sand mobility. The associated mechanism may be increased lake levels destabilizing dune faces, thereby increasing available sand exposed to wind erosion along the shore (Anderton and Loope, 1995). Such conclusions have also been made by Fisher and Loope (2005), Timmons et al. (2007), and Fisher et al. (2010). High lake levels are associated with increased precipitation, typically brought on by increased storminess.

In response to findings by Fisher et al. (2012), using correlations from this study, very little can be said for the relationship of PDSI and sand percentage found in lake cores from the statistical tests. It has been suggested that eolian activity is more active in winter months in the Great lakes region (Marsh and Marsh, 1997), and that sand moves with snow further out into the lake basin during winter time across a frozen surface (Lewis et al., 2002; Fisher et al., 2007, 2012) - potentially due stronger wind conditions in winter. Winter conditions (highly gusty winds and sand-laden snow) should lead to an increase in eolian sand mobility, which was not observed statistically in this study. In fact the strongly negative statistically significant results would support the decrease of sand transport during time of high wind, including winds focused in fall and winter. Visual comparisons between trends of Winter PDSI, wind >7 m/s, and sand percent support a relationship between them, and are generally a positive one.

6.5 Sources of Error

The variability of wind directions at the study site has the potential to blow sand into Oxbow Lake from all of the dunes surrounding it, affecting the sand signal retrieved from the cores. These are details that may need to be considered during more in depth

studies of sand movement at this site. The proximity of all dunes surrounding Oxbow Lake allows for the possibility that the activity of multiple dunes may have been recorded in the sand signals; those signals would be indistinguishable from each other. This study primarily considers sand signals from the foredune ridge separating Oxbow Lake from Lake Michigan, and the nearest dunes on the north side of the lake (Figure 6-1). The highest wind speeds occur during fall and winter, from the NW to SW quadrant. These winds move large amounts of sand from all areas where eolian erosion is possible. Shown in Figure 6.1, winds from all directions have the potential to introduce sand from dunes surrounding Oxbow Lake, diluting consideration that the sand is sourced from the foredune ridge to the west and dunes along the north side of the lake.

There are very few strong correlations between wind and sand concentration, and no consistently positive or negative connections found. At times, R^2 values were as high as 0.50 to 0.33 for all Glew cores but dated core G3. Core G3 had the lowest R^2 highs between the cores (Appendix E); however, the R^2 values from these correlations show wind and sand concentrations having both positive and negative relationships, even between the same variables. A possible cause for the inconsistency in results between wind and sand concentrations stems from the variety of sand sources surrounding the lake. Sediment traps deployed around and in the lake could be necessary to better understand this relationship. If the dunes bordering Oxbow Lake contribute sand at different times and from different directions (Figure 5-17), correlations between sand concentrations in lake sediment and specific combinations of wind directions and speeds will be ineffective. Thus, connections between wind and eolian sand transported into

Oxbow Lake could exist, but are weak and inconclusive due to the noise in the data from sand signals of surrounding dunes, unrelated to those used in this study.

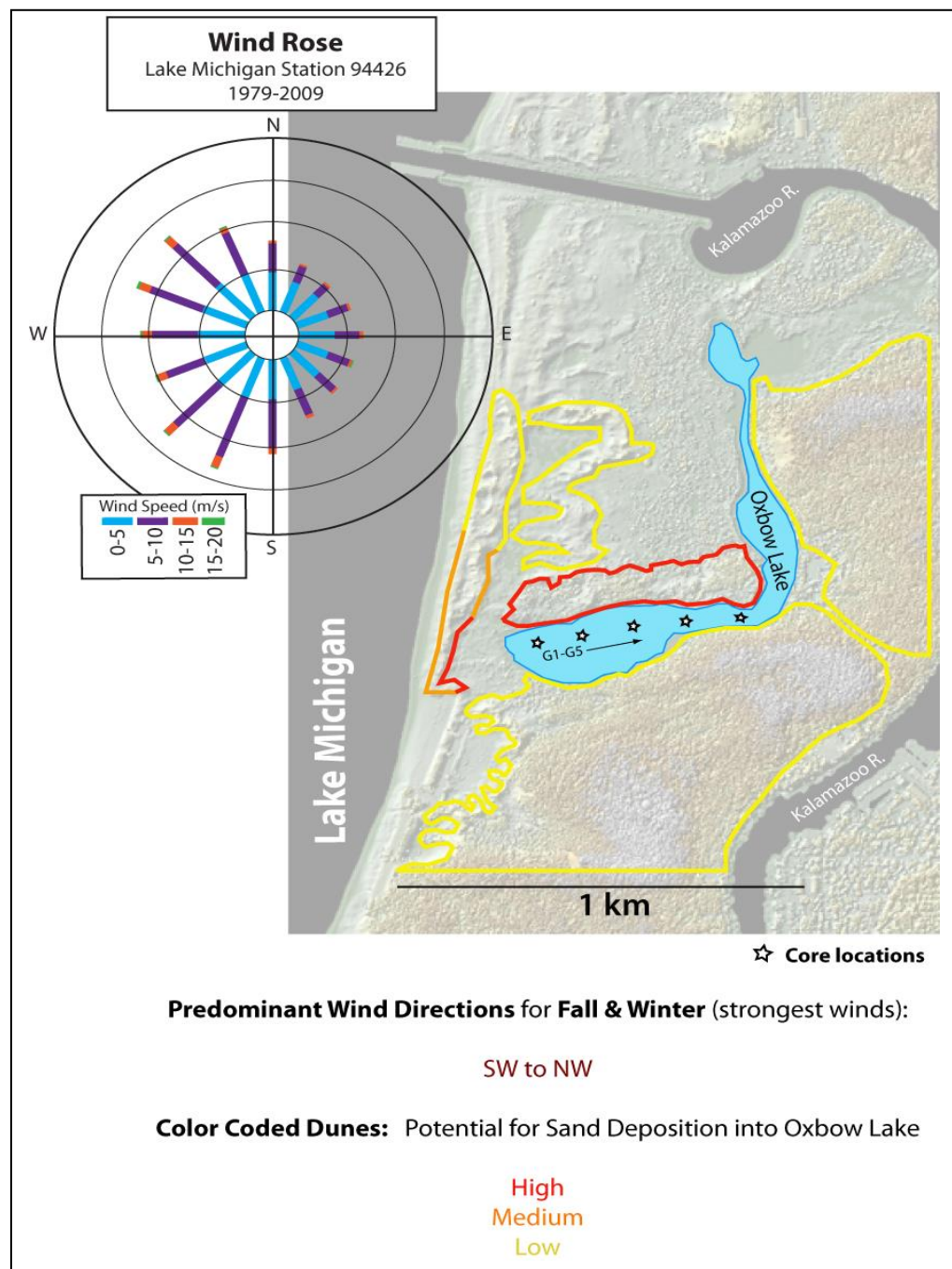


Figure 6-1 Potential sources of sand to be transported into Oxbow Lake from adjacent dunes. Winds from the southwest and northwest are strongest during winter.

Chapter 7

Conclusion

7.1 Infilling of the Kalamazoo River Mouth

It was the objective of this study to show that historical photographs, sediment cores, and GPR can be cross-referenced, and used to reconstruct the processes of infilling of a channel mouth within the time frame of photographic evidence. This work elucidates processes along the Lake Michigan coastline, and the results indicate that historical photographs can be used in conjunction with GPR profiles and core samples to reconstruct the depositional history of the Kalamazoo River mouth through time. Sediment packages revealed by GPR were correlated with different stages of infilling the abandoned Kalamazoo River mouth, as seen in selected photographs. It was determined using this method that the channel went from a fluvial system in 1905, to a low-energy, mostly closed body of water separated from Lake Michigan by a beach by 1920. During this time several meters of sand were deposited in the west end of the lake, and overlain by finer sediment. After 1920, sedimentation switched from muddy sand to a sapropel. The dates for these organic sediments coincide with the growth of foredune ridges, shielding Oxbow Lake from storm surges. The organic sediment continues to accumulate within the small lake with episodic influxes of eolian sand.

7.2 Sand Percent and Climate

Eolian sand concentrations in the sediment cores (sand signals) from Oxbow Lake were hypothesized to correlate to trends in climate (aridity, storminess and high lake level) through time. Visual comparisons (wiggle matching) between climate data and sand percentages through time correlate within the dating error of the sediment. Specifically, it was noted that peaks in sand correlate with peaks in wetter conditions (high PDSI), elevated lake level, and sustained high winds.

Following correlations between sand percent and various climate factors the most significant were the negative correlations between precipitation, evaporation, and lower cumulative hours of high winds with sand percentage by weight found within lake sediment cores. These results suggest that drier conditions (low precipitation and low evaporation) lead to higher concentrations of sand. Also, fewer cumulative hours of strong winds both in fall and winter, and the ratio of fall and winter hours to annual hours (fall and winter being the time of the strongest winds from NW to SW) lead to greater amounts of sand in the cores. Cumulatively, these results would suggest that periods of drier climates (low precipitation) where wind is not constant (low wind and evaporation), but perhaps more gusty, leads to greater sand concentrations.

Linear correlation and regression analyses of sand percentages with various individual climate variables (lake level, temperature, precipitation, evaporation, and wind), were mostly low to non-existent. These results indicate a low predictability of one variable with the other. When correlations were statistically significant (95%), they were neither consistently positive nor negative. Only precipitation gave consistently negative correlations to sand percentage. The conclusion is that the statistical methods employed

in this study, between individual measures of climate and eolian sand activity may have been inadequate means of analysis. Conversely, as illustrated by visual comparisons of plots for lake level, PDSI, and sand concentration through time, the correlation only exists when there are sand peaks, suggesting that high lake levels, cyclonic activity and strong winds are conditions necessary for eolian activity in the study area.

7.3 Future Work

During the course of this project, various aspects of this research were examined and ideas for future work considered. Further studies done to the dunes surrounding Oxbow Lake would be beneficial to this study as well as any studies done in this area on eolian sand movement, such as those being performed 0.5 km north, on a dune instrumented by researchers from Hope College. Their research activity is designed to quantify sand transport, erosion and deposition on a small parabolic dune. Observations of dunes surrounding Oxbow Lake could include measuring sand transport gauged by seasonal sediment traps and measuring heights of sand in the air column. During winter, sand surveys in snow and on the lakes would quantify the volume of sediment moving during the winter months by suspension and saltation. The knowledge of sand movement of surrounding dunes would even benefit the community around the study site, concerning future human development on and around the dunes.

Another difficulty encountered in this study was the statistical analysis. Many of the statistics were only rudimentary. Using single variable linear regressions was a good method for checking for year to year or lagging yearly correlations; however, after considering the variability of each core, and lack of correlation between sand percent

values and a single climatic variable, a multivariate linear regression may be a better suited technique. This method for analysis would use a single core, and by simultaneously comparing different climatic variables to sand percentage, may elucidate stronger statistical correlations with sand signals.

Because it was found that stronger sand signals were generally found eastward in Oxbow Lake, determining the source of the sand at each coring location is important. While it has been assumed that eolian processes brought the sand to the coring sites (lake sediment), this was not proven in this study. The study was concerned with regional climate factors affecting the dune ridge to the west of Oxbow Lake, but the same climatic factors would be affecting the surrounding dunes. Whether all dunes surrounding the lake behave the same way in response to climate factors remains unknown.

References

- Alley, W. M. (1985), The Palmer Drought Severity Index as a Measure of Drought. JAWRA Journal of the American Water Resources Association, 21: 105–114. doi: 10.1111/j.1752-1688.1985.tb05357.
- Anderton, J. B., and Loope, W. L., 1995, Buried soils in a perched dunefield as indicators of Late Holocene lake-level change in the Lake Superior Basin: Quaternary Research, v. 44, p. 190-199.
- Arbogast, A., Loope, W. (1999). Maximum-limiting ages of Lake Michigan coastal dunes: their correlation with Holocene lake level history. *Journal of Great Lakes research*, v. 25 (2), p. 372-382.
- Arbogast, A., Hansen, E., Van Oort, M. (2002). Reconstructing the geomorphic evolution of large coastal dunes along the southeastern coast of Lake Michigan. *Geomorphology*, v. 46, p. 241-255.
- Arbogast, A., Schaetzl, R.J., Hupy, J.P., and Hansen, E.C. (2004). The Holland Paleosol: An Informal Pedostratigraphic Unit in the Coastal Dunes of Southeastern Lake Michigan. *The Canadian Journal of Earth Sciences*, v. 14, p. 1385-1400.
- Argyilan, E.P. and Forman, S.L. (2003). Lake level response to seasonal climatic variability in the Lake Michigan-Huron system from 1920 to 1995. *Journal of Great Lakes Research*, v. 29, p. 488-500.
- Baird, W.F., et al. Saugatuck Harbor Impact Assessment. Detroit District USACE.
- Baedke, S.J., and Thompson, T.A. (2000). A 4,700-year record of lake level and isostacy for Lake Michigan. *Journal of Great Lakes Research*, v.26, p. 416-426.

Bishop, C.T. (1990). Historical Variation of Water Levels in Lakes Erie and Michigan-Huron. *Journal of Great Lakes Research*, v. 16 (3), p. 406-425.

Donnelly, J.P., Roll, S., Wengren, M., Butler, J., Lederer, R., Webb, T. (2001) Sedimentary evidence of intense hurricane strikes from New Jersey. *Geology*, v.29 (7), p.615-618.

Fisher, T. G., and Loope, W. L., (2005). Aeolian sand preserved in Silver lake: A reliable signal of Holocene high stands of Lake Michigan: *The Holocene*, 15(7): 1072–1078.

Fisher, T.G., Loope, W.L., Pierce, W.C., and Jol, H.M., (2007). Big lake records preserved in a little lake's sediment: an example from Silver Lake, Michigan, USA. In: Karrow, P. and Lewis, C.F.M. (Eds.) *The Greater and Lesser Great Lakes, Journal of Paleolimnology* 37: 365–382.

Fisher, T. G., Weyer, K. A., Boudreau, A. M., Martin-Hayden, J. M., Krantz, D. E., and Breckenridge, A., 2012, Constraining Holocene lake levels and coastal dune activity in the Lake Michigan basin: *Journal of Paleolimnology*, v. 47, no. 3, p. 373-390.

Fraser, G.S., Larsen, C.E., Hester, N.C. (1990). Climatic control of lake levels in the Lake Michigan and Lake Huron basins. In: Schneider, A.F., and Fraser, G.S., eds., Late Quaternary history of the Lake Michigan basin: Boulder, CO, Geological Society of America Special Paper, v. 251, p. 75-89.

Gottgens, J.F. (1996). Radionuclide dating of sediment cores. In: Protocol for Estimating Historic Atmospheric Mercury Deposition, M.E. Keirstead, D.B. Porcella (Eds.), EPRI, Palo Alto, CA: 4.4-4.9

Hanes, B.E. (2010). Paleo-storminess in the southern Lake Michigan basin, as recorded by eolian sand downwind of dunes. Published MS Thesis, Dept. of Environmental Sciences, University of Toledo, Toledo, OH.

Hansen, E., Fisher, T., Arbogast, A., Bateman, M. (2010). Geomorphic history of low-perched, transgressive dune complexes along the southeastern shore of Lake Michigan. *Aeolian Research*, v. 1, p. 111–127.

Hansen, E., DeVries-Zimmerman, S., Van Dijk, D., Yurk, B. (2009). Patterns of wind flow and aeolian deposition on a parabolic dune on the southeastern shore of Lake Michigan. *Geomorphology*, v. 105, p. 147–157

Heiri, O., Lotter, A.F., Lemche, G. (1999). Loss on ignition as a method for estimating organic and carbonate content in sediments: reproducibility and comparability of results. *Journal of Paleolimnology*, v. 25, p. 101-110.

Jol, H. M., Bristow, C.S. (2003). GPR in sediments: advice on data collection, basic processing and interpretation, a good practice guide. *Geologic Society of London*, v. 211, p. 9-27.

Malvern Instruments, Ltd. (2007). Operators Guide, MAN 0247, Issue 2.0. Worcestershire, UK.

Malvern Instruments, Ltd. (1999). User's Manual, MAN 0387, Issue 2.0. Worcestershire, OK.

Kiesel, D., Mickelson, D. (2005). Influence of Lake Michigan Holocene lake level on fluvial sediments of the Lower Pigeon River, Wisconsin. *Journal of Great Lakes Research*, v. 31, p. 343-359.

Kirchner, G. (2011). ^{210}Pb as a tool for establishing sediment chronologies: examples of potential and limitations of conventional dating models. *Journal of Environmental Radioactivity*, v. 102, p. 490-494.

Lane, Kit. (2006). The Kalamazoo: Rivers of Michigan Series. Pavillion Press: Douglas, Michigan, p.114-118.

Lewis, T., Gilbert, R., and Lamoureux, S. F., 2002, Spatial and temporal changes in sedimentary processes at proglacial Bear Lake, Devon Island, Nunavut, Canada: *Arctic and Alpine Research*, v. 34, no. 2, p. 119-129.

Livingstone, D.A. (1955). A lightweight piston sampler for lake deposits. *Ecology*, v.36 (1), p. 137-139.

Loope, H.M., Loope, W.L., Goble, R.J., Fisher, T.G., and Jol, H.M. (2010). Early Holocene dune building linked to meltwater-driven lowering of glacial Lake Minong in eastern Upper Michigan, USA. *Quaternary Research* 74(1) 73-81

MacKenzie, A., Hardie, S., Farmer, J., Eades, L., Pulford, I. (2011). Analytical and sampling constraints in ^{210}Pb dating. *Science of the Total Environment*, v. 409, p. 1298-1304.

Olson, J. S. 1958. Lake Michigan dune-development. 3 Lake level, beach and dune oscillations. *Journal of Geology* 66, 473-483.

Peterson, J. M., and Dersch, E. 1981. A Guide to Sand Dune and Coastal Ecosystem Functional Relationships. Extension Bulletin E-1529, MICHU-SG-81-501, 18 pages.

Rust, B. (1982). Sedimentation in fluvial and lacustrine environments. *Hydrobiologia*, v. 91, p. 59-70.

Schnurrenberger, D., Russel, J., Kelts, K. (2003). Classification of lacustrine sediments based on sedimentary components. *Journal of Paleolimnology*, v.29, p.141-154.

Scileppi, E., Donnelly, J.P. (2007). Sedimentary evidence of hurricane strikes in western Long Island, New York. *Geochemistry Geophysics Geosystems*, v. 8(6), p.1-25.

Thompson, T.A., and Baedke, S.J. (1997). Strand-plain evidence for the late Holocene lake-level variations in Lake Michigan. *Geological Society of America Bulletin*, v. 109, p. 666-682.

Thompson, T. A., Lepper, K., Enders, A., Johnson, J., Baedke, S. J., Argyilan, E. P., Booth, R. K., and Wilcox, D. A. 2011. Mid-Holocene lake level and shoreline behavior during the Nipissing phase of the upper Great Lakes at Alpena, Michigan, USA. *Journal of Great Lakes Research* 37, 567-576.

Timmons, E., Fisher, T., Hansen, E., Eisaman, E., Daly, T. Kashgarian, M. (2007). Elucidating aeolian dune history from lacustrine sand records in the Lake Michigan Coastal Zone, USA. *The Holocene*, v. 17(6), p. 789–801.

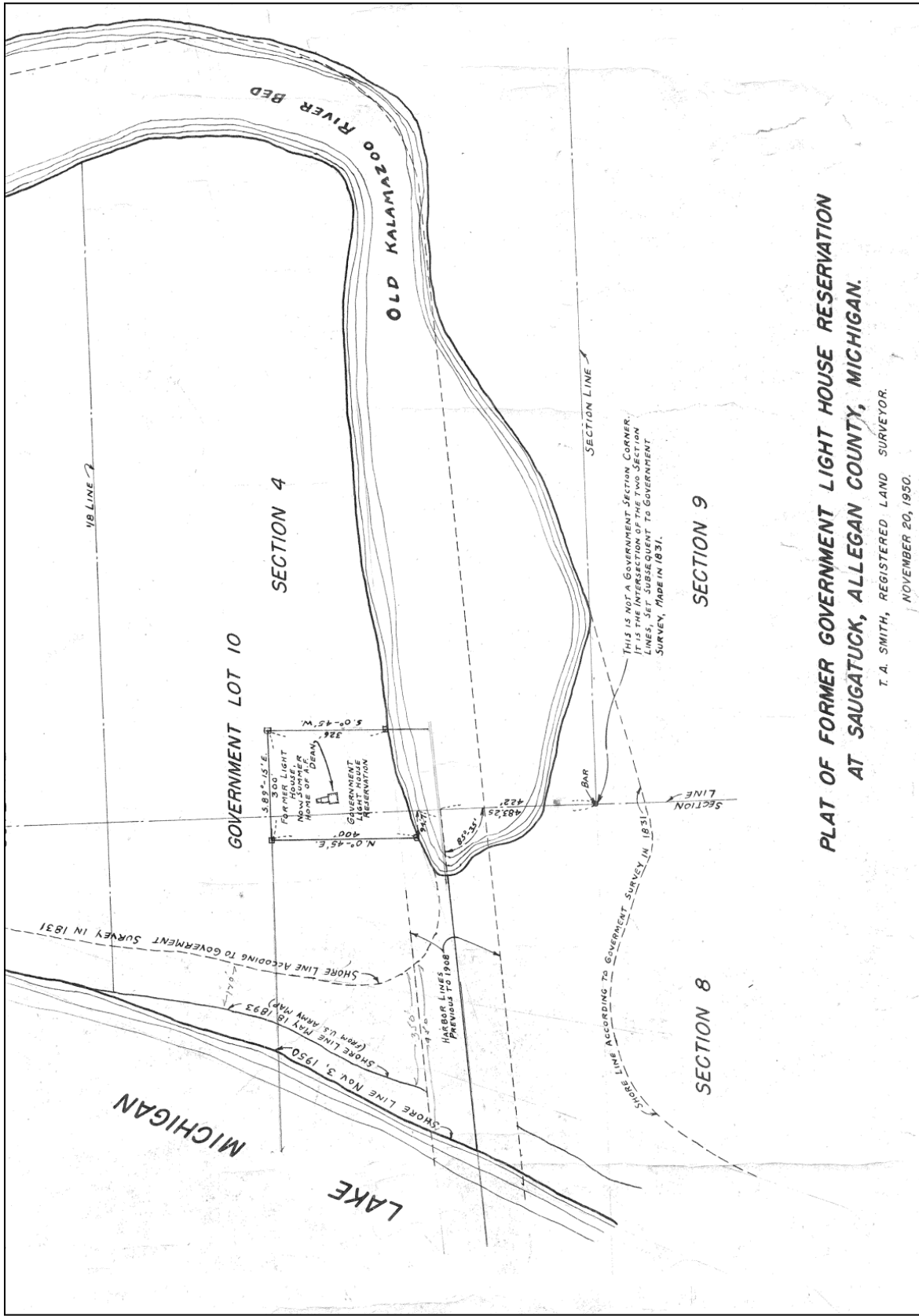
Tomkins, J.D., Antoniades, D., Lamoureux, S.F., Vincent, W.F. (2007). A simple and effective method for preserving the sediment-water interface of sediment cores during transport. *Journal of Paleolimnology*, v. 40 (1), p. 577-582.

van Dijk, D., 2004, Contemporary geomorphic processes and change on Lake Michigan coastal dunes: an example from Hoffmaster State Park, Michigan: Michigan Academician, v. 35, no. 4, p. 425-453.

Wright, H.E., Mann, D.H., Glaser, P.H. (1984). Piston corers for peat and lake sediments. *Ecology*, v.65(2), p.657-659.

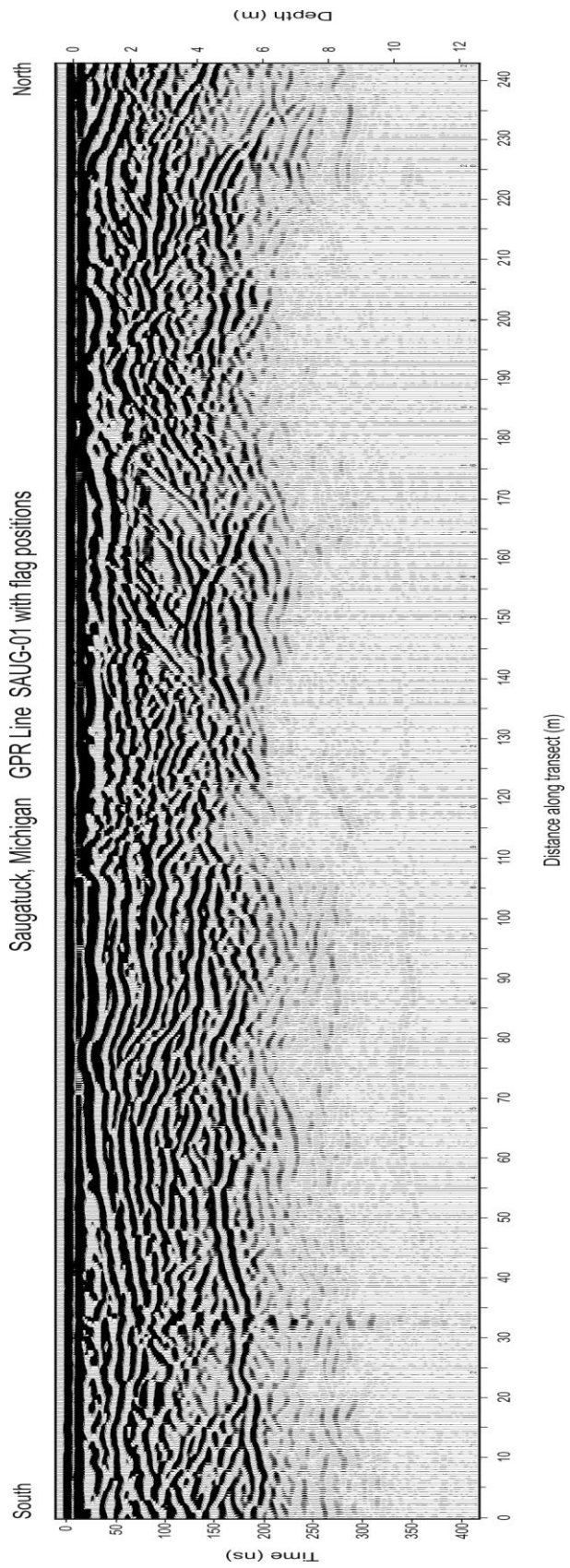
A.

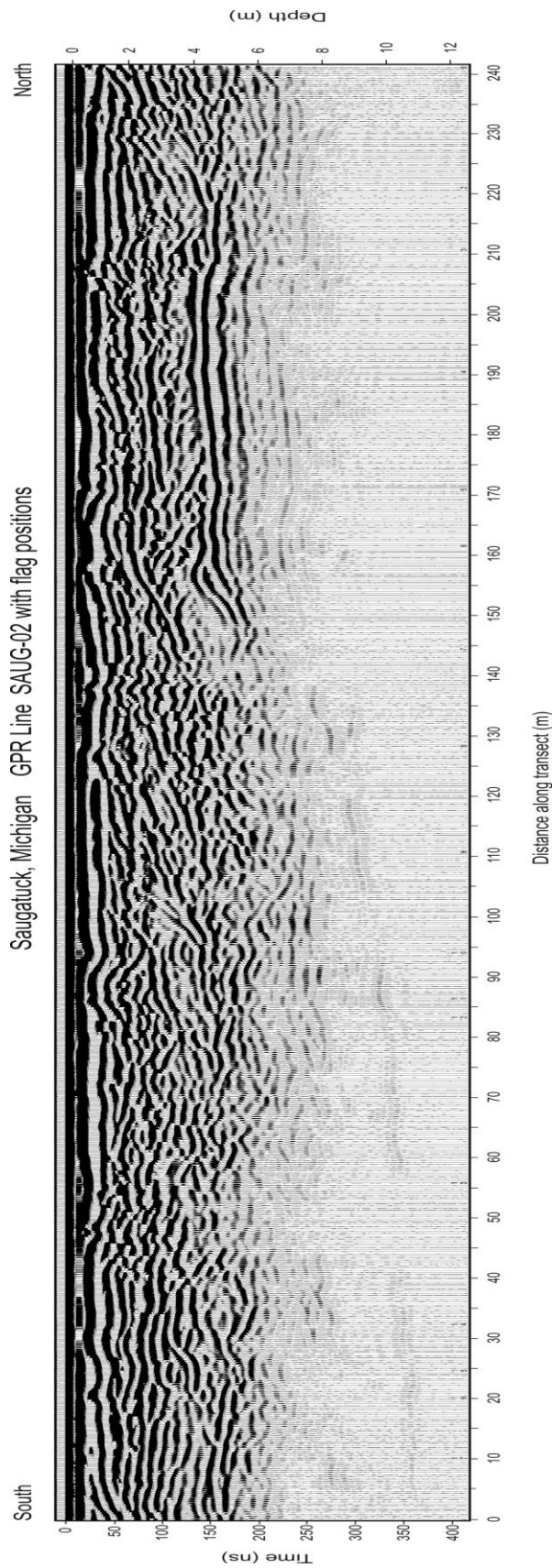
Historic Maps and Images

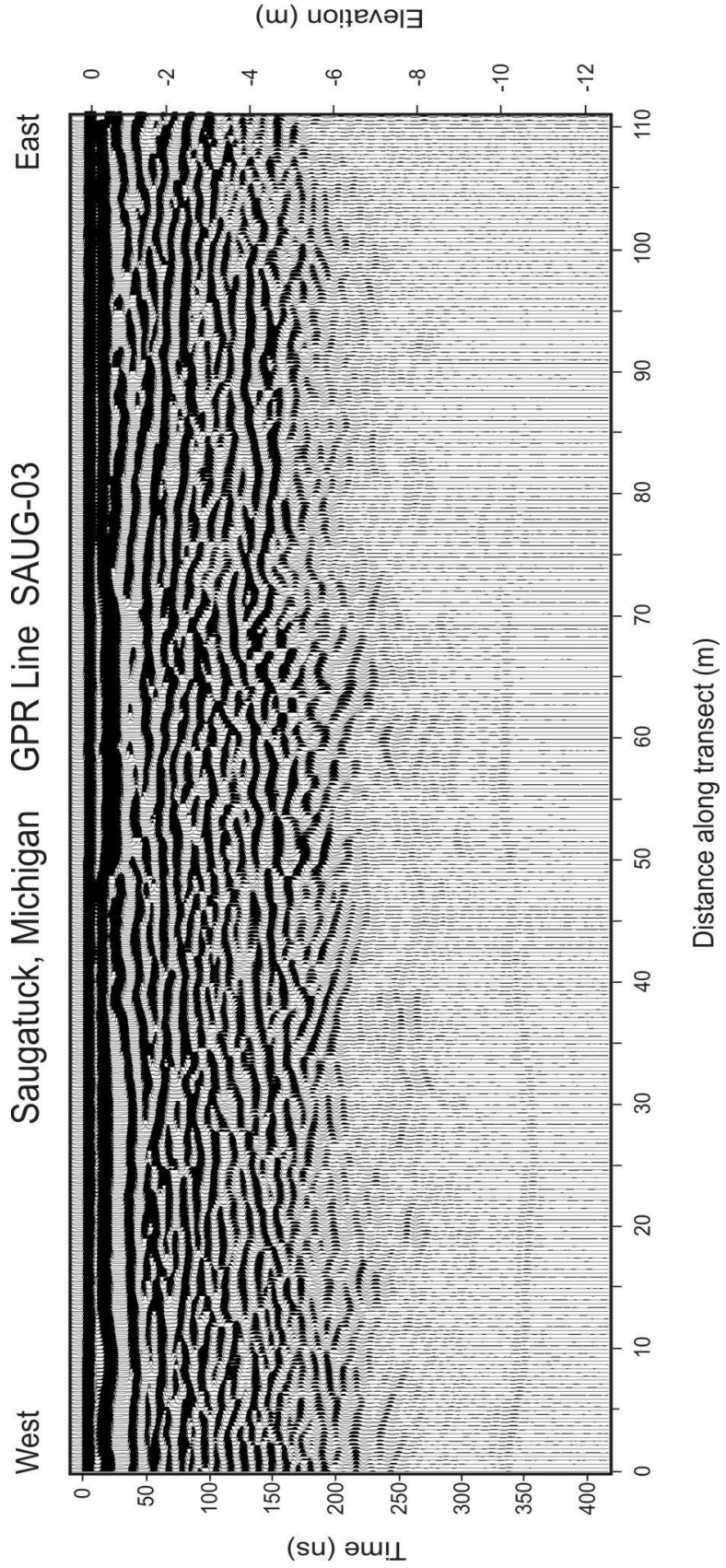


B.

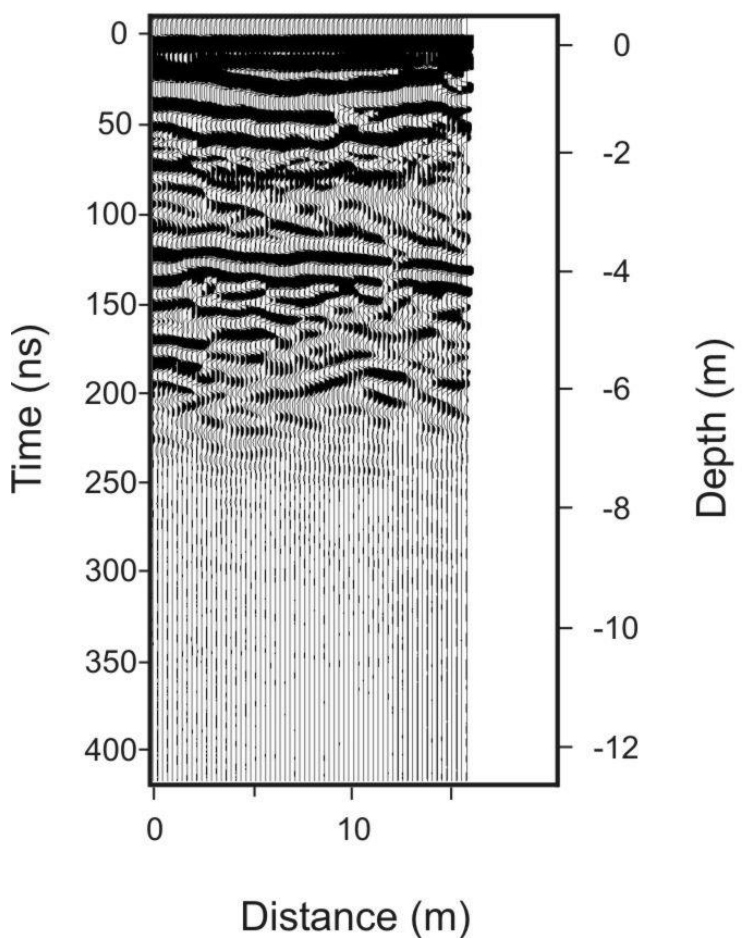
Raw GPR Data

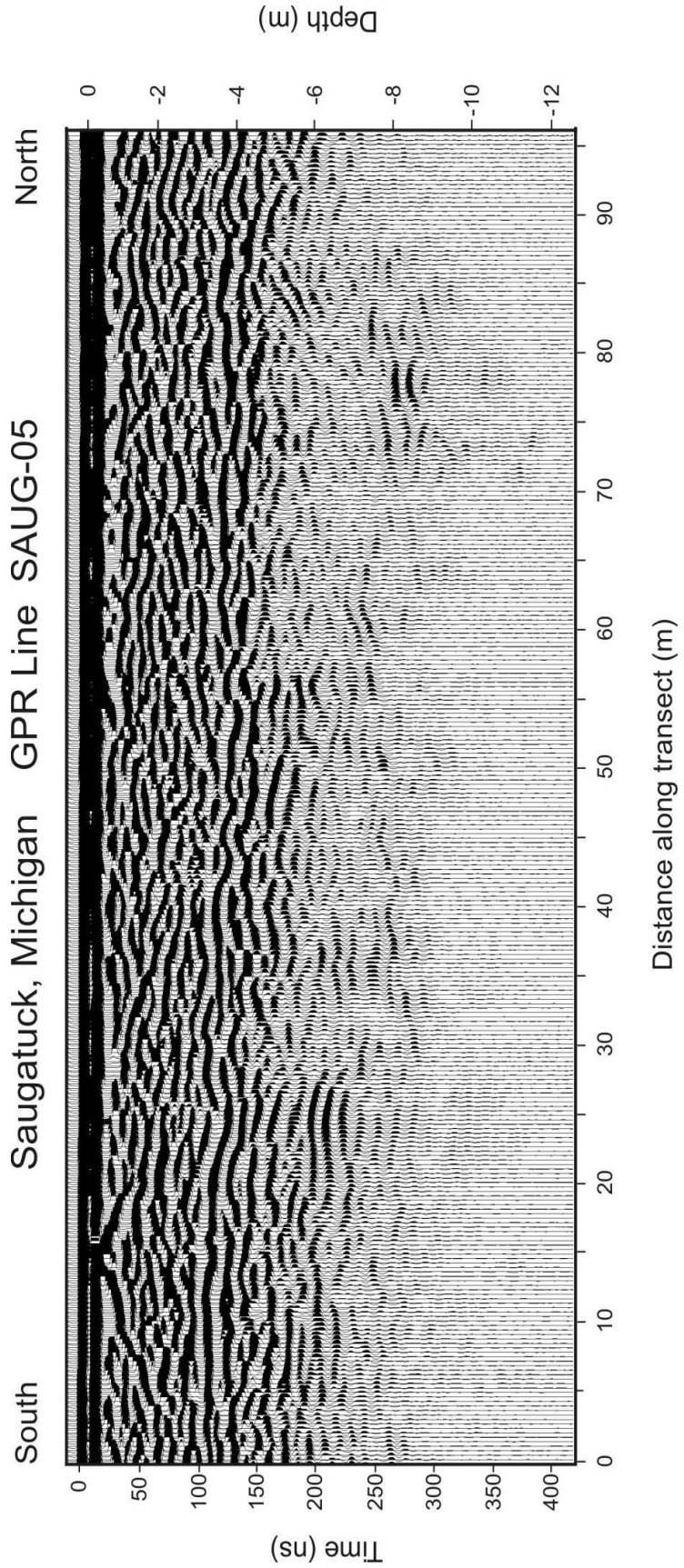


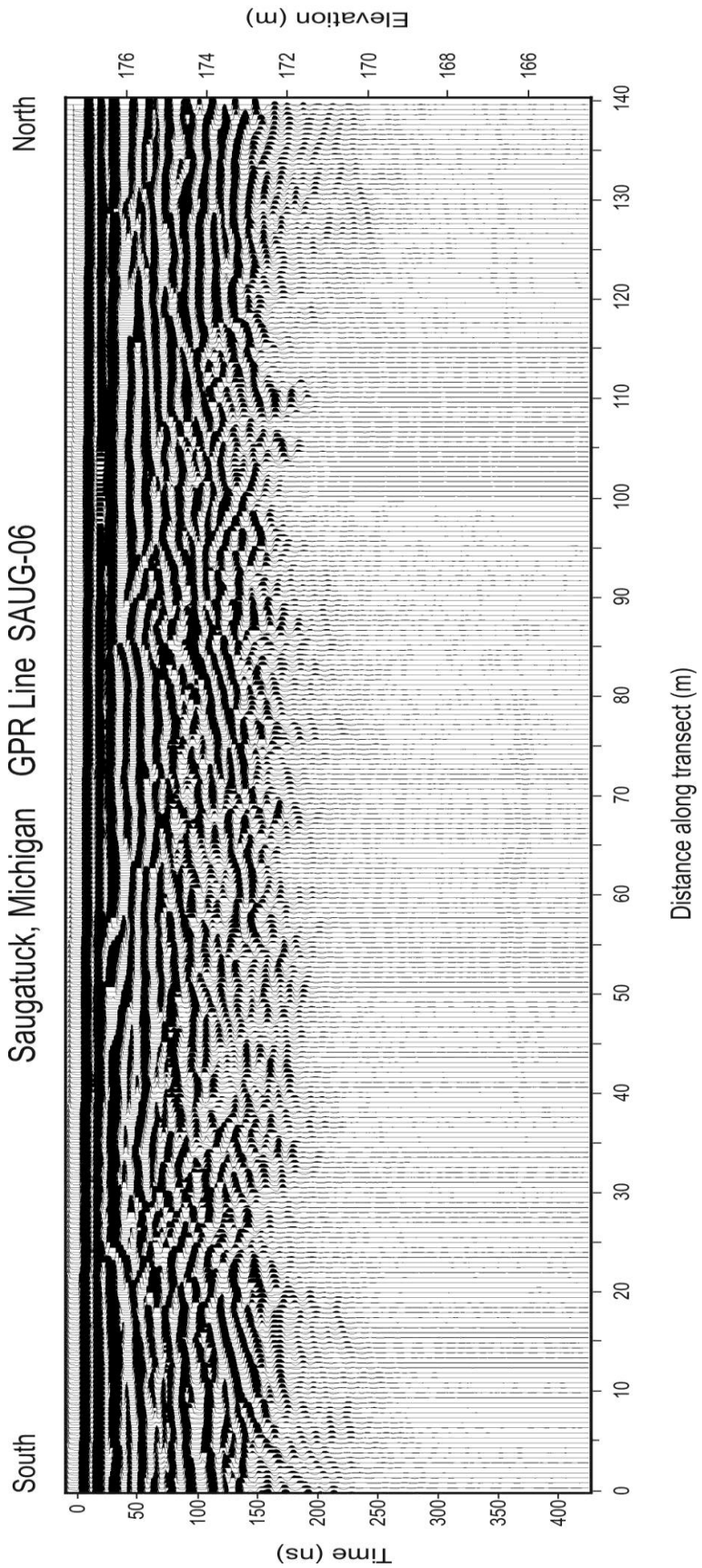




W SAUG-04 E







C.

Sediment Analysis Data

BULK DENSITY CALCULATIONS (OL-G3)				
Sample #	Avg Depth (cm)	Wet Sed. (g)	Dry Sed. (g)	Bulk Density
1	0.5	0.9314	0.0224	0.0224
2	1.5	0.8802	0.0381	0.0381
3	2.5	0.957	0.0492	0.0492
4	3.5	1.0871	0.0705	0.0705
5	4.5	0.9791	0.0719	0.0719
6	5.5	1.0401	0.0734	0.0734
7	6.5	0.9926	0.0748	0.0748
8	7.5	0.9702	0.0808	0.0808
9	8.5	1.0571	0.0853	0.0853
10	9.5	1.0022	0.0679	0.0679
11	10.5	1.0387	0.0955	0.0955
12	11.5	1.0484	0.1091	0.1091
13	12.5	1.0061	0.0856	0.0856
14	13.5	1.1156	0.1093	0.1093
15	14.5	1.0629	0.1138	0.1138
16	15.5	1.0495	0.1027	0.1027
17	16.5	1.0323	0.1028	0.1028
18	17.5	1.0762	0.1242	0.1242
19	18.5	1.0625	0.1211	0.1211
20	19.5	1.1474	0.1288	0.1288
21	20.5	1.0867	0.1408	0.1408
22	21.5	1.0779	0.1261	0.1261
23	22.5	1.0838	0.1633	0.1633
24	23.5	1.126	0.1733	0.1733
25	24.5	1.0639	0.1467	0.1467
26	25.5	1.1078	0.1668	0.1668
27	26.5	1.0881	0.1826	0.1826
28	27.5	1.22	0.2984	0.2984
29	28.5	1.2161	0.2933	0.2933
30	29.5	1.5941	0.8541	0.8541
31	30.5	2.1074	1.5817	1.5817
32	31.5	1.833	1.2932	1.2932
33	32.5	2.055	1.4916	1.4916
34	33.5	2.0442	1.5958	1.5958

35	34.5	2.0418	1.5532	1.5532
36	35.5	1.7976	1.4377	1.4377
37	36.5	1.9081	1.5257	1.5257
38	37.5	1.9145	1.5027	1.5027
39	38.5	1.9176	1.5413	1.5413
40	39.5	2.0678	1.6751	1.6751
41	40.5	1.835	1.4721	1.4721
42	41.5	2.006	1.5871	1.5871
43	42.5	1.792	1.397	1.397
44	43.5	1.8966	1.4928	1.4928
45	44.5	1.9812	1.5857	1.5857
46	45.5	1.8349	1.263	1.263
47	46.5	1.9263	1.398	1.398
48	47.5	2.1172	1.6914	1.6914

Organic Loss on Ignition for OL-G3 with Depth					
Avg Depth	G1	G2	G3	G4	G5
0.5	22.5674571	13.0306022	34.1433779	30.296827	33.4957369
1.5	19.5469256	23.4210526	31.1184939	29.0262172	25.3558719
2.5	16.4477441	19.7461213	31.2348668	31.0344828	28.5714286
3.5	18.5325743	17.0679508	31.4496314	28.7332647	29.4234592
4.5	22.2977566	20.2991453	30.6122449	29.2982456	27.6657061
5.5	18.115942	11.7085863	30.1546392	30.1818182	27.21843
6.5	19.3002257	16.7249417	28.2110092	26.619965	26.0667184
7.5	20.9812782	18.9171559	25.0676285	27.7580071	24.6130031
8.5	11.2601483	14.5953118	28.8968825	26.6819572	16.3567
9.5	12.5084289	13.9554795	27.9912184	23.0651341	20.6455952
10.5	10.6532357	13.5303266	28.460039	24.6049661	20.7614515
11.5	14.4880615	16.2149955	26.8798617	24.6051538	25.9651308
12.5	16.172043	7.14285714	24.3794326	23.4672304	23.0858469
13.5	20.7931404	4.3961276	26.9589552	23.7077877	16.0203139
14.5	21.3997986	5.66793893	26.7080745	5.64292322	26.6267764
15.5	11.6773442	2.06196468	27.9182879	25.6055363	25.1784555
16.5	12.3068117	1.87160184	28.3472803	26.2443439	24.6753247
17.5	8.18791946	0.49542363	28.4428443	24.4262295	24.3421053
18.5	1.90514795	0.58027079	26.6426643	21.464108	20.7656613
19.5	0.84259259	0.85790885	27.7727683	19.1807542	26.4099037
20.5	1.30027215	0.29913252	27.0962048	10.3136309	30.7438017
21.5	0.7547513	0.22791575	19.5037507	4.82333146	31.3669065
22.5	1.08632955	0.21880128	9.37779101	3.24611207	31.6653636
23.5	1.38124312	0.18768498	20.6042296	5.07042254	12.0189773
24.5	2.50926238	0.08114249	23.0267449	2.68154414	11.1566618
25.5	0.25998582	0.10906711	24.1299304	2.37835875	2.99412368
26.5	1.63689167	0.11618619	20.8015267	1.79531728	1.09714103
27.5		0.16723624	9.03062835	1.60271977	0.76987575
28.5		0.21452651	7.37386805	5.74497315	0.74104855
29.5		0.22871477	9.93330993	5.55491925	0.64564192
30.5		0.21397477	1.04924068	4.65241216	0.62509193
31.5		0.25559439	0.68790049	3.49885139	
32.5		0.38374906	0.8941094	5.20811099	0.78586738
33.5			1.0488616	2.21481101	0.7405778
34.5			0.71519034	1.97353833	0.79659004
35.5			1.18890357	1.97993664	0.62964159
36.5			0.85985285	0.90546602	0.93917382
37.5			0.39315259	7.03408267	0.67862969
38.5			0.36418547	3.22786541	0.54882538
39.5			0.40528634	1.07491857	0.52704577
40.5			0.39786743	1.44301258	0.5261971
41.5			0.6292095	0.79113924	0.54923499
42.5			1.95787325		0.73180931
43.5			4.29140697		0.6958458
44.5					0.62709328
45.5					0.41514977
46.5					0.36273259
47.5					0.46337308
48.5					0.5608525
49.5					2.87175117

OL-G1 CORE GRAIN SIZE ANALYSIS

SAMPLE	Depth (cm)	Clay	V.F. Silt	F. Silt	M. Silt	C. Silt	V.F. Sand	F. Sand	M. Sand	C. Sand
OL-G1-01	1	8.212	7.335	11.4875	13.7375	16.342	17.9855	13.951	8.6755	2.2735
OL-G1-02	2	7.439	6.347	9.4395	10.619	12.4535	13.866	16.4595	16.8205	6.556
OL-G1-03	3	7.321	6.4895	9.912	11.2	13.111	13.7405	18.2235	18.8205	1.182
OL-G1-04	4	6.4725	5.1625	7.604	8.903	11.074	12.859	19.237	22.0375	6.65
OL-G1-05	5	6.4725	5.1625	7.604	8.903	11.074	12.859	19.237	22.0375	6.65
OL-G1-06	6	6.887	5.914	8.904	10.288	12.094	14.238	15.967	17.367	8.343
OL-G1-07	7	5.296	4.448	6.811	8.138	9.883	10.808	18.58	25.463	10.574
OL-G1-08	8	5.845	4.973	7.524	8.769	10.608	12.768	16.366	20.023	13.124
OL-G1-09	9	5.002	4.355	6.85	8.439	10.349	11.776	21.528	26.056	5.645
OL-G1-10	10	7.314	6.045	8.8975	9.8535	11.486	12.3575	17.1385	20.005	6.904
OL-G1-11	11	7.314	6.045	8.8975	9.8535	11.486	12.3575	17.1385	20.005	6.904
OL-G1-12	12	5.318	4.6985	7.2165	8.4075	9.4605	10.004	17.3195	24.481	13.0945
OL-G1-13	13	3.96	3.547	5.668	6.839	7.929	9.32	22.168	30.187	10.381
OL-G1-14	14	3.893	3.667	6.075	7.441	8.362	9.082	20.242	29.645	11.593
OL-G1-15	15	5.002	5.645	10.946	14.717	13.996	12.201	16.761	17.427	3.305
OL-G1-16	16	4.187	4.859	9.655	13.053	12.942	10.812	15.799	20.454	8.239
OL-G1-17	17	3.032	2.598	4.169	5.427	6.87	7.863	22.98	35.123	11.939
OL-G1-18	18	2.647	2.077	3.357	4.721	6.246	5.639	25.022	39.814	10.478
OL-G1-19	19	0	0	0	0.5785	1.7665	0.0735	29.5035	62.564	5.5145
OL-G1-20	20	0	0	0	0.708	1.648	0.407	32.953	57.324	6.96
OL-G1-21	21	0	0	0	0	0	0.155	32.242	61.036	6.567
OL-G1-22	22	0	0	0	0	0	0.116	33.355	59.988	6.541
OL-G1-23	23	1.169	0.627	0.731	0.927	1.927	0.101	27.629	60.36	6.529
OL-G1-24	24	0	0	0	0	0	0.08	30.604	62.1165	7.1995
OL-G1-25	25	0	0	0	0	0	0.039	28.792	65.218	5.95
OL-G1-26	26	0.958	0.434	0.376	0	0	-0.003	29.826	62.741	5.669
OL-G1-27	27	3.898	1.7265	1.8315	2.0425	2.42	0	22.519	58.512	7.05

OL-G2 CORE GRAIN SIZE ANALYSIS

SAMPLE	Depth (cm)	Clay	V.F. Silt	F. Silt	M. Silt	C. Silt	V.F. Sand	F. Sand	M. Sand	C. Sand
OL-G2-01	1	4.5595	5.102	8.9075	8.8805	8.378	9.29	16.3605	25.677	12.845
OL-G2-02	2	4.9185	5.1815	9.7255	9.39	7.654	6.577	14.419	28.909	13.226
OL-G2-03	3	3.1005	2.729	4.5075	5.276	6.518	9.2425	21.013	32.108	15.505
OL-G2-04	4	4.1375	4.3185	7.894	9.0895	9.4255	9.1535	15.6385	25.0985	15.2445
OL-G2-05	5	4.7855	5.4525	10.273	10.278	8.207	6.614	15.7285	27.366	11.295
OL-G2-06	6	5.6435	6.1645	10.425	9.096	6.7565	3.7165	16.176	33.4625	8.5595
OL-G2-07	7	4.5475	4.4135	8.136	9.0295	9.432	10.347	18.725	24.9735	10.396
OL-G2-08	8	4.3455	5.2605	8.374	8.0425	7.8895	9.118	17.5975	26.5225	12.8485
OL-G2-09	9	5.757	6.3515	10.615	9.692	7.5375	6.8735	15.131	26.109	11.9345
OL-G2-10	10	4.123	5.1765	7.5675	6.251	5.251	4.7925	17.598	33.287	15.9535
OL-G2-11	11	4.532	4.0085	4.9805	4.287	4.347	3.3365	21.0765	40.564	12.868
OL-G2-12	12	4.0155	4.103	7.381	8.349	8.7655	8.967	19.272	28.9545	10.193
OL-G2-13	13	2.282	2.079	3.0045	2.5105	2.7205	1.0955	19.795	46.8705	19.6435
OL-G2-14	14	5.3995	5.0505	8.2185	8.3935	7.514	7.006	19.2025	28.4465	10.769
OL-G2-15	15	2.0925	1.7715	2.721	2.876	3.4925	2.1755	20.743	45.734	18.395
OL-G2-16	16	1.3205	0.922	1.528	2.3215	4.1405	3.7015	27.19	47.7345	11.141
OL-G2-17	17	1.037	0.6915	0.978	1.34	2.841	0.4245	23.955	57.6235	11.109
OL-G2-18	18	1.5085	0.9555	1.327	1.6635	2.4475	0.1405	24.1215	59.7575	8.0785
OL-G2-19	19	1.2015	0.6025	0.602	0.072	0	0	22.47	61.908	13.144
OL-G2-20	20	1.3215	0.601	0.5935	0.2405	0.6835	0	21.8045	64.3725	10.3825
OL-G2-21	21	0	0	0	0	0	0.068	28.3315	62.565	9.0355
OL-G2-22	22	0	0	0	0	0	0	15.0855	72.5085	12.406
OL-G2-23	23	0	0	0	0	0	0	21.3228	70.449	8.2235
OL-G2-24	24	0	0	0	0	0	0	11.7245	65.239	23.0365
OL-G2-25	25	0	0	0	0	0.0115	25.8235	65.931	8.2345	
OL-G2-26	26	0	0	0	0	0	0	23.148	68.6055	8.247
OL-G2-27	27	0	0	0	0	0	0	24.0285	66.7475	9.2245
OL-G2-28	28	0	0	0	0	0	0	21.903	66.6775	11.4195
OL-G2-29	29	0	0	0	0	0	0	19.458	71.8545	8.687
OL-G2-30	30	0	0	0	0	0	0	19.3045	73.8295	6.865
OL-G2-31	31	0	0	0	0	0	0	21.038	69.062	9.9
OL-G2-32	32	0	0	0	0	0	0	22.2855	67.8425	9.8715
OL-G2-33	33	0	0	0	0	0	0	19.865	71.9155	8.2195

OL-G3 CORE GRAIN SIZE ANALYSIS

SAMPLE	Depth (cm)	Clay	V.F. Silt	F. Silt	M. Silt	C. Silt	V.F. Sand	F. Sand	M. Sand	C. Sand
OL-G3-01	1	9.8285	7.1885	16.094	18.2	15.227	11.427	6.475	7.7835	7.776
OL-G3-02	2	10.641	8.4205	17.618	19.6575	16.622	12.6215	6.8625	5.1435	2.413
OL-G3-03	3	15.2065	12.5625	22.1855	21.426	16.014	12.05	0.5565	0	0
OL-G3-04	4	13.678	12.348	22.046	22.084	17.075	11.644	1.126	0	0
OL-G3-05	5	12.808	10.73	20.972	22.573	18.288	13.027	1.603	0	0
OL-G3-06	6	12.431	11.529	21.255	22.058	17.636	13.017	2.074	0	0
OL-G3-07	7	10.767	10.323	18.718	19.914	17.767	14.92	5.48	0.982	1.129
OL-G3-08	8	10.344	9.372	16.973	17.996	15.481	12.584	7.57	6.19	3.489
OL-G3-09	9	11.317	10.093	17.747	18.67	16.468	13.399	6.201	3.677	2.429
OL-G3-10	10	10.233	8.562	15.333	16.829	15.301	13.417	8.815	7.574	3.938
OL-G3-11	11	9.552	7.311	13.334	16.095	17.421	17.181	9.256	5.935	3.915
OL-G3-12	12	9.34	7.446	13.559	16.262	17.136	15.942	8.862	7.019	4.435
OL-G3-13	13	8.059	7.116	12.596	14.877	16.053	15.933	12.324	9.418	3.626
OL-G3-14	14	9.998	8.654	14.655	16.489	16.472	15.056	8.974	5.814	3.888
OL-G3-15	15	10.653	9.415	14.913	16.111	15.431	14.201	10.023	6.817	2.436
OL-G3-16	16	7.964	7.952	13.009	14.272	13.873	13.401	11.773	11.215	6.541
OL-G3-17	17	8.092	8.447	13.867	15.408	14.483	13.491	10.97	9.836	5.406
OL-G3-18	18	9.954	9.636	15.631	17.264	16.227	14.967	9.025	5.793	1.503
OL-G3-19	19	7.934	7.576	11.965	13.729	14.072	14.034	11.09	10.678	8.923
OL-G3-20	20	6.777	7.1445	11.3735	13.3865	13.257	12.463	9.169	11.931	14.499
OL-G3-21	21	7.217	7.383	11.348	13.095	13.169	12.815	10.425	12.155	12.392
OL-G3-22	22	9.501	8.999	14.289	17.444	18.848	17.548	11.719	1.651	0
OL-G3-23	23	5.935	6.49	10.397	11.843	11.228	10.816	10.894	16.152	16.246
OL-G3-24	24	7.274	7.02	10.541	11.891	12.24	12.112	11.661	14.739	12.525
OL-G3-25	25	6.991	6.909	10.121	10.876	10.384	9.651	9.992	17.224	17.851

OL-G3-26	26	6.359	6.611	10.534	12.404	11.998	11.567	12.69	15.678	12.159
OL-G3-27	27	7.565	7.69	11.265	12.365	10.998	9.545	11.917	16.837	11.818
OL-G3-28	28	9.33	8.701	10.506	10.392	10.116	9.762	13.229	16.583	11.38
OL-G3-29	29	4.44	3.923	4.936	5.6005	5.9055	5.107	26.7815	35.496	7.8115
OL-G3-30	30	6.371	6.324	8.141	8.736	8.222	7.721	19.951	24.491	10.042
OL-G3-31	31	4.844	4.381	4.865	5.738	6.581	7.986	28.82	29.756	7.028
OL-G3-32	32	1.186	0.616	0.707	1.733	2.446	1.59	38.557	49.745	3.42
OL-G3-33	33	0	0.364	0.408	1.234	2.04	1.537	39.789	51.527	3.1
OL-G3-34	34	1.352	0.617	0.737	2.126	3.385	1.523	38.016	49.369	2.876
OL-G3-35	35	1.106	0.476	0.51	1.522	2.676	1.315	37.93	51.189	3.276
OL-G3-36	36	0.06	0.499	0.472	1.249	2.219	0.82	35.816	54.209	4.655
OL-G3-37	37	1.544	0.664	0.786	1.553	2.299	0.34	34.922	54.459	3.434
OL-G3-38	38	1.451	0.568	0.645	1.359	2.488	0.16	29.728	58.74	4.861
OL-G3-39	39	0	0	0	0	0	0.533	38.729	56.824	3.915
OL-G3-40	40	0	0	0	0	0	1.787	49.248	47.974	0.991
OL-G3-41	41	0	0	0	0	0	2.877	54.718	41.932	0.473
OL-G3-42	42	0	0	1.127	0.547	5.648	59.526	33.123	0.028	

OL-G4 CORE GRAIN SIZE ANALYSIS

SAMPLE	Depth (cm)	Clay	V.F. Silt	F. Silt	M. Silt	C. Silt	V.F. Sand	F. Sand	M. Sand	C. Sand
OL-G4-01	1	9.2685	9.78	17.016	16.8685	14.0165	13.7835	11.4245	7.0295	0.8135
OL-G4-02	2	8.1045	8.612	15.0725	14.7955	12.51	13.1035	11.0615	9.674	7.066
OL-G4-03	3	8.2745	9.421	17.956	19.4245	15.6775	12.5105	7.287	4.7715	4.6785
OL-G4-04	4	9.864	9.1865	16.225	16.461	14.744	14.7305	8.605	4.707	5.4775
OL-G4-05	5	9.6455	11.163	20.469	21.2245	15.9135	11.774	5.1095	1.42	3.281
OL-G4-06	6	6.602	6.476	12.255	14.324	14.095	14.6165	12.1405	11.1175	8.373
OL-G4-07	7	5.838	6.921	12.5135	14.4955	13.5375	12.167	10.0845	12.4245	12.0185
OL-G4-08	8	5.9215	6.862	12.322	14.033	13.4495	12.3775	10.5445	13.4205	11.0685
OL-G4-09	9	6.334	6.5125	11.9435	13.401	12.5545	12.7035	11.677	14.178	10.6965
OL-G4-10	10	5.9455	6.715	11.9815	13.4535	12.908	13.167	11.127	13.3595	11.343
OL-G4-11	11	6.274	7.633	13.2895	14.9505	13.374	10.877	9.727	13.2875	10.5875
OL-G4-12	12	6.275	6.352	10.68	12.3525	11.919	10.5955	10.6395	17.172	14.014
OL-G4-13	13	6.2222	6.9445	11.4975	13.6035	13.995	12.2175	9.927	13.8165	11.778
OL-G4-14	14	4.48	4.861	8.4655	11.554	14.421	14.4725	12.206	15.479	14.061
OL-G4-15	15	4.218	4.902	9.372	13.1185	14.865	13.899	11.905	15.552	12.1685
OL-G4-16	16	4.7785	5.2445	9.291	12.9445	15.1025	15.3415	11.446	12.0805	13.771
OL-G4-17	17	4.5275	4.847	8.687	12.0795	14.022	13.82	11.3755	16.0385	14.603
OL-G4-18	18	3.89	4.4465	8.379	12.2585	14.857	14.6355	11.092	14.915	15.527
OL-G4-19	19	3.558	4.299	7.465	10.186	12.457	14.3065	12.106	16.426	19.196
OL-G4-20	20	3.815	4.366	7.501	10.2	12.867	14.7275	12.0235	16.88	17.62
OL-G4-21	21	4.6855	5.0735	7.98	9.597	9.9165	10.108	10.837	21.268	20.5345
OL-G4-22	22	2.7405	2.389	2.9895	3.456	5.6145	7.8835	12.0975	37.7985	25.032
OL-G4-23	23	1.872	1.37	1.8505	2.714	4.834	8.6975	14.601	38.3685	25.6935
OL-G4-24	24	2.459	1.895	2.5975	3.95	6.7385	9.329	12.8445	36.267	23.9195
OL-G4-25	25	1.666	1.0605	1.543	2.191	4.139	4.884	8.286	44.103	32.127

OL-G4-26	26	2.87	1.599	2.1965	3.4195	6.0065	6.346	9.381	41.1875	26.9945
OL-G4-27	27	1.7865	0.9785	1.3575	1.68	3.131	3.838	8.8065	46.216	32.2065
OL-G4-28	28	2.82	1.6645	2.404	2.945	4.1675	4.08	8.283	44.146	29.4905
OL-G4-29	29	3.796	2.4375	3.394	3.8185	4.3155	3.4475	5.2155	43.0275	30.549
OL-G4-30	30	3.37	2.192	3.1865	4.106	5.624	6.4525	8.1365	38.181	28.7515
OL-G4-31	31	4.5555	2.9535	4.3055	5.6265	7.3825	8.282	10.495	34.241	22.1585
OL-G4-32	32	5.3385	3.379	4.4085	5.1075	5.9755	5.964	6.865	35.0005	27.9615
OL-G4-33	33	2.368	1.614	2.284	2.695	4.2505	5.459	8.1395	41.7965	31.3935
OL-G4-34	34	3.2295	2.062	2.6605	2.788	4.143	3.954	6.501	44.2735	30.3885
OL-G4-35	35	1.614	0.861	1.1135	0.881	1.592	1.5025	2.259	53.534	36.6425
OL-G4-36	36	3.335	1.6535	1.815	1.5655	2.463	2.5655	3.2015	50.7155	32.6855
OL-G4-37	37	2.597	1.5885	1.7995	1.6535	2.134	7.224	15.3925	41.2225	26.3885
OL-G4-38	38	7.94	5.7025	6.966	5.582	4.209	7.072	13.206	30.5915	18.7315
OL-G4-39	39	5.5595	3.177	3.514	3.125	3.603	1.965	4.0335	45.656	29.3665
OL-G4-40	40	4.534	2.9055	2.8835	2.4185	3.3465	2.1565	6.3865	47.341	28.0285
OL-G4-41	41	3.397	2.198	2.2505	1.8005	2.53	1.745	3.4735	49.471	33.1345
OL-G4-42	42	0	0	0	0	0	0	3.143	57.457	39.4005

OL-G5 CORE GRAIN SIZE ANALYSIS

SAMPLE	Depth (cm)	Clay	V.F. Silt	F. Silt	M. Silt	C. Silt	V.F. Sand	F. Sand	M. Sand	C. Sand
OL-G5-01	1	7.348	7.378	11.08	12.5565	17.904	21.687	12.7295	7.418	1.898
OL-G5-02	2	7.3965	7.588	11.564	12.8565	16.451	19.18	12.0145	8.3565	4.5925
OL-G5-03	3	5.8795	6.664	10.899	11.816	13.994	15.9605	12.2535	13.359	9.175
OL-G5-04	4	7.857	10.5035	17.663	16.8645	14.049	12.4395	8.089	7.0335	5.5015
OL-G5-05	5	5.236	6.9425	12.063	12.499	13.988	16.535	11.3575	11.3205	10.059
OL-G5-06	6	7.676	7.65	12.182	14.8725	19.308	18.3975	9.0115	6.305	4.5975
OL-G5-07	7	6.861	7.223	11.4125	13.5165	16.024	14.9355	10.2415	11.2865	8.4995
OL-G5-08	8	6.5145	7.1425	11.7325	13.705	15.976	14.4135	10.5945	13.627	6.295
OL-G5-09	9	5.54	5.8105	9.505	11.8625	16.2485	16.834	12.1025	13.742	8.3545
OL-G5-10	10	9.791	12.597	19.121	17.0385	13.7365	11.9685	7.5505	5.6295	2.567
OL-G5-11	11	6.1295	6.707	10.443	10.6525	12.2725	12.045	11.3405	19.554	10.8565
OL-G5-12	12	5.7225	5.4655	9.187	12.2575	15.7725	13.7215	10.37	16.9405	10.563
OL-G5-13	13	4.622	4.2805	6.7565	9.3055	13.7695	14.5855	12.5825	19.1095	14.9835
OL-G5-14	14	5.79	5.582	8.6825	11.2365	14.549	14.099	10.902	15.1825	13.9775
OL-G5-15	15	6.498	6.441	10.098	12.9525	16.295	15.1645	10.761	12.2145	9.576
OL-G5-16	16	5.5425	5.675	9.036	11.7235	15.3205	14.756	11.591	15.146	11.21
OL-G5-17	17	5.5285	5.561	8.7555	11.1895	14.4595	13.7295	10.48	15.6565	14.64
OL-G5-18	18	5.467	5.374	8.472	10.9825	14.2035	13.5925	11.548	16.8395	13.521
OL-G5-19	19	4.721	4.549	7.497	10.265	14.3595	14.837	12.8875	17.6805	13.203
OL-G5-20	20	4.7175	4.4885	7.2445	9.9085	13.71	13.838	12.221	18.31	15.5625
OL-G5-21	21	5.2005	5.0865	8.3525	11.555	15.8	14.516	10.76	15.7085	13.0215
OL-G5-22	22	5.545	5.349	8.5605	11.7	15.888	14.5715	10.142	14.233	14.011
OL-G5-23	23	5.196	5.039	8.021	10.902	14.593	13.4465	12.039	18.519	12.245
OL-G5-24	24	4.871	4.602	6.689	7.5175	7.6315	6.333	12.1535	30.737	19.4655
OL-G5-25	25	3.4945	3.3475	4.9845	5.73	6.363	5.089	11.5385	36.1225	23.33

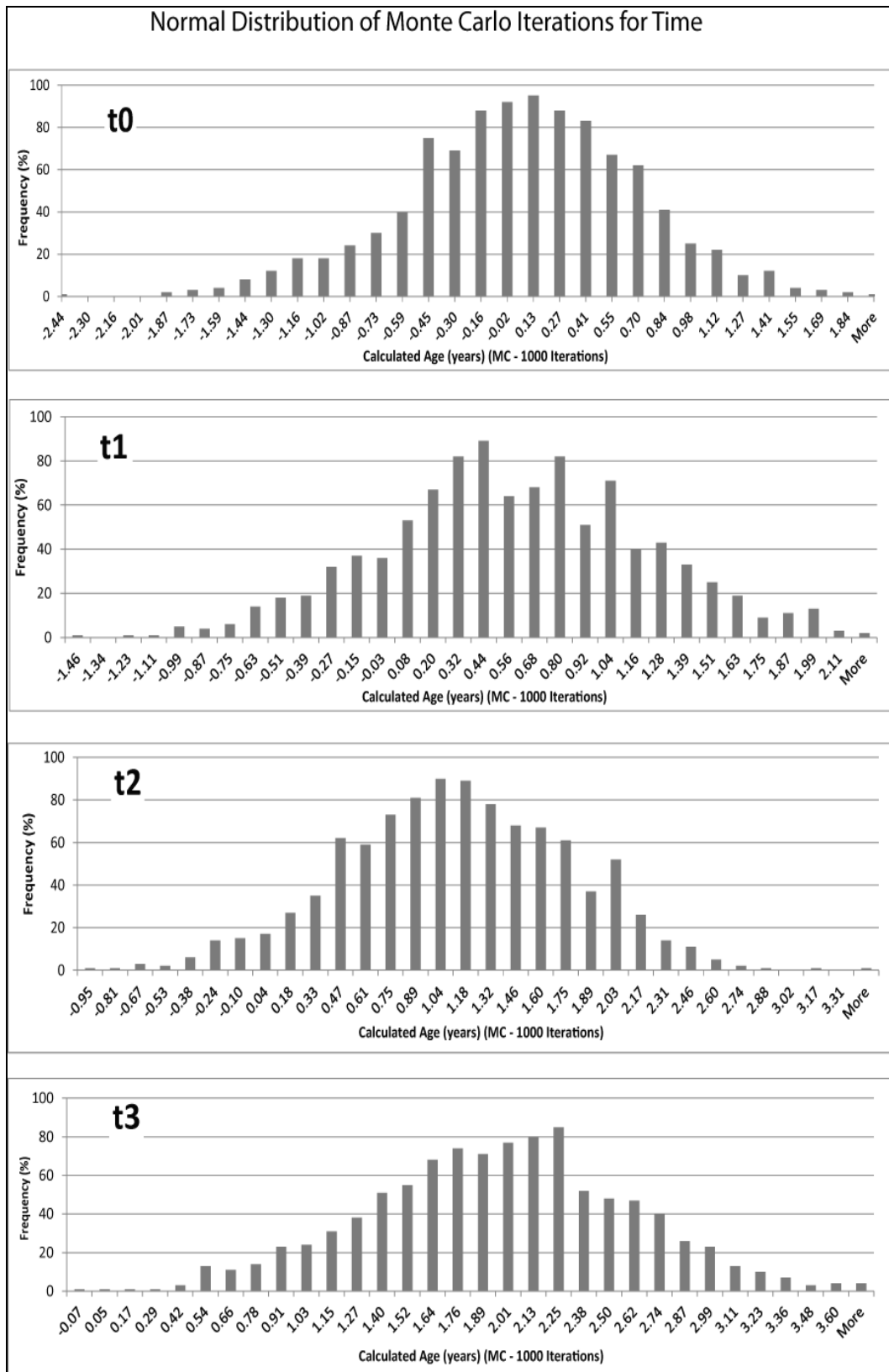
OL-G5-26	26	1.624	1.3645	2.1415	2.3415	3.6035	1.195	8.2	58.164	21.3655
OL-G5-27	27	1.25	1.0065	1.843	2.2275	3.748	1.431	8.8055	59.803	19.886
OL-G5-28	28	0	0.3085	0.8165	0.51	1.88	0.5385	7.712	69.2925	18.942
OL-G5-29	29	0	0	0	0	0	0	9.354	69.696	20.9495
OL-G5-30	30	0	0	0	0	0	0	10.9625	70.4485	18.5885
OL-G5-31	31	0	0.312	0.9265	0.8895	2.365	0.7455	8.478	69.5915	16.6915
OL-G5-32	32	0	0	0	0.106	1.932	0.5015	8.197	71.724	17.539
OL-G5-33	33	0	0	0	0	0	0	8.7835	74.3935	16.8235
OL-G5-34	34	1.054	0.6215	0.837	0.194	0	0	5.9685	75.881	15.4435
OL-G5-35	35	0	0	0	0	0	0	6.885	78.0205	15.095
OL-G5-36	36	0	0	0	0	0	0	5.8465	76.9565	17.1975
OL-G5-37	37	2.246	1.0495	1.2075	0.8535	2.0515	0.4644	5.394	69.9965	16.7365
OL-G5-38	38	0	0	0	0	0	0	7.0785	78.0025	14.9195
OL-G5-39	39	0	0	0	0	0	0	6.5715	77.417	16.0115
OL-G5-40	40	0	0	0	0	0	0	9.1115	71.99	18.899
OL-G5-41	41	0	0	0	0	0	0	7.1975	78.2225	14.5805
OL-G5-42	42	0	0	0	0	0	0	7.3275	77.872	14.8005
OL-G5-43	43	0	0	0	0	0	0	10.5345	72.522	16.944
OL-G5-44	44	0	0	0	0	0	0	11.369	70.226	18.4055
OL-G5-45	45	0.646	0.2025	0.201	0.001	0	0	10.135	73.677	15.138
OL-G5-46	46	0	0	0	0	0	0	10.62	74.061	15.319
OL-G5-47	47	0.6215	0.171	0.15	0	0	0	14.003	71.7355	13.3185
OL-G5-48	48	1.7095	0.582	0.592	0.07	0	0	19.0435	64.001	14.002
OL-G5-49	49	2.627	1.046	1.0465	0.9665	1.959	1.9385	22.5275	53.125	14.764
OL-G5-50	50	3.724	1.599	1.463	1.2435	2.353	6.545	24.1405	45.9515	12.98

PERCENTAGE SAND BY WEIGHT for ALL CORES with DEPTH					
Depth (cm)	G1	G2	G3	G4	G5
0.5	20	41.15272	3.445851	12.42824	2.270816
1.5	30.14544	41.19561	7.74359	13.02782	15.74451
2.5	41.87161	42.4993	5.807711	13.03215	13.86355
3.5	33.93325	41.06434	6.705119	14.42904	11.53846
4.5	34.32078	51.26382	8.844065	12.34266	8.475669
5.5	34.70348	49.33879	13.4058	13.11249	7.838808
6.5	28.7569	46.9429	7.515473	13.4106	12.66899
7.5	26.978	45.15209	12.46439	16.67014	28.17417
8.5	47.38462	45.75416	10.05996	16.24738	35.93988
9.5	50.84067	50.63623	10.3681	21.05263	38.18218
10.5	49.50298	45.38633	8.222433	22.6709	32.23777
11.5	46.95122	46.47799	9.586535	17.22982	26.07986
12.5	40.70189	64.95005	13.76535	23.80892	25.43129
13.5	30.98888	78.4885	13.14232	23.71337	18.47877
14.5	28.66456	70.39567	9.73025	20.40457	18.57988
15.5	42.3863	84.5927	9.693252	18.0805	18.72021
16.5	47.15893	93.48148	10.7359	19.74338	18.37624
17.5	68.36857	97.6723	7.566616	20.4244	21.67108
18.5	93.95822	98.15898	8.148992	22.79804	28.93172
19.5	95.34591	97.73104	8.528341	24.63223	19.92329
20.5	94.75516	98.08274	6.651088	49.96981	8.896034
21.5	96.50419	98.90974	18.49964	62.81942	13.27434
22.5	95.81945	98.95074	30.45893	72.52901	20.05089
23.5	96.15192	98.81983	20.14431	56.09402	67.20617
24.5	97.05354	98.74307	14.2125	81.78817	76.83991
25.5	96.19026	98.63416	18.40098	83.59222	91.14366
26.5	84.33183	98.67795	27.51189	79.98118	96.09245
27.5		98.61069	56.28909	82.19978	97.35595
28.5		98.72636	62.06331	58.6707	97.6862
29.5		98.67995	52.9837	55.26347	98.65437
30.5		98.88511	86.34982	61.31537	98.01041
31.5		98.17306	93.59012	62.18949	97.26649
32.5		98.76747	95.29455	64.18226	97.99455
33.5			90.06265	85.67471	98.23583
34.5			89.91806	89.62807	97.47061
35.5			93.25248	91.07115	98.12119
36.5			96.02967	89.24884	96.63518
37.5			90.13391	72.99584	98.55604
38.5			95.93011	71.03958	98.86009
39.5			97.36961	93.66266	98.92717
40.5			97.16949	95.9461	98.63849
41.5			93.55646	97.76029	98.7142
42.5			93.34412		98.21029
43.5			75.643		98.34254
44.5					98.43448
45.5					98.35657
46.5					98.62741
47.5					97.4021
48.5					92.10362
49.5					80.74809

D.

^{210}Pb ERROR CALCULATIONS

RESULTS OF MONTE CARLO SIMULATION FOR ^{210}PB DATING ERROR				
Depth	Variable	Mean	StDev	95% CI
1.5	t1	0.5265	0.617	1.234
2.5	t2	1.0615	0.6465	1.293
3.5	t3	1.9011	0.6372	1.2744
4.5	t4	1.8919	0.6405	1.281
5.5	t5	4.2442	0.641	1.282
6.5	t6	5.4862	0.6587	1.3174
7.5	t7	6.5234	0.6643	1.3286
8.5	t8	7.6497	0.7046	1.4092
9.5	t9	8.9956	0.7326	1.4652
10.5	t10	10.294	0.751	1.502
11.5	t11	11.487	0.753	1.506
12.5	t12	13.415	0.756	1.512
13.5	t13	14.795	0.788	1.576
14.5	t14	16.711	0.832	1.664
15.5	t15	18.914	0.895	1.79
16.5	t16	21.044	0.944	1.888
17.5	t17	23.201	0.967	1.934
18.5	t18	25.875	1.054	2.108
19.5	t19	28.307	1.078	2.156
20.5	t20	31.628	1.244	2.488
21.5	t21	34.789	1.26	2.52
22.5	t22	37.418	1.422	2.844
23.5	t23	40.995	1.523	3.046
24.5	t24	45.282	1.752	3.504
25.5	t25	48.857	1.966	3.932
26.5	t26	52.739	2.232	4.464
27.5	t27	56.814	2.467	4.934
28.5	t28	60.639	2.664	5.328
29.5	t29	67.823	3.289	6.578
30.5	t30	70.408	3.71	7.42
31.5	t31	76.009	4.134	8.268
32.5	t32	74.612	3.194	6.388
33.5	t33	115	9.7	19.4
34.5	t34	181.66	37.85	75.7



E.

CLIMATE AND SAND CONCENTRATION CORRELATION

Regression Statistics	
Multiple R	0.144886
R Square	0.020992
Adjusted R Square	-0.01164
Standard Error	0.377632
Observations	32

Average Annual Lake Level

ANOVA					
	df	SS	MS	F	Significance F
Regression	1	0.091732	0.091732	0.643258836	0.428840943
Residual	30	4.278176	0.142606		
Total	31	4.369909			

Regression Statistics	
Multiple R	0.537418
R Square	0.288818
Adjusted R Square	0.264294
Standard Error	24.92356
Observations	31

Annual Average Precipitation

ANOVA					
	df	SS	MS	F	Significance F
Regression	1	7315.785546	7315.785546	11.77716902	0.001822855
Residual	29	18014.32759	621.18371		
Total	30	25330.11313			

Regression Statistics	
Multiple R	0.263888
R Square	0.069637
Adjusted R Square	0.037555
Standard Error	28.50663
Observations	31

Average Winter Precipitation

ANOVA					
	df	SS	MS	F	Significance F
Regression	1	1763.909684	1763.909684	2.170624596	0.151441394
Residual	29	23566.20345	812.6277052		
Total	30	25330.11313			

Regression Statistics	
Multiple R	0.263994
R Square	0.069693
Adjusted R Square	0.037613
Standard Error	28.50577
Observations	31

Average Summer Precipitation

ANOVA					
	df	SS	MS	F	Significance F
Regression	1	1765.327514	1765.327514	2.172500049	0.15127099
Residual	29	23564.78562	812.5788145		
Total	30	25330.11313			

Regression Statistics		Average Fall Precipitation			
Multiple R	0.369527				
R Square	0.13655				
Adjusted R Square	0.106776				
Standard Error	27.46238				
Observations	31				

ANOVA					
	df	SS	MS	F	Significance F
Regression	1	3458.831704	3458.831704	4.586202218	0.040761646
Residual	29	21871.28143	754.1821183		
Total	30	25330.11313			

Regression Statistics		Average Annual Evaporation			
Multiple R	0.623033				
R Square	0.38817				
Adjusted R Square	0.362677				
Standard Error	15.028				
Observations	26				

ANOVA					
	df	SS	MS	F	Significance F
Regression	1	3438.783841	3438.783841	15.22658791	0.000674511
Residual	24	5420.177697	225.8407374		
Total	25	8858.961538			

Regression Statistics		Average Summer Evaporation			
Multiple R	0.7094				
R Square	0.503249				
Adjusted R Square	0.482551				
Standard Error	13.54114				
Observations	26				

ANOVA					
	df	SS	MS	F	Significance F
Regression	1	4458.262545	4458.262545	24.31393313	4.95268E-05
Residual	24	4400.698994	183.3624581		
Total	25	8858.961538			

Regression Statistics		Average Fall Evaporation			
Multiple R	0.245612				
R Square	0.060325				
Adjusted R Square	0.021172				
Standard Error	18.62407				
Observations	26				

ANOVA					
	df	SS	MS	F	Significance F
Regression	1	534.4209411	534.4209411	1.540758008	0.226500738
Residual	24	8324.540597	346.8558582		
Total	25	8858.961538			

Regression Statistics		Average Winter Evaporation			
Multiple R	0.224884				
R Square	0.050573				
Adjusted R Square	0.011014				
Standard Error	18.72046				
Observations	26				

ANOVA					
	df	SS	MS	F	Significance F
Regression	1	448.0239598	448.0239598	1.278403856	0.269368906
Residual	24	8410.937579	350.4557324		
Total	25	8858.961538			

Regression Statistics		Average Annual Temperature			
Multiple R	0.062816175				
R Square	0.003945872				
Adjusted R Square	-0.039360829				
Standard Error	16.15401157				
Observations	25				

ANOVA					
	df	SS	MS	F	Significance F
Regression	1	23.77653981	23.77653981	0.091114579	0.765477477
Residual	23	6001.898068	260.9520899		
Total	24	6025.674608			

Regression Statistics		Average Summer Temperature			
Multiple R	0.151084138				
R Square	0.022826417				
Adjusted R Square	-0.019659391				
Standard Error	16.00017669				
Observations	25				

ANOVA					
	df	SS	MS	F	Significance F
Regression	1	137.54456	137.54456	0.537271571	0.470970863
Residual	23	5888.130048	256.0056542		
Total	24	6025.674608			

Regression Statistics		Average Winter Temperature			
Multiple R	0.116227251				
R Square	0.013508774				
Adjusted R Square	-0.029382149				
Standard Error	16.07627895				
Observations	25				

ANOVA					
	df	SS	MS	F	Significance F
Regression	1	81.39947595	81.39947595	0.314956476	0.58008191
Residual	23	5944.275132	258.4467449		
Total	24	6025.674608			

Regression Statistics		Average Fall Temperature			
Multiple R	0.089649296				
R Square	0.008036996				
Adjusted R Square	-0.03509183				
Standard Error	16.1208025				
Observations	25				

ANOVA					
	df	SS	MS	F	Significance F
Regression	1	48.42832473	48.42832473	0.186348599	0.669992839
Residual	23	5977.246283	259.8802732		
Total	24	6025.674608			

Regression Statistics		Annual Average PDSI			
Multiple R	0.094962				
R Square	0.0090178				
Adjusted R Square	-0.024015				
Standard Error	29.231142				
Observations	32				

ANOVA					
	df	SS	MS	F	Significance F
Regression	1	233.2632811	233.2632811	0.272995079	0.605167032
Residual	30	25633.78962	854.4596541		
Total	31	25867.0529			

Regression Statistics		Average Fall PDSI			
Multiple R	0.1478485				
R Square	0.0218592				
Adjusted R Square	-0.010746				
Standard Error	29.041132				
Observations	32				

ANOVA					
	df	SS	MS	F	Significance F
Regression	1	565.4322914	565.4322914	0.670430128	0.419358686
Residual	30	25301.62061	843.3873537		
Total	31	25867.0529			

Regression Statistics		Average Summer PDSI			
Multiple R	0.0753156				
R Square	0.0056724				
Adjusted R Square	-0.027472				
Standard Error	29.280439				
Observations	32				

ANOVA					
	df	SS	MS	F	Significance F
Regression	1	146.7292153	146.7292153	0.171143898	0.682039792
Residual	30	25720.32369	857.3441229		
Total	31	25867.0529			

Regression Statistics	
Multiple R	0.0611068
R Square	0.003734
Adjusted R Square	-0.029475
Standard Error	29.308966
Observations	32

Average Winter PDSI

ANOVA

	df	SS	MS	F	Significance F
Regression	1	96.58852435	96.58852435	0.112440959	0.739715698
Residual	30	25770.46438	859.0154793		
Total	31	25867.0529			

Regression Statistics	
Multiple R	0.1979
R Square	0.0392
Adjusted R Square	-0.0249
Standard Error	208.23
Observations	17

ST 94055 – Cumulative Annual Hours >7 m/s

ANOVA

	df	SS	MS	F	Significance F
Regression	1	26516.32339	26516.32339	0.611563354	0.446369427
Residual	15	650373.9119	43358.26079		
Total	16	676890.2353			

Regression Statistics	
Multiple R	0.50943
R Square	0.25952
Adjusted R Square	0.20256
Standard Error	11.5997
Observations	15

ST 94055 – Cumulative Annual Hours >10 m/s

ANOVA

	df	SS	MS	F	Significance F
Regression	1	613.0347665	613.0347665	4.556096925	0.052417729
Residual	13	1749.184027	134.5526174		
Total	14	2362.218793			

Regression Statistics	
Multiple R	0.48495
R Square	0.23518
Adjusted R Square	0.17635
Standard Error	11.7888
Observations	15

ST 94055 – Cumulative Annual Hours >15 m/s

ANOVA

	df	SS	MS	F	Significance F
Regression	1	555.5458802	555.5458802	3.997456536	0.066916516
Residual	13	1806.672913	138.9748394		
Total	14	2362.218793			

Regression Statistics		ST4055 – RATIO of Fall & Winter Hours to Annual Hours			
Multiple R	0.65244				
R Square	0.42567				
Adjusted R Square	0.38149				
Standard Error	10.2157				
Observations	15				

ANOVA					
	df	SS	MS	F	Significance F
Regression	1	1005.53046	1005.53046	9.635150287	0.008381113
Residual	13	1356.688333	104.360641		
Total	14	2362.218793			

Regression Statistics		ST94055 – Cumulative Annual Fall and Winter Hours			
Multiple R	0.44769				
R Square	0.20042				
Adjusted R Square	0.13892				
Standard Error	12.0536				
Observations	15				

ANOVA					
	df	SS	MS	F	Significance F
Regression	1	473.4450348	473.4450348	3.258614445	0.094251153
Residual	13	1888.773758	145.2902891		
Total	14	2362.218793			

Regression Statistics		ST 92446 – Cumulative Annual Hours >6.5 m/s			
Multiple R	0.3028				
R Square	0.0917				
Adjusted R Square	0.0218				
Standard Error	91.005				
Observations	15				

ANOVA					
	df	SS	MS	F	Significance F
Regression	1	10868.66777	10868.66777	1.312345189	0.27262201
Residual	13	107664.2656	8281.866582		
Total	14	118532.9333			

Regression Statistics		ST 94226 – Cumulative Annual Hours >10 m/s			
Multiple R	0.14448				
R Square	0.02087				
Adjusted R Square	-0.0444				
Standard Error	2.18612				
Observations	17				

ANOVA					
	df	SS	MS	F	Significance F
Regression	1	1.528275245	1.528275245	0.319780346	0.580100664
Residual	15	71.68710944	4.779140629		
Total	16	73.21538468			

Regression Statistics	
Multiple R	0.13153
R Square	0.0173
Adjusted R Square	-0.0482
Standard Error	2.19011
Observations	17

ST 94226 – Cumulative Annual Hours >15 m/s

ANOVA

	df	SS	MS	F	Significance F
Regression	1	1.266648357	1.266648357	0.264073093	0.614822162
Residual	15	71.94873632	4.796582422		
Total	16	73.21538468			

Regression Statistics	
Multiple R	0.30816
R Square	0.09496
Adjusted R Square	0.03463
Standard Error	2.10179
Observations	17

ST94226 – RATIO of Fall & Winter Hours to Annual Hours

ANOVA

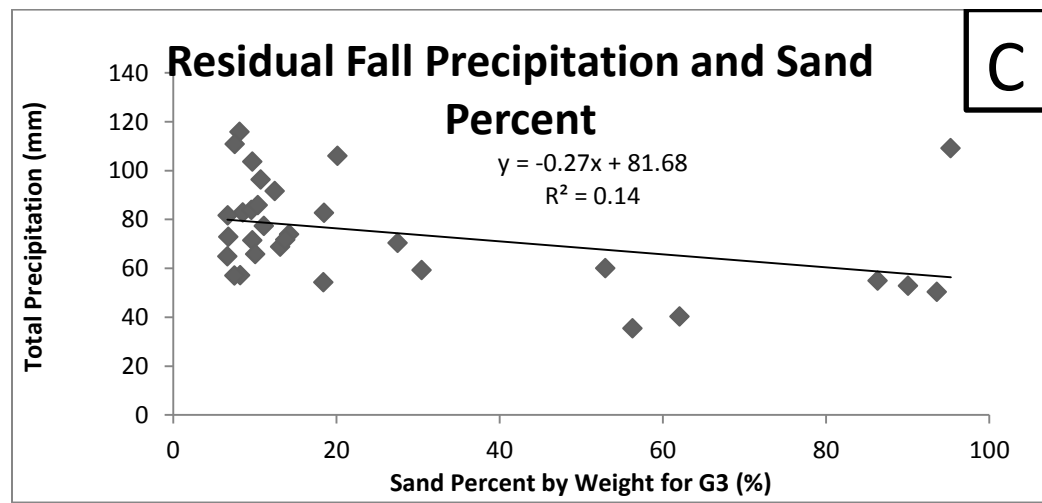
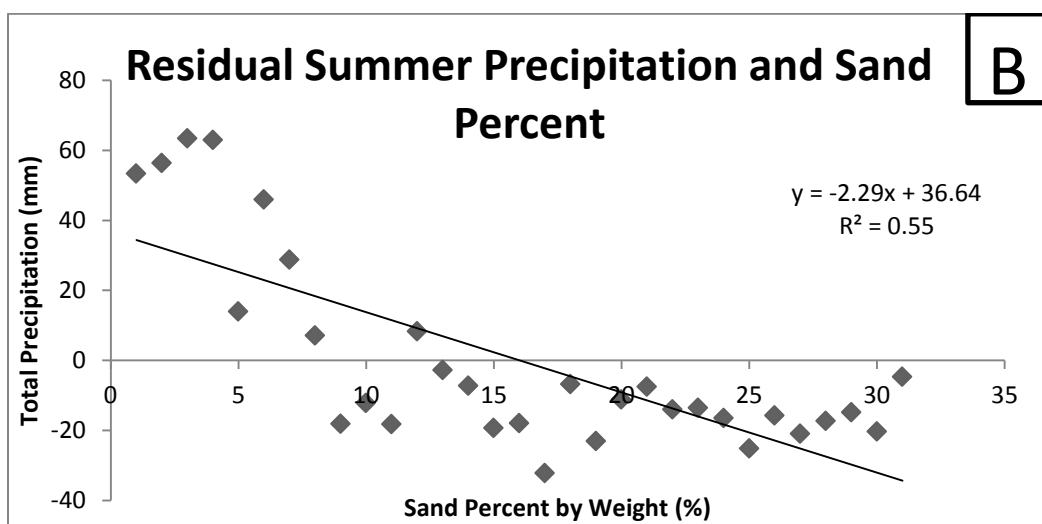
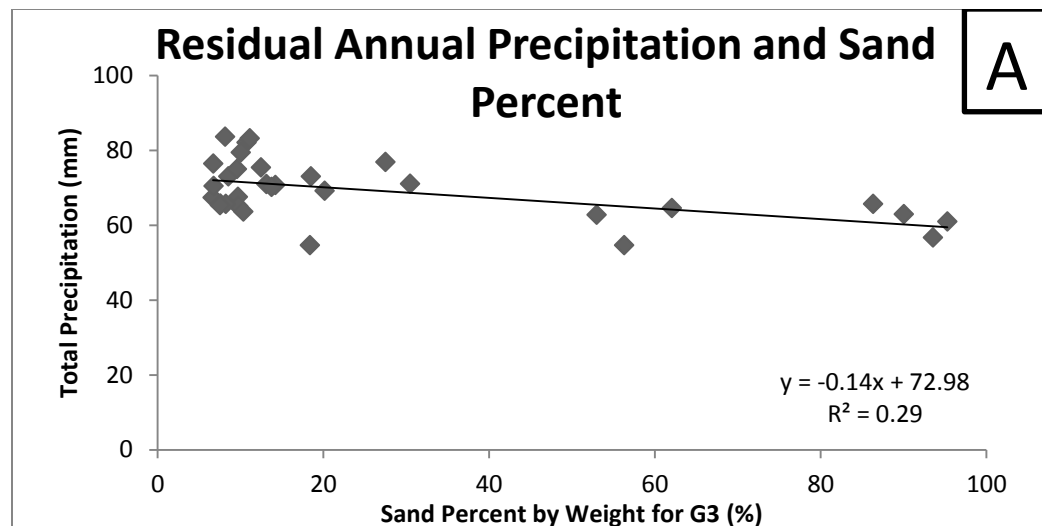
	df	SS	MS	F	Significance F
Regression	1	6.952678954	6.952678954	1.573889613	0.228839884
Residual	15	66.26270573	4.417513715		
Total	16	73.21538468			

Regression Statistics	
Multiple R	0.11483
R Square	0.01319
Adjusted R Square	-0.0526
Standard Error	2.19469
Observations	17

ST94226 – Cumulative Annual Fall and Winter Hours

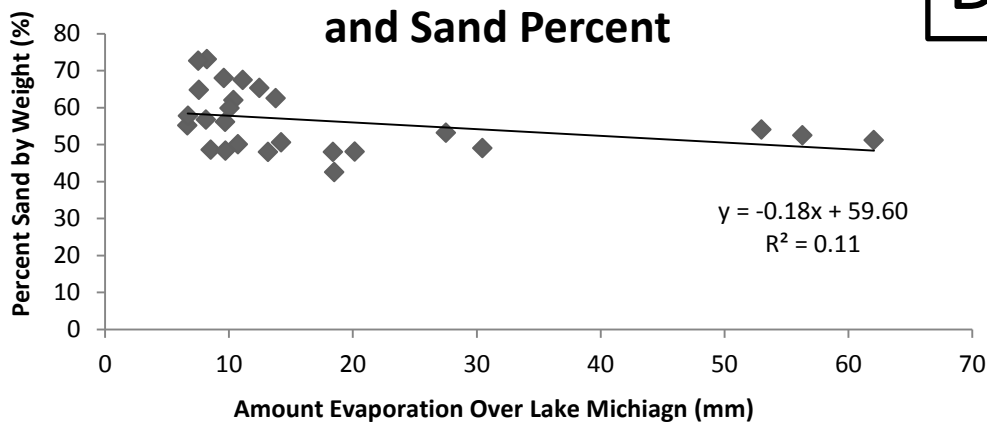
ANOVA

	df	SS	MS	F	Significance F
Regression	1	0.965459861	0.965459861	0.200441702	0.660762569
Residual	15	72.24992482	4.816661655		
Total	16	73.21538468			



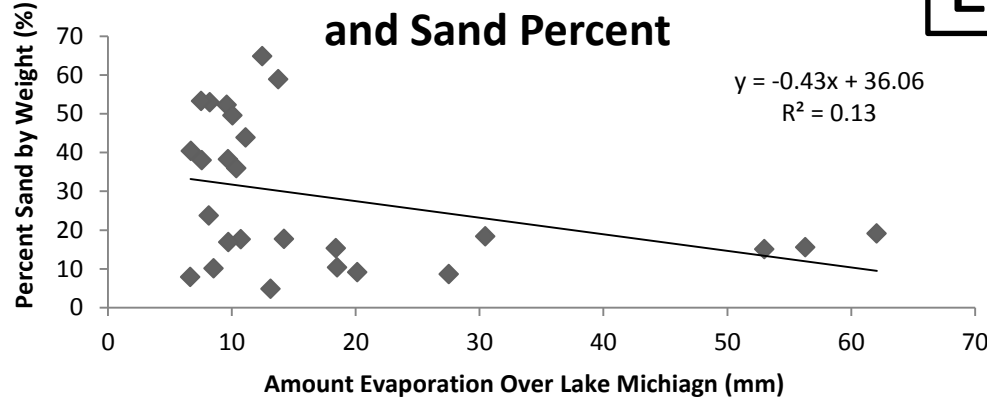
Residual Average Annual Evaporation and Sand Percent

D



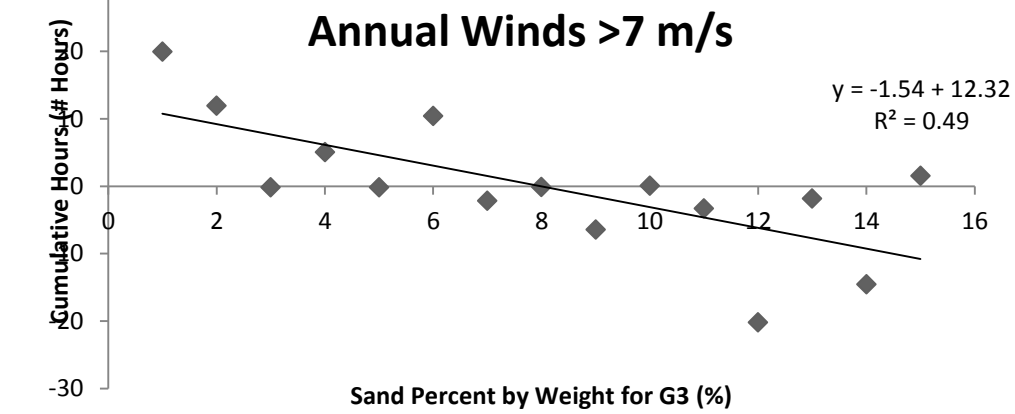
Residual Average Summer Evaporation and Sand Percent

E



Residual Ratio ST94055: Fall & Winter to Annual Winds >7 m/s

F



Residual Annual Wind >10 m/s Cumulative Hours

G

